Development and Application of Multiscale Methods for Simulating Polymer Properties

Entwicklung und Anwendung von Multiskalenverfahren zur Simulation von Polymereigenschaften

Vom Fachbereich Chemie der Technischen Universität Darmstadt zur Erlangung des Grades Doctor rerum naturalium (Dr. rer. nat.)

Dissertation von Jurek Schneider

1. Gutachten: Prof. Dr. Florian Müller-Plathe
2. Gutachten: Prof. Dr. Nico van der Vegt
Darmstadt 2021

TECHNISCHE UNIVERSITÄT DARMSTADT

Eduard-Zintl-Institut für Anorganische und Physikalische Chemie

Development and Application of Multiscale Methods for Simulating Polymer Properties
Entwicklung und Anwendung von Multiskalenverfahren zur Simulation von Polymereigenschaften

Dissertation von Jurek Schneider

1. Gutachten: Prof. Dr. Florian Müller-Plathe
2. Gutachten: Prof. Dr. Nico van der Vegt

Tag der Einreichung: 20. Juli 2021
Tag der Prüfung: 27. September 2021

Darmstadt 2021

Acknowledgment

When I signed up my studies to become a chemist ten years ago, I could not have possibly imagined how this chapter – probably the so-far most important one in my life – would challenge my skills, persistence, and sanity. I want to dedicate some lines to thank the people I have met along the way, who helped me overcome all kinds of obstacles and really made this memory a pleasant one.

I firstly want to thank Florian Müller-Plathe, who has been a great teacher and supervisor not only during my Ph.D., but in all theses and many practicals throughout my studies. Florian always found a good balance between providing guidance and the freedom to follow my own interests. His scientific skills are renowned, but I equally appreciate his efforts to keep close personal contact to all members of his group and maintain a healthy working atmosphere, especially in the recent times of social distancing.
I want to express my gratitude to Nico van der Vegt for examining this thesis and for providing help and suggestions in- and outside of our shared group seminar. Further, I'm grateful to Markus Biesalski, Arash Nikoubashman, and Boris Schmidt for being part of my evaluation committee.

My studies would have probably been very different if it wasn't for Michael Böhm. A long time ago, Michael insisted that I would talk to Florian, who I only knew as a scary thermodynamics professor back then, about a potential bachelor's thesis in his group. I never really left again, which was also due to Michael's kind, welcoming attitude and his genuine interest in the scientific and personal well-being of everybody around him. I deeply regret that we have never published anything together.
I am profoundly grateful to Dana Voss for her endeavors to make our group a kinder and more social place. Also, I believe the professional effortlessness with which she wiped away all possible bureaucratic obstacles cannot be appreciated enough.
Of course, I also want to thank the many friends and colleagues I am lucky to have in the Müller-Plathe group. Over the years, I have met so many amazing people and bright scientists there, and I sincerely miss our discussions about cultural peculiarities, world politics, science, and everything in between. Among them, I am especially grateful to Gustavo, Yash, and Tobias for their support in all kind of IT-related crises. I also want to thank my former students Melissa, Han, Leo, and Simon for their contributions to my work. Even though it might not be my achievement, I am proud of how many of you stayed to become colleagues.

I cannot imagine the time at TU Darmstadt without the friends I made along the way. I am deeply grateful for all the good times we had and for reminding me that university life is not only about studying. I am yet especially indebted to Sonja, Viktor, Jasmin, and Tobias for somehow motivating me to show up for Sunday morning learning sessions every now and then.
My last and deepest gratitude goes out to my old group of friends, my family, and of course Ines. Despite me not reaching out for weeks, canceling meetings, and working evenings and weekends, I could always trust that you had my back and would cheer me up when I needed it most. Thank you.

Die vorliegende Dissertation wurde der unter Leitung von Herrn Prof. Dr. Florian Müller-Plathe in der Zeit vom 01. August 2017 bis zum 31. Januar 2021 im Fachbereich Chemie der Technischen Universität Darmstadt durchgeführt.

Teile dieser Arbeit sind bereits veröffentlicht:

J. Schneider, L. D. Süss, F. Müller-Plathe, *The Influence of Entanglements on the Dynamics of Flash Nanoprecipitation: A Slip-Spring Dissipative-Particle-Dynamics Investigation*, J. Chem. Eng. Data **65**, 1264-1272 (2020).

J. Schneider, M. K. Meinel, H. Dittmar, F. Müller-Plathe, *Different Stages of Polymer-Chain Collapse Following Solvent Quenching – Scaling Relations from Dissipative Particle Dynamics Simulations*, Macromolecules **53**, 8889-8900 (2020).

J. Schneider, F. Fleck, H. A. Karimi-Varzaneh, F. Müller-Plathe, *Simulation of Elastomers by Slip-Spring Dissipative Particle Dynamics*, Macromolecules **54**, 5155-5166 (2021).

In dieser Dissertation nicht enthalten, aber im gleichen Zeitraum und Kontext entstanden sind:

J. Schneider, A. Z. Panagiotopoulos, F. Müller-Plathe, *Polymer Chain Collapse upon Rapid Solvent Exchange: Slip-Spring Dissipative Particle Dynamics Simulations with an Explicit-Solvent Model*, J. Phys. Chem. C **121**, 27664-27673 (2017).

Z. Wu, S. A. N. Alberti, J. Schneider, F. Müller-Plathe, *Knotting Behaviour of Polymer Chains in the Melt State for Soft-Core Models with and without Slip-Springs*, J. Phys.: Condens. Matter **33**, 244001 (2021).

S. A. N. Alberti, J. Schneider, F. Müller-Plathe, *Mobility of Polymer Melts in a Regular Array of Carbon Nanotubes*, Macromolecules, in revision (2021).

Von dieser Dissertation unabhängig veröffentlicht oder eingereicht wurden:

M. Jäger, J. Schneider, R. Schäfer, *Size- and Charge-Dependent Optoelectronic Properties of CdSe Clusters: Evolution of the Optical Gap from Molecular to Bulk Behavior*, J. Phys. Chem. A **124**, 185-196 (2020).

T. Zhou, J. Schneider, Z. Wu, F. Müller-Plathe, *The Compatibilization Efficiency of Additives in Homopolymer Blends: A Dissipative Particle Dynamics Study*, Macromolecules, in revision (2021).

Zusammenfassung

Eine vollständige Betrachtung der Bewegung und Relaxation weicher Materie, wie beispielsweise von Polymerschmelzen, -lösungen und -netzwerken, reicht von der quantenmechanischen Beschreibung von Bindungsfluktuationen bis zu den makroskopischen viskosen Moden von Elastomeren. Die gleichzeitige Simulation aller Eigenschaften ist unmöglich, sodass drastische Vereinfachungen vorgenommen werden müssen. Beispiele hierfür sind die Betrachtung von Atomen als starre Objekte und die Zusammenfassung mehrere Atome, Monomere oder Kettensegmente zu Superatomen, sogenannten *beads*. Eine generische, chemisch unspezifische Polymerkette kann durch eine Reihe von mit Federn verbundenen *beads* in einer vergröberten, mesoskaligen Darstellung modelliert werden. Diese mesoskalige Kette verliert Aspekte der physikalischen Beschreibung ihres detaillierteren Stammmodells. Das resultierende, unphysikalische Verhalten kann korrigiert werden, indem andersskalige Eigenschaften artifiziell in das Modell eingeführt werden. Eine der dazu fähigen Multiskalenmethoden ist die hier vorgestellte *Slip-Spring Dissipative-Particle-Dynamics*-Methode.
Die mesoskalige *Dissipative-Particle-Dynamics*-Methode erlaubt eine Beschreibung von Polymeren durch ein einfaches Kugel-Feder-Modell. Die Wechselwirkungen der *beads* sind schwach repulsiv. Durch die weichen Potentiale können sich mehrere *beads* am selben Ort aufhalten, was ein Durchkreuzen verschiedener Polymerketten ermöglicht. In realen Polymerschmelzen sind die Moleküle durch ihre Nachbarketten eingeschränkt, wobei die topologischen Begrenzungen einen schlauchartigen Freiraum bilden. Die Translationsfreiheitsgrade der Polymerkette werden auf eine kriechende, „reptierende“ Bewegung entlang ihrer Hauptachse reduziert. In konventionellen *Dissipative-Particle-Dynamics*-Simulationen wird dieses Verhalten nicht beobachtet, da die Kette seitlich aus ihrer Begrenzung entweicht. Um die physikalisch korrekte Dynamik wieder herzustellen, muss diese laterale Bewegung eingeschränkt werden. Eine Möglichkeit hierzu bieten artifizielle, entlang der Kette mobile Bindungen, sogenannte *slip springs*. Die vor einigen Jahren vorgestellte *Slip-Spring Dissipative-Particle-Dynamics*-Methode wurde erfolgreich zur Untersuchung von Polymerschmelzen und -lösungen eingesetzt. In dieser Arbeit erfolgt eine Erweiterung auf andere Systeme, in denen eine entscheidende Rolle topologischer Wechselwirkungen erwartet wird. Die korrekte Anwendung der *Slip-Spring Dissipative-Particle-Dynamics*-Methode ermöglicht zudem Einblicke in die Rolle von Verschlaufungen in solchen Systemen.

Ein erstes Ziel ist die Anwendung der *Slip-Spring Dissipative-Particle-Dynamics*-Methode zur Modellierung von Blitznanofällung. Diese experimentelle Technik zur Herstellung von Nanopartikeln basiert auf dem schnellen Mischen einer Polymerlösung mit einem Nichtlösungsmittel. Durch die Durchmischung kommt es zum Kollaps der Polymerketten und der Fällung der Polymerlösung. In dieser Arbeit werden zwei Studien vorgestellt, die den Kollapse einer einzelnen, isolierten Kette und die Fällung einer Polymerlösung untersuchen.
In der ersten Studie wird eine einzelne, lange Kette aus einem gelösten in einen ungelösten Zustand

gequencht. Bei der Untersuchung der Kollapstrajektorie werden drei Stufen identifiziert: zunächst kollabiert die Kette in Tröpfchen entlang ihrer ursprünglichen Ausdehnung. Diese Tröpfchen werden durch überschüssige Polymer-*beads* verbunden. Anschließend werden letztere von den Tröpfchen absorbiert, bis das Molekül die Form einer Perlenkette annimmt. Drittens kollabiert der bis dahin undeformierte Hauptstrang der Kette. Für jede der Stufen wird eine charakteristische Skalierung mit der Kettenlänge identifiziert, die sich, ebenso wie die Kollapstrajektorie, in hervorragender Übereinstimmung mit einem literaturbekannten theoretischen Modell befindet. Gefundene Diskrepanzen können leicht durch das Zusammenwirken verschiedener dissipativer Mechanismen erklärt werden.
Im Fall der Polymerfällung wechselwirken die kollabierenden Ketten miteinander und bilden eine netzwerkartige Struktur, in der die Tropfen von stark gestreckten Ketten verknüpft werden. Der Fällungsweg wird unter der Arbeitshypothese untersucht, dass die Stabilität dieser Struktur durch eine unterschiedliche Anzahl an *slip springs* beeinflussbar ist, sofern topologische Wechselwirkungen eine Rolle spielen. Durch das schnelle Auflösen des zwischenzeitigen Netzwerkes in räumlich getrennte Nanopartikel ohne Einfluss der *slip springs* kann diese Hypothese jedoch nicht bestätigt werden.

In einer dritten Studie wird die *Slip-Spring Dissipative-Particle-Dynamics*-Methode zur Untersuchung der topologischen Wechselwirkungen in Elastomeren erweitert. Hier wird eine Wiederherstellung der topologischen Effekte benachbarter Netzwerkstänge durch *slip springs* beobachtet. Die resultierende Änderung des Beitrags von Verschlaufungen zum Schermodul der untersuchten Netzwerke ist in hervorragender Übereinstimmung mit Referenzsimulationen. Darüber hinaus können die dynamischen Speicher- und Verlustmodule von experimentellen Polyisopren-Kautschuken durch Quervernetzung einer Polymerschmelze vorhergesagt werden, deren Parameter zuvor für die Simulation von (unvernetztem) Polyisopren optimiert wurden. Diese erfolgreiche Erweiterung der Methode auf Netzwerke ermöglicht zukünftige Untersuchungen von Systemen von großem wissenschaftlichen und industriellen Interesse, wie beispielsweise von Netzwerkdefekten und gefüllte Elastomeren.

Abstract

A full inspection of the motion and relaxation of soft matter systems, such as polymer melts, solutions, and networks, spans from the quantum mechanical derivation of bond fluctuations to the macroscopic viscous modes of rubbers. The simulation of all properties at once is impossible, and crucial simplifications have to be made. For example, atoms can be viewed as rigid objects, and multiple atoms, monomers, or chain segments can be displayed by a single “bead”. A generic polymer chain, stripped of its chemical details, might be modeled by a number of beads that are connected by springs, in a so-called coarse-grained, mesoscale description. This mesoscale chain does no longer obey all physical laws of its more detailed parent model, and they must be reintroduced as artifacts from a different scale. One of the multiscale methods capable of doing so is the slip-spring dissipative-particle-dynamics method presented here.
Dissipative particle dynamics is a mesoscale method that allows a description of polymers by a simple bead-and-spring model. The interactions of beads are repulsive and soft, so that multiple beads can occupy the same point in space, and chains can pass through each other. In a real system, a polymer chain in a melt can be imagined as being confined in a tube by its neighboring chains. Its translational degrees of freedom are reduced to a creeping, “reptating” motion along its main axis. In regular dissipative-particle-dynamics simulations, this behavior is no longer obeyed, and the chain can escape its tube in a lateral motion. Restoring the correct physics means to confine this motion, which is done by slip springs, that is, artificial, mobile bonds that travel along the chain by their own dynamics. The slip-spring dissipative-particle-dynamics method has been proposed some years ago and was successfully applied to study polymer melts and solutions. Here, it is extended to further systems where a crucial role of topological interactions is anticipated. By correctly applying the slip-spring dissipative-particle-dynamics method, the role of entanglements in these systems can be studied.

A first objective is to model flash nanoprecipitation by slip-spring dissipative particle dynamics. Flash nanoprecipitation is an experimental technique to produce nanoparticles based on the rapid mixing of a polymer solution with a nonsolvent. As solvent and nonsolvent mix, polymer chains collapse, and the polymer solution precipitates. Here, two studies are presented that investigate the collapse pathway of a single, isolated chain, and the precipitation of a polymer solution.
In the first study, a single, long chain is quenched from solvent into nonsolvent conditions. The collapse pathway exhibits three stages: first, the chain collapses into blobs along its backbone, which are initially connected by bridges of slack polymer. Second, the bridges are absorbed by the blobs, until the chain resembles a pearl necklace. Third, the so-far undeformed chain backbone collapses. For each of the collapse stages, a characteristic scaling with the chain length is identified. Both the collapse pathway as well as the scaling are in excellent agreement with a theoretical model, and discrepancies can be readily explained by the mergence of different dissipative mechanisms.
In the case of precipitating polymer solutions, the collapsing chains interact with each other and form a

network-like structure, where blobs are spanned by highly stretched chains. The study's working hypothesis is that the stability of this intermediate structure would be altered by varying numbers of slip springs if topological interactions played a role. However, no influence of slip springs is found, and the intermediate network structure quickly dissolves into spatially separated nanoparticles.

In a third study, the slip-spring dissipative-particle-dynamics method is extended to study the topological interactions of elastomers. In these network structures, slip springs successfully recover the topological effects of neighboring network strands. The resulting change in the entanglement contribution to the shear modulus of the inspected networks is in excellent agreement with reference simulations. Moreover, the dynamic storage- and loss moduli of experimental polyisoprene rubbers can be predicted by cross-linking a polymer melt mapped onto polyisoprene. The successful extension of the slip-spring dissipative-particle-dynamics method to networks will allow future investigations of systems of scientific and industrial interest, such as network defects and filled elastomers.

Contents

1 Introduction **1**

2 Problems Addressed in this Thesis **9**
2.1 Objective 9
2.2 Application to Elastomers 9
2.3 Application to Single-Chain Collapse and Flash Nanoprecipitation 10
2.4 Structure of this Thesis 11

3 The Slip-Spring Dissipative-Particle-Dynamics Method **13**
3.1 Implementation of Slip-Spring Dynamics 13
3.2 Choice of Parameters 15
3.3 Further Development of Slip-Spring DPD in this Thesis 16

4 Results **17**
4.1 Different Stages of Polymer-Chain Collapse Following Solvent Quenching 17
4.2 The Influence of Entanglements on the Dynamics of Flash Nanoprecipitation 29
4.3 Simulation of Elastomers by Slip-Spring Dissipative Particle Dynamics 39

5 Conclusion and Outlook **51**

References to Chapters 1–3 and 5 **55**

Appendix **xi**

1 Introduction

Simulation of polymeric systems is one out of many research areas that have immensely benefited from the progresses made in computational power over the last years. By now, they have the ability to act as an "*in silico*" addition – or alternative – to *in vitro* experiments[1]. Other contributions to this success are the recent improvements in simulation software and algorithms[1]. The latter are necessary for the same reasons that draw interest to these soft-matter systems: while the chemistry of polymers might be dominated by interactions on the ångström and sub-picosecond scale, properties of the whole chain are described on scales of $10 - 100$ nanometers and seconds[2]. Thus, a certain resolution must be chosen for the simulation of soft-matter systems. This simplification is achieved by coarse-graining, a technique which focuses on a specific scale of interest, while details of lower scales are discarded[3]. A polymer could be described by an atomistic model, a united atom model with one bead per monomer (mildly coarse-grained), a bead-spring model with multiple monomers or Kuhn segments per bead (mesoscopic), or a single bead or volume element (super-coarse-grained and continuum models)[2, 3]. Coarse-grained models can be obtained by matching specific quantities from fine-grained simulations in bottom-up approaches[4]. On the other hand, generic mesoscopic models are employed to study the universal behavior and physics of polymer chains[1]. However, the separation of scales is usually challenging or impossible, which motivated the use of multi-scale simulation methods. They are a class of methods that combine different resolutions, or reintroduce effects of one scale into a simulation on a different scale[5]. Here, the extension of the mesoscopic dissipative-particle-dynamics method to incorporate effects based on atomistic chain-uncrossability is presented.

The **dissipative-particle-dynamics simulation technique** (DPD) was firstly proposed by Hoogerbrugge and Koelman[6] in 1992 as one of several "physicist intuitive, quick and dirty"[7] approaches. The present-day standard model was completed after a revision of Español and Warren[8] and the addition of a velocity-Verlet integration algorithm by Groot and Warren[9] in 1997. The DPD force consists of conservative, dissipative, and random contributions. In the standard model, the conservative potential is described by a soft, linearly repulsive force. The dissipative or drag force incorporates a friction coefficient weighted by the relative velocity between two particles. It is counteracted by a pairwise random force accounting for stochastic collisions with surrounding particles. If the noise level of this random contribution is sufficiently linked to the friction coefficient, DPD samples the canonical ensemble[8]. All DPD interactions are pairwise and hydrodynamics is explicitly accounted for. In their simplest representation, bonds are modeled by a harmonic spring with an equilibrium length of zero, which is added upon the nonbonded potential of bonded beads[9].

In a recent perspective, Español and Warren[7] highlighted that there is no universal answer as to what a dissipative particle represents. For example, Spaeth *et al.*[10] simulated an aqueous solution of diblock copolymers where equally-sized DPD beads represented 11 water molecules, 2 polystyrene monomers, and 3.4 polyethylene glycol monomers. Further up the coarse-graining spectrum, a DPD bead could also mean

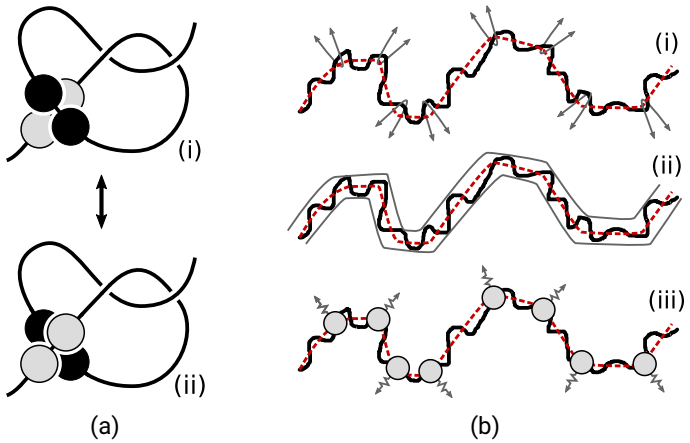

Figure 1: Consequences of the absence of topological interactions in polymer models and methods to restore their influence on the chain dynamics. **(a)** In hard-core models, dissolving of knotted or self-entangled polymers ((i)) into an unknotted state ((ii)) requires diffusion of a chain end trough the "loop", which happens on the time scale of chain diffusion. Soft-core chain dynamics allow bond crossing and thus bring the knotted-to-unknotted transition to the scale of monomer diffusion. **(b)** In melts of long chains, a single chain is confined by neighboring chains hooked and entwined with it ((i), gray arrows). Tube models ((ii)) describe this entanglement effect as the confinement of a single chain by a parabolic potential orthogonal to the chain's primitive path (red line). In slip-spring models ((iii)), the tube is replaced by additional bonds ((iii), depicted as springs) which attach a number of chain segments to the background (single-chain models) or surrounding chains (multi-chain models).

a glassy domain in a filled rubber[11] or a chain of 800 carbon atoms[12]. A reason for the versatility of the mesoscopic DPD method is that it can be approached from the atomistic and continuum scale alike. Bottom-up parametrization of DPD uses atomistic simulations to map groups of atoms into DPD beads. The conservative and friction forces can, for example, be parameterized from the parent simulation's potential of mean force[13, 14]. Top-down approaches, such as smoothed DPD[15] and many-body DPD[16], aim to discretize continuum models to obtain dissipative particles from volume elements. A summary of these and more specialized recent advances can be found in the review by Español and Warren[7].
The standard bead-spring DPD model, on the other hand, is nowadays sometimes considered a "toy model"[7]. It is yet, despite its simplistic approach, obeying all dynamic and static scaling laws of unentangled linear and star polymers in melts and solutions[17–19]. Bead-spring DPD thus remains a popular tool to study generic soft-matter systems, with a special focus on scaling relations and universal behavior[1].

The coarse nature of mesoscopic DPD models, which commonly merge multiple monomers into a single bead, introduces a number of shortcomings. Besides the high compressibility and the loss of chemical detail, the soft-core model is unable to reproduce physical torsional and **topological constraints between beads**[1]. A simple consequence is outlined in Figure 1a: to dissolve an overhand knot, or "self-entanglement", in a long polymer chain in a physical way, one chain end has to pass through the loop constructed by the remainder of the chain. The knotted-to-unknotted transition time is associated with the center-of-mass diffusion of a larger chain segment. In contrast, the reduced (or fully neglected) topological constraints of soft-core models cannot prevent chain crossing. The transition time is thus accelerated to the scale of single-bead diffusion[20]. While knots are likely of minor importance for the physical properties of polymer chains[21], more severe issues arise when neglecting topological interactions between multiple, long chains. Figure 1b(i) illustrates a single chain in a polymer melt. The chain is entangled with the surrounding chains,

which are hooked around its backbone (gray arrows). The confinement arising from these topological interactions is commonly visualized as a tube in which the chain is moving (Figure 1b(ii))[22, 23]. The environment thus restricts the lateral motion of the chain, which can only translate ("reptate") along the tube. Provided that all chains are above a critical length, their entangled dynamics is significantly slower than that of unrestricted chains.* While the tube model is discussed in more detail below, it is evident that the standard, soft-core DPD model can *not* capture its effects due to the weak topological interactions[17, 18]. Instead, DPD chains follow unentangled Rouse dynamics irrespective of their length[17]. DPD is thus unable to sample the physically correct dynamics of entangled chains.

The inability to correctly sample topological effects, especially those related to entanglements, is common among strongly coarse-grained models due to their necessarily soft potentials[3]. Over the last 20 years, different approaches were developed to explicitly reintroduce chain uncrossability, mostly by monitoring the bond-bond distances[24]: in 2001, Padding and Briels[25] introduced the elastic-band method for mesoscopic simulations of polyethylene. As soon as their algorithm detected the crossing of two bonds, they were replaced by elastic bands, slowing down their relative motion and eventually preventing bond crossing. Despite the complicated implementation and the additional computational burden, Padding and Briels successfully studied the scaling behavior of polyethylene chains of up to 500 monomers mapped into 50 beads[26]. For their systems in equilibrium and under a planar flow, their diffusion coefficients scaled according to the reptation theory, and their shear viscosity, tube diameter and other entanglement-related rheological properties matched experimental reference systems[26, 27]. A segmental repulsive potential (SRP) approach was proposed by Kumar and Larson[28], who added a Lennard-Jones potential between bonds to enforce segmental repulsion for their Brownian-dynamics system. Multiple authors[29, 30] adapted this approach into DPD by replacing the Lennard-Jones potential with the conservative DPD interaction. These studies were able to reproduce the onset of entanglements[29] as well as the scaling of the diffusion coefficient[30] shown by entangled experimental polymer melts. However, the conformation of short chains showed deviations from the Rouse model due to the artificial chain stiffness. This was later adjusted in a parameterized SRP by Goujon *et al.*[31], which was successfully used to study the friction and viscosity of sheared linear chains[32] and polymer brushes[33]. Other approaches to restore the conformational behavior of undisturbed DPD chains included the change of the segmental distance criterion[34] and the implementation of multi-point interactions[35]. As an alternative to SRPs, changes in the conservative DPD potential have been evaluated to make DPD beads hard-core[36] or avoid bond-crossing by a suitable combination of strongly repulsive conservative interactions and stiff chains[37, 38]. A disadvantage of hard-core repulsion is, however, the limitation to small time steps. Despite some attempts to improve their efficiency[39], none of the approaches to explicitly avoid bond crossing maintains the speed of the original DPD method. While they might offer interesting reference systems, an alternative is the implicit incorporation of uncrossability effects commonly found in mesoscopic models. Here, the focus shifts from the conservation of topological entanglements to the restoration of their characteristic dynamics.

Even though the subject of topological interactions in soft matter is usually discussed in the framework of polymer melts and dense solutions, some of the most prominent approaches are based on, or co-developed for, **models of rubber elasticity**. Early attempts to theoretically describe the elastic properties of elastomers,

*Note that the observation of entangled dynamics is indeed the common definition of entangled matter[24]. An entangled system is thus not defined by the existence or absence of hooked and entwined chains, but rather by how strongly this affects their dynamics. In the scope of this introduction, however, the term "entangled" is used equivalently to "hooked" and "entwined".

or rubbery networks, assumed unentangled, non-interacting “phantom” strands that are spanned between network junctions, that is, cross-links. In the affine network model[40–44], these junctions are assumed to displace affinely with the background upon deformation, so that any strand would experience the same strain as the macroscopic rubber. In contrast, the phantom network model[45–49] assumes fully fluctuating network strands and junctions. Here, only the macroscopic “edges” of the network are affinely displacing with the elastic background. The affine and phantom network models differ in how strongly the experienced stress is coupled to the inflicted strain, and were thus thought to define the upper and lower limits of a network’s shear modulus[50]. It was soon realized that the stress-strain relations observed in experimental systems could not be understood without consideration of topological interactions[51]: first, the shear modulus of weakly cross-linked networks exceeds the affine prediction. Second, the stress-strain coupling is overestimated upon deformation. Both observations can only be explained by topological interactions of long network strands, which add an additional, strain-dependent contribution to the shear modulus. In 1975, Ronca and Allegra suggested the constrained-junction model[52–56], where all junctions are pinned to the elastic background by virtual springs. These springs effectively act as a confining potential and are additionally modeled to be strain-dependent to account for strain thinning. In a slightly different approach, Edwards and co-workers[57, 58] considered the confinement to be constructed by so-called slip links between network strands: in their first slip-link model, a link connecting two strands can slide along them but cannot cross network junctions. The slip-link model is able to predict both strain thinning and a joint contribution of cross-links and slip links to the shear modulus. It was later shown that the slip-link and constrained-junction models can be related by their constraint and slippage parameters[59]. Combining the approaches of constrained strands and junctions with the upcoming understanding of entanglement-induced reptation by early tube models[22, 23, 60, 61], Edwards and Vilgis reviewed the tube model of rubber elasticity in 1988[62]. They assumed the constraints to not only act upon network junctions or some selected monomers, but on every monomer in any network strand. The resulting confining potential can be expressed in terms of virtual springs attached to any monomer and the elastic background; however, the more prominent description is that of a confining tube. Here, entanglements with their environment restrict the fluctuations of network strands in the same way as a parabolic lateral potential. This tube is characterized by its diameter and the so-called entanglement length, which is the shortest strand length necessary to experience entanglements.

While being able to describe the experimentally observed entanglement contribution to the shear modulus in equilibrium, the original tube model fails for strained networks due to its strain-independent tube diameter. Consequently, Rubinstein and Panyukov corrected this affine tube deformation in their non-affine tube model[63]. In this combination of the constrained-junction model and Edwards tube model, the monomers are attached to the elastic background by virtual chains with a strain-dependent potential. This effectively introduces an affine change of the tube diameter with the background. In a further extension, the same authors replaced the junctions between virtual chains and monomers by slip links[64]. This non-affine slip-tube model combines the tube model with the concept of slip links. There are further extensions to the non-affine tube model, such as the extended tube model[65] or the non-affine network model[66]; however, the non-affine slip-tube model captures the entanglement behavior of networks well enough to remain one of the standard tools to extract cross-link and entanglement contributions in accurate fits to experimental[64] and computational[67] results. Lastly, it has to be mentioned that these theories only discuss elastically active network strands. The contribution of network defects, such as loops or dangling

ends, are debated in a still growing number of network theories, some of which were recently reviewed by Danielsen *et al.*[68].

Melts or solutions of long polymer chains, cross-linked or not, are viscoelastic materials. The similarity of cross-linked elastomers and the "entanglement network" in **dense soft matter systems** has been understood very early[22]. The tube model for polymer melts is based on the initial works of Edwards[22], de Gennes[23], and Doi and Edwards[60, 61]. They all share the same single-chain description of a polymer confined into a tube by a mean field. While this is very similar to the confinement experienced by network strands, a free polymer chain can escape its tube by creeping ("reptating") out of it, a single relaxation process with a characteristic disentanglement time. More elaborated tube models know additional relaxation mechanisms: for example, the so-called contour-length fluctuation describes a contraction and expansion of the chain in its tube. This affects the tube length and effectively reduces the disentanglement time[69]. Another relaxation mechanism is constraint-release: here, the chain can additionally relax due to the relaxation of the chains framing its confinement, which challenges the original thought of a fixed environment. While contour-length fluctuations are relatively well-established in modern tube models[70], different competing models for constraint-release dynamics exist. A detailed discussion of different approaches addressing more complex dynamics, including those of star polymers, polydisperse chains, and systems under a shear flow, is given by Masubuchi[24]. It has to be noted that some of these models, such as the Likhtman-McLeish theory[71], became established tools to access rheological parameters from respective experimental data. However, generally speaking, single-chain models such as the tube model struggle to incorporate multi-chain effects such as constraint-release dynamics by implication.

As an alternative representation of tube models, the concept of slip links was developed for melts and elastomers alike[72]. In a first slip-link approach, Doi and Edwards[73] replaced the tube by a number of fixed rings. Reptation was described by the one-dimensional motion of chains through them. In 1998, Hua and Schieber[74] proposed a more elaborate model for an ensemble of multiple, non-interacting chains. Here, slip links can be created in space if a terminal chain segment beyond the last slip link exceeds a critical length. Accordingly, slip links are destroyed once the last chain segment reptates through them. In addition, a second, randomly chosen slip link is destroyed as well if it is older than the original one. Chains thus experience a disintegration of their tubes due to reptation in their environment, a mechanism meant to introduce constraint-release dynamics. Doi and co-workers[75, 76] further refined this mechanism by coupling not random, but permanently paired links that were created and destroyed together. Their model also explicitly allows contour-length fluctuations. All of these concepts consider slip links as immobile rings pinned onto the background. A model allowing thermal fluctuations of slip links was proposed by Masubuchi *et al.*[77]. They also added a structural aspect by requiring a pair of coupled slip links to share a spatial position; a pair of formally entangled chains thus has to be spatially close. Masubuchi *et al.* simulated the chains of their resulting "primitive chain network" (PCN) by Brownian dynamics. Their model is considered an important connection between the realms of molecular simulations and slip-link models. The PCN model is capable of reproducing linear and nonlinear rheological properties for a variety of soft-matter systems, some of which can be found in the review of Masubuchi[24]. An extension for elastomeric networks was, for example, realized by Oberdisse *et al.*[78]. This list of slip-link models is far from complete, and some, including the PCN model, are still subject of recent research[79, 80]. As an example, a hierarchical model employing Schieber's discrete slip-link theory was recently reported to

predict rheological properties from first principles[81]. In the scope of this work, slip links do, however, only serve as a forerunner for the family of slip-spring models.
The first slip-spring model was proposed by Likhtman in 2005[82]. It can be viewed as an extension of the slip-link model of Doi and Takimoto[76] but introduces a novel description of the links: inspired by the slip-tube network models of Rubinstein and Panyukov[63, 64], links are not affinely attached to the background but connected by a phantom chain, represented by a single spring. The links thus have a certain spatial mobility. Likhtman additionally modeled the chain beads explicitly and allowed them to move in a three-dimensional, Brownian fashion; the chains can thus show Rouse motion below the entanglement level on top of the automatically considered reptation and contour-length fluctuations. Figure 1b schematically compares the slip-spring model ((iii)) to the microscopic picture ((i)) and the tube model ((ii)): if the virtual springs in (iii) are not connected to the background but to different chains, an extension to a multi-chain model is straightforward.

Indeed, Likhtman's single-chain slip-spring model inspired the development of different **multi-chain slip-spring** (MC-SS) approaches. The following sections are meant to introduce them and give an overview over their different characteristic features and key applications. The existing MC-SS models choose from a number of ingredients, some of which are interchangeable, some mutually exclusive. The advantages and disadvantages of, for example, different slip-spring ensembles will be discussed later.
The first MC-SS models were published – independently and within a scope of two weeks – by Chappa *et al.*[83] and Uneyama and Masubuchi[84]. Both models aim to utilize Likhtman's slip-spring model to address shortcomings of the PCN model, among them the connection of slip links to the background and the insufficient modeling of chain segments below the entanglement level. They also consider a fluctuating number of slip springs to emulate entanglements, controlled in a grand-canonical way by a predefined activity coefficient. Here, slip springs are mobile bonds that connect two beads on either different or the same chain and migrate along the polymer chains by a series of discrete hopping moves. Both the grand-canonical description and the discrete hopping motion were inherited from earlier single-chain models[85, 86]. The model of Chappa *et al.*[83] implements slip springs in a classical DPD simulation to model the motion of chain beads. At every simulation step, their algorithm chooses between a short sequence of DPD steps, where slip springs remain stationary, or a Monte-Carlo move of the slip springs. The slip-spring moves are either a migration move, or, if slip springs populate a chain end, a destruction or relocation to a different end. Similarly, slip springs can be created at chain ends. In contrast, the model of Uneyama and Masubuchi[84] is based on a free-energy description of Rouse chains incorporating terms for bonded, slip-spring, and nonbonded interactions. The chain motion is governed by Brownian dynamics. The probabilities for hopping, creation, and destruction moves are not fixed but connected to the resulting changes in the system's free energy. Both models were found to reliably reproduce the dynamics and linear rheology of hard-core models. Chappa *et al.* also probed the nonlinear rheology of their chains under a shear flow, which yielded a depletion of entanglements and shear thinning. In a second study, Masubuchi[87] reported similar findings for their system, such as a correct shear-rate dependence of the viscosity.
Shortly after the publication of the original model, Langeloth *et al.*[88] proposed a DPD version of Uneyama's and Masubuchi's model. This model uses some simplifications meant to ease the understanding of the effect of the artificial slip springs: for instance, the number of slip springs is kept constant, and the motion of DPD

beads and slip springs is separated into different blocks called with a pre-defined frequency. Details on this model are given in chapter 3. Langeloth's DPD model was, despite its simplicity, successful in reproducing reptation dynamics and linear rheology. Langeloth *et al.*[89] and Nikoubashman *et al.*[90] also showed its applicability to describe constraint-release dynamics in bidisperse melts and shear thinning. Masubuchi *et al.*[91] used a related model to simulate dense polymer solutions, a system that naturally suits DPD due to its explicit incorporation of hydrodynamic interactions.
In all these approaches, intermolecular interactions between chains are either fully neglected or only governed by comparatively weak DPD interactions. In order to simulate systems with a reasonable compressibility, Ramírez-Hernández *et al.*[92, 93] developed the so-called theoretically informed entangled polymer simulation (TIEPOS) method in a series of papers. This method is based on the theoretically informed coarse-grained model[94], which describes ideal Rouse chains with intermolecular interactions based on a compressibility and a Flory-Huggins interaction parameter. In the TIEPOS method[92, 93], Ramírez-Hernández *et al.* additionally use slip springs to restore reptation dynamics. In contrast to other MC-SS models, their slip springs are interacting by a repulsive potential. Over the years, Ramírez-Hernández *et al.* made their model fit to study inhomogeneous systems such as thin copolymer films by exchanging the canonical treatment of slip springs for a grand-canonical one[95]. In a second step, they adjusted the probability of slip-spring creation to not only consider an activity coefficient, but also the local environment of the chain ends in question[96]. The TIEPOS model was applied to, for example, show a depletion of slip springs on the interface of microstructured melts of diblock-copolymers[97].

In 2017, MC-SS methods already provided a powerful tool to efficiently perform physically consistent mesoscale simulations of large, computationally demanding systems. Since then, further efforts were directed towards the development of new simulation methods, the application to new systems, and the elaboration of well-defined parameters to allow a linkage to the microscale, which is a crucial step for hierarchical models. Masubuchi extended his MC-SS model by a hierarchical relaxation mechanism to study branched polymers[98]. Together with Uneyama, he also used their method to model both linear and branched polyisoprene melts[99] and study the kinetics of network formation by adding an end-linking reaction mechanism[100]. The same authors compared their MC-SS and PCN models to reference hard-core systems in equilibrium[101] and under a strong shear flow[102]. They found the results of all simulations to be transferable by conversion of time, length, and the number of segments per bead. In a later study, Masubuchi *et al.*[103] reported a similar transferability between MC-SS simulations with different slip-spring densities, a strong indicator that these coarse-grained models allow an arbitrary choice of slip-spring numbers or activities. Very recently, Uneyama[104] paired their MC-SS scheme with the responsive-particle-dynamics model of Kindt and Briels[12]. The latter is a successful coarse-grained model were polymer chains are reduced to single beads, and entanglements are modeled by transient bonds between them based on their distance. Uneyama showed that these transient bonds can be replaced by a fluctuating number of slip springs governed by a simplified version of the MC-SS algorithm. In a first study, Uneyama applied this extremely fast transient bond method to a melt of ideal gas particles, that nonetheless were entangled by slip springs. While the model fails to reproduce the diffusive behavior of actual polymer melts, the chain-length dependence of the shear modulus is met surprisingly well.
The DPD model of Chappa *et al.*[83] was recently utilized in an attempt to hierarchically model polybutadiene melts: in a study of Behbahani *et al.*[105], it was used to describe 12 monomers per DPD bead. The parameters

of this model were chosen to reproduce the viscoelastic properties of moderately coarse-grained systems with one monomer per bead, which itself was derived from atomistic simulations by bottom-up coarse-graining.

At the same time, two new MC-SS models based on particle-field methods were introduced. Theodorou and co-workers[106, 107] presented a highly coarse-grained particle-field method where beads comprise up to 50 monomers. Their method employs a well-defined equation of state derived by bottom-up coarse-graining. Nonbonded interactions are computed as a functional of the local density and communicated on a grid, and beads are governed by a Brownian-dynamics (BD) equation of motion. The soft-core interactions are compensated by either a fixed[106] or fluctuating[107] number of slip springs, whose dynamics follow a kinetic Monte Carlo (kMC) scheme adopted from Chappa *et al.*[83]. The authors aimed to derive all parameters from an atomistic parent model. Successful applications of this kMC/BD model include linear melts of polyisoprene[106], polyethylene[107], and polyisoprene rubber networks[108]. Later, Sgouros *et al.* paired the equation-of-state model with a square-gradient theory to allow studies of the depletion of slip springs on liquid-gas[109] and solid-liquid[110] interfaces. In a similar approach, Wu *et al.*[111] extended the hybrid particle-field (hPF) simulation method by slip springs. The original hPF model[112] simulates atomistic or coarse-grained chains which explicitly consider bonded interactions, while non-bonded interactions are modeled through a density-functional field of a variable resolution. Combined with the slip-spring model of Langeloth *et al.*[88], Wu *et al.* were able to efficiently reproduce the behavior of polyethylene melts where the model resolution could be changed at will. In a second publication, Wu *et al.*[113] showed that the hPF/SS model is suitable to derive chemically specific coarse-grained simulations where almost all parameters are extracted from atomistic reference systems.

The slip-spring DPD model of Langeloth *et al.* was applied for additional studies in the past years: Wu *et al.* compared the knotting behavior of hPF and DPD simulations with and without slip springs[20]. Consistent with a similar study, they reported that the soft-core models failed to correctly sample the knotting probabilities of a hard-core reference system when applied to flexible chains[114]. Additionally, they showed that the knotting-to-unknotting transition is accelerated towards the time scale of monomer motion for soft-core simulations. As a method to restore the dynamic effects of bond crossing on long time scales without explicitly preventing it, slip springs are not suited to address this issue[20]. Recently, Alberti *et al.* investigated the dynamics of a polymer melt confined by an array of nanotubes using slip-spring DPD[115]. They were able to show that the scaling behavior of temporal properties was surprisingly unaffected by the confinement. Additionally, they described the influence of slip springs on the hopping mechanism of chains through the vicinities between nanotubes.

2 Problems Addressed in this Thesis

2.1 Objective

This thesis exploits a tremendous advantage of slip-spring DPD over other methods: given the access to long time- and length scales while being able to correctly sample polymer dynamics as well as hydrodynamics, it is suited to investigate the dynamic properties of computationally demanding soft-matter systems where topological interactions are expected to play a role. The aim of this thesis is the investigation of such systems by improving the model and algorithm, that before had only been applied to mono- and bidisperse polymer melts and solutions[88, 89, 116], to fit a broader range of applications. Also, the influence of topological interactions, modeled *via* slip springs, in these systems is studied. In the following two sections, the systems chosen for these investigations are described.

2.2 Application to Elastomers

An intuitive application of the slip-spring DPD method are elastomeric networks. Computer simulations became a convenient tool to study these and related systems due to their ability to model networks with well-defined structures[68]. Structural details are usually inaccessible by experiments, which makes the prediction of material properties based on the molecular design a tremendous challenge[117]. Topological interactions between network strands are either of an adjacent or trapped nature. Interactions between unentangled strands decelerate the network dynamics but fully relax under shear stress. Trapped entanglements, on the other hand, appear between hooked strands that are fully cross-linked. Due to their inability to dissolve under shear, they contribute to the network's plateau modulus[118]. Topological interactions thus play a crucial role and are usually explicitly modeled in coarse-grained network simulations: the standard Kremer-Grest model, consisting of hard-core Lennard-Jones beads connected by finitely extensible springs[119], was used for the vast majority of early network simulations[120–129]. Mesoscopic models, in particular DPD, were equipped with either a segmental repulsion potential[130] or excluded volume interactions[131, 132]. However, recent studies still stress the challenge to fully sample the rheology of hard-core systems (for example, their storage and loss moduli), due to high computational costs[133, 134]. Macroscopic properties of rubbers, on the other hand, are strongly affected by network defects such as dangling ends and loops, which can only be modeled by reasonably large systems[133]. The requirements for a computationally efficient method that still incorporates entanglements make elastomeric networks, as well as related systems such as gels, interesting fields for the application of slip-spring DPD. A useful feature of network simulations is the possibility to manipulate repulsive interactions between network strands. This trick has been utilized in the literature to investigate the influence of topological interactions on static

network properties such as the shear modulus[124, 127, 128, 134, 135]. The (at least qualitative) influence of topological interactions on some network properties is thus relatively well understood[134–136], which leaves some reference systems to directly investigate the role of slip springs in comparable systems. The application of slip-spring DPD after necessary changes to the simulation code is documented in section 4.3[137]. Here, an in-depth introduction to elastomeric systems and some results of the successes and shortcomings of their investigation by slip-spring DPD are provided. This study focuses on the method's general applicability but also discusses the ability of slip springs to emulate static and dynamic topological effects by comparing them to hard-core molecular dynamics reference data and experiments.

2.3 Application to Single-Chain Collapse and Flash Nanoprecipitation

As a perhaps less apparent application for slip-spring DPD, the collapse behavior and role of (self-)entanglements in single-chain collapse and flash nanoprecipitation is studied. Flash nanoprecipitation (FNP) is a technique to produce kinetically frozen nanoparticles. Invented in 2003 by Johnson and Prud'homme[138][139], FNP is based on the rapid mixing of a polymer solution with a nonsolvent, which leads to a controlled assembly of the dissolved chains into nanoparticles of well-defined, nearly monodisperse size. Depending on the ingredients, FNP can be used for the controlled production of, for example, microstructured nanoparticles such as patchy[140, 141] or Janus[142] particles. An interesting observation is that nanoparticle dispersions show a long-time stability even if homopolymers without stabilizers are used[143]. Electrostatic[143] and steric repulsion[144] are the most likely explanations for this behavior; however, some open questions remain. For example, the role of topological interactions and (self-)entanglements of the precipitating chains is elusive. Due to its short time- and length scales, only the initial and final states of the precipitation process are experimentally accessible. Understanding of the precipitation dynamics is pursued by computer simulations. As an intuitive starting point for this task, many studies attempted the modeling of single-chain collapse[143, 145], which itself has been a subject of scientific interest for a long time[146].
Single-chain collapse is observed as a result of either thermal or chemical quenching. Different models suggest a varying number of collapse stages, each of which is identified by the scaling of its characteristic time with the chain length. By now, it is relatively well-understood that long, isolated polymer chains follow a so-called pearl-necklace pathway. This picture of Halperin and Goldbart[147] describes a chain quenched into blobs along its primitive path, followed by stretching of the bridges between blobs until the structure resembles a pearl necklace. Finally, the pearl necklace collapses into a globule. The first model of single-chain collapse, however, was given 15 years prior by de Gennes[148]: he suggested a two-stage process where a chain would firstly collapse into an elongated, sausage-like shape, that would later crumple into an equilibrated globule. Grosberg *et al.*[149] adjusted the initial process to a collapse into a fractal globule, and argued that only chains longer than their entanglement length experienced a second stage. Only then could the fractal structure relax in a reptation-like fashion. In an extension to multi-chain systems, Grosberg and Kuznetsov[150] proposed a third stage for chain collisions. The collapse- and precipitation behavior would then depend on the interplay of four relaxation processes: initial single-chain collapse into a fractal globule, formation of self-entanglements (knots), inter-chain aggregation, and inter-chain entanglement formation. The different stages would crucially depend on the time scales of these processes, which itself depended on the chains' concentration and entanglement lengths.

It is, for the reasons sketched above, believed that topological interactions play an important role in the collapse of single chains as well as the process of flash nanoprecipitation[151]. However, different complications have to be dealt with in the simulation of physically sane systems. For instance, the importance of an explicit solvent model (as opposed to considering the solvent implicitly by bead-bead interactions) has been pointed out for a physical modeling[10] and the prevention of trapping in metastable collapse stages[152–155]. Likewise, hydrodynamic interactions should be considered[156]. On the other hand, long-ranged hydrodynamic processes can artificially alter the static and dynamic chain properties, and their prevention requires large simulation cells[157]. Thus, the number of explicitly considered particles can easily reach 10^6 and more, especially for dilute multi-chain systems. These prerequisites can be met by slip-spring DPD, which is utilized here to learn about the applicability of slip springs as well as the general importance of entanglement effects in these systems.

In a first study, we investigated the influence of slip springs on single-chain collapse[158]. Even though some results were obtained during my PhD studies, this work is based on the results of my master thesis and is thus not considered a part of this thesis. Among other findings, we reported the trapping of good solvent in the globular final chain configurations, which confirms the need to use an explicit solvent model. We were, however, not able to find an influence of self-entanglements on the collapse process or the final globular structures. We also reported a smooth, apparently single-staged collapse of $N = 100$ bead chains, but were able to identify intermediate pearl-necklace structures.
Starting from this, our studies progressed in two directions: in section 4.1[159], we discuss the collapse behavior of single chains under explicit-solvent DPD. This study focuses on the description of the collapse pathway, investigated by a specific clustering algorithm. The observed pearl-necklace pathway is consistent with the well-known model of Halperin and Goldbart[147], who also predict scaling coefficients for the characteristic times of the different collapse stages. We study and report, for the first time, the scaling coefficients of all three stages, and relate them to the literature. Even though this study does, for the reasons discussed above, not consider slip springs, it is an excellent example of the applicability of DPD to large systems where hydrodynamic interactions must be considered.
Second, the slip-spring studies of single-chain collapse were extended to a multi-chain system to investigate the influence of slip springs, as an embodiment of entanglements, on the dynamics of flash nanoprecipitation. In section 4.2[160], we present and discuss simulation results for the collapse of a $1\ \%$ solution of polymers of different lengths which precipitate as $50\ \%$ of the solvent particles are replaced by nonsolvent. The systems exhibit an intermediate, network-like stage, where some elongated chains connect others that are already globular. We use different numbers of slip springs as artificial entanglements to study their effect on the stability of this structure.

2.4 Structure of this Thesis

This thesis is constructed as follows: in chapter 3, the slip-spring DPD algorithm is described as introduced by Langeloth *et al.*[88]. My own changes to the code are presented as well as different algorithms utilized in other multi-chain slip-spring models. My publications containing the results of the investigations mentioned above are presented in chapter 4. They are given in a logical rather than the chronological order, starting

with the study on single-chain collapse (section 4.1, ref. [159]). It is followed by the applications of slip-spring DPD to precipitating polymer solutions (section 4.2, ref. [160]) and elastomeric networks (section 4.3, ref. [137]). In chapter 5, a brief summary and conclusion are given, and different applications and improvements of the slip-spring DPD method are suggested for future works.

3 The Slip-Spring Dissipative-Particle-Dynamics Method

This section describes the multichain slip-spring (MC-SS) algorithm developed by Langeloth *et al.*[88]. It is meant to introduce the method and the employed parameters. In the past years, different studies suggested alternative treatments for many key ingredients of MC-SS simulations. Here, an overview over other approaches is given wherever relevant. We do, however, refrain from a detailed comparison or discussion. Some of these alternatives will be discussed to in chapter 5. This chapter focuses on the slip-spring part of the slip-spring dissipative-particle-dynamics (DPD) model. For the DPD equation of motion, we refer to the pioneering work of Groot and Warren[9].

3.1 Implementation of Slip-Spring Dynamics

The MC-SS model of Langeloth *et al.*[88] treats the dynamics of slip springs and DPD beads separately. This allows a separation of the algorithm into sequences. A schematic overview of a simulation of a fictitious system of free polymer chains (light gray) and cross-linked chains (dark gray) is given in Figure 2. Slip springs and cross-links are depicted by red and black springs, respectively. The slip-spring algorithm starts from an *initial configuration* where slip springs connect inter- and intramolecular beads alike (Figure 2a). This is followed by a sequence of DPD bead motion, while slip springs remain fixed and act as additional bonds (or cross-links) between their respective anchors (Figure 2b). After the DPD sequence, the beads remain stationary and slip springs located at a chain end are allowed to perform *relocation moves* to a different chain end and any suitable partner bead (Figure 2c). Lastly, slip springs perform a number of *migration steps* governed by a Metropolis Monte Carlo (MC) criterion, where they attempt discrete hopping moves along their chains (Figure 2d). Migration to cross-linked beads (black beads) is forbidden. The simulation software iterates over (b), (c), and (d) until the sum of DPD sequences equals the desired simulation time. Further details of the sequences are given below.

The **initial insertion of slip springs** at the start of any slip-spring simulation is straightforward. A slip spring is inserted by choosing an anchor from a list of all beads capable of carrying slip springs. The second end is attached to any other suitable bead within a distance between $r_{\min} = 0\ r_c$ and $r_{\max} = 2\ r_c$ to the first one. r_c is the DPD cutoff radius serving as the unit of length. The choice of parameters is reasoned below. This model uses a number of slip springs that is constant at any time; thus all slip springs are inserted until the desired number is reached.

A single **slip-spring relocation** move is attempted by any spring that populates a chain end at the end of a DPD sequence. This move can be thought of as a balanced destruction and reinsertion of slip springs, a

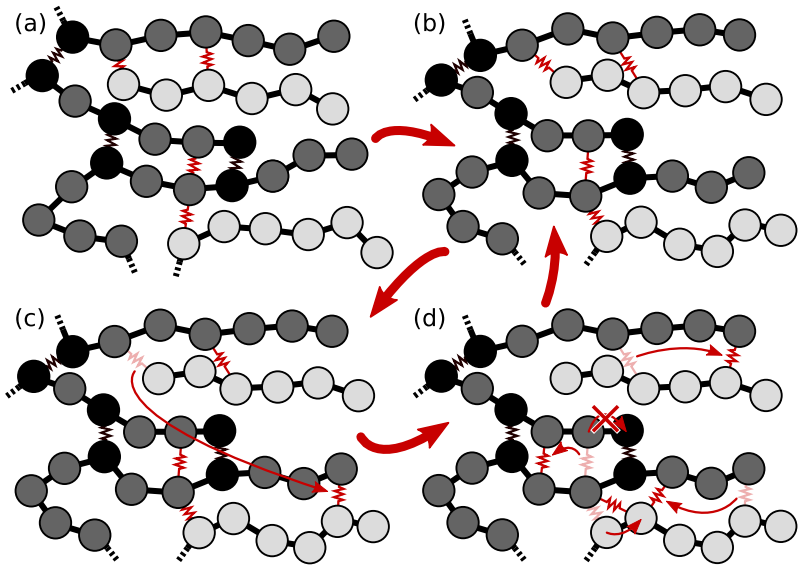

Figure 2: Sequences in the slip-spring dissipative-particle-dynamics model of Langeloth *et al.*[88]. Shown is a fictitious system of unconnected bead-spring chains (light gray) and cross-linked chains (dark gray). Cross-links and their anchor points are shown in black, slip springs are depicted in red. Starting from an initial configuration (a), the sequences are motion of DPD beads (b), slip-spring relocation (c), and slip-spring migration (d). For more details, see the text.

mechanism necessary to model constraint-release dynamics. In a relocation attempt, a slip-spring insertion between a randomly chosen chain end and any bead within a distance r with $r_{\mathrm{min}} \leq r \leq r_{\mathrm{max}}$ of this chain end is probed. The relocation, that is, deletion of the old slip spring and insertion of the new one, is accepted if the energy difference between both slip springs fulfills a Metropolis criterion. The parameters r_{min} and r_{max} must be chosen carefully to ensure a certain relocation efficiency. Strictly speaking, detailed balance additionally demands the same distance criterion to be fulfilled for the removed slip springs. Thus, a lower limit of $r_{\mathrm{min}} = 0\ r_c$ is chosen. A relocation of slip springs longer than $r_{\mathrm{max}} = 2\ r_c$ is, however, still allowed, as this is a rather rare event.

Other MC-SS models with a fixed number of slip springs consider very similar relocation dynamics. However, if the number of slip springs is allowed to vary, the relocation move is replaced by slip-spring creation and destruction dynamics which are usually coupled to fulfill detailed balance. An exception is the model of Chappa *et al.*[83], where relocation is allowed additionally to creation/destruction events. Slip-spring creation is usually controlled by an activity coefficient[84]. The later versions of Ramírez-Hernández' TIEPOS model[96] and the kMC/BD model of Theodorou and co-workers[106] also consider the number of potential partners for a creation move, and thus a dependence on the local environment.

In the **slip-spring migration sequence**, every spring performs n_{MC} trial moves, each corresponding to a migration attempt. In every attempt, both mounting points of the slip spring hop to a random bead bonded to their original anchor. This migration attempt is again accepted or rejected by a Metropolis criterion. Migration moves are automatically rejected if they would collapse both slip-spring anchors onto the same bead. After n_{MC} steps, the slip springs are fixed to act as bonds in the next DPD sequence. Notably, slip springs are only allowed to attempt a relocation move from one chain end to another if they populate it at the end of the MC sequence.

While some other models follow this approach to attempt migration at fixed intervals, other works use a certain probability to initiate migration every few steps[84, 106, 113]. For example, Uneyama and Masubuchi[84] propose a hopping probability that depends on the time since the last hop and a sliding friction. In the kMC/BD model[106], the acceptance of migration moves does not depend on the energy change but is proportional to the slip-spring potential. This approach is combined with short migration sequences, so that slip springs can easily realize unfavorable positions but are unlikely to remain there for a longer period. A completely different approach is proposed in the first version of the TIEPOS model[92], where slip springs are interacting and have their own dynamics governed by a one-dimensional, stochastic differential equation of motion.

3.2 Choice of Parameters

An important decision is the choice of the **slip-spring number and ensemble**. The method of Langeloth *et al.*[88] uses a fixed number of slip springs, that is, it handles them in a canonical approach. In a monodisperse melt, the number of slip springs N_{SS} is related to the topological entanglement length of the chains as $N_{\mathrm{e}}^{\mathrm{SS}} \approx N \times N_{\mathrm{chains}} / \left(2 N_{\mathrm{SS}}\right)$, where N and N_{chains} are the number of beads per chain and chains in the system. Everaers[136] found the relation $N_{\mathrm{e}} \approx 2 N_{\mathrm{e}}^{\mathrm{SS}}$ between the rheological and topological entanglement length. If mapping to a specific system is attempted, the number of slip springs can thus be chosen accordingly. Since this is not the case for the systems considered in this thesis, the number of slip springs is arbitrarily set to $N_{\mathrm{SS}} = 0.1 N \times N_{\mathrm{chains}}$ for melts, which is small enough to allow Rouse motion between entangled segments, yet large enough to reproduce reptation dynamics in melts[88]. Recently, Masubuchi *et al.*[103] showed that systems with different N_{SS} were transferable withing some limits, which justifies an arbitrary choice if no target system is addressed.
An alternative to a fixed number of slip springs is to control N_{SS} in a grand-canonical ensemble. This is done by defining a slip-spring activity, which is coupled to a, somewhat ambiguous, chemical potential of slip springs. This approach is used for simulations of polymers under shear flow[83, 87] or inhomogeneous systems containing inter- and surfaces[97, 109]. For monodisperse melts, Vogiatzis *et al.*[106] compared both ensembles and found them to yield identical simulation results.

Other parameters that must be chosen carefully are the **sequence lengths** of MC and DPD blocks, n_{MC} and n_{DPD}. One attempt to balance the number of DPD and MC steps is to match the spatial decorrelation time of the slip-spring bond vector. In their original work, Langeloth *et al.*[88] reported that this was best fulfilled for $n_{\mathrm{DPD}} = n_{\mathrm{MC}}$. They derived the sequence length by a simple consideration: by monitoring the ratio of accepted to attempted relocation moves per chain and MC sequence, a success (or relocation) rate of $\alpha = 0.13$ is derived. The rate α is independent of the chain length if n_{MC} is large enough that any slip spring would be allowed to travel the whole chain within one MC block. There is thus a characteristic time $\tau_c = n_{\mathrm{DPD}} / \alpha$ after which a chain experiences an entanglement effect by relocation of a slip spring to it. For consistency, this should equal the entanglement time τ_{e}, which is the relaxation time of a chain segment of length $N_{\mathrm{e}}^{\mathrm{SS}}$. Thus, for a measured entanglement time of 4000 time steps, $n_{\mathrm{DPD}} = n_{\mathrm{MC}} \approx 500$ steps can be derived[88]. Note that these sequence lengths only depend on the topological entanglement length $N_{\mathrm{e}}^{\mathrm{SS}}$ and hold as long as $n_{\mathrm{MC}} = 500$ is sufficient for a slip spring to travel the whole chain length in one block.

While this standard value is employed in simulations of polymer melts and networks, different slip-spring mobilities are investigated in solutions (section 4.2).
Some other MC-SS works also use fixed sequences for bead motion and slip-spring migration[95, 105]. In a different, previously described approach, the entanglement topology is not allowed to equilibrate in the MC section but controlled *via* short retention times of slip springs far from equilibrium[107, 113].

Additional considerations address the interaction of slip springs. The work in this thesis follows the majority of MC-SS models by considering slip springs as noninteracting objects. As such, multiple slip springs can pass each other and populate the same beads (bosonic model). In contrast, the first TIEPOS-approaches of Ramírez-Hernández *et al.*[92] model slip-spring interactions by a harmonic potential. In their later works, slip springs are additionally forbidden to occupy the same beads (fermionic model).
A different problem arises for MC-SS models with weak intermolecular interactions. Since slip springs introduce an additional attractive term into the total free energy of the system, the overall pressure reduces and simulated chains are compressed. To counter this, the models of Chappa *et al.*[83], Uneyama and Masubuchi[84], and the Theodorou group[109] introduce a compensating repulsive potential. Precise compensation of the slip-spring attraction is possible but comes at high computational costs[108]. On the other hand, models considering chain compressibilities[93, 106, 111] or strong repulsions such as DPD[88] experience only weak artificial compressions. For DPD, this was also observed for polymer solutions[91].

3.3 Further Development of Slip-Spring DPD in this Thesis

Most changes made to the simulation code are of no direct influence to the simulation outcome. They concern, for example, the flexibility of choice in input parameters, the performance, or correct the code to comply with rare events that were of no significance in the studies of Langeloth and co-workers[88, 89]. A particular example that gains importance in more dilute systems is the treatment of slip springs on bonded beads[91]. As polymers are diluted, the number of intra-chain slip springs increases. Since slip springs are modeled by a harmonic spring with zero equilibrium length, and since the collapse of both slip-spring anchors to the same bead is forbidden, the equilibrated entanglement topology contains a number of intra-chain slip springs that connect neighboring, already bonded beads. The force constant between these bonded pairs is thus effectively doubled. In the model of Chappa *et al.*[83], moves yielding this topology are forbidden. This however simply transfers the problem to third neighbor beads. Our approach is to make these slip springs inactive for the next DPD sequence but allow them to migrate (or relocate) freely in the MC block. Thus, these entanglements vanish temporarily but can still migrate and re-emerge. While highly diluted polymer solutions have a high number of inactive slip springs at all times, the individual slip spring is found to stay inactive very briefly.
To allow simulations of elastomeric networks, the simulation code has been extended by cross-links. Their creation mechanism is laid out in section 4.3. Cross-links can, similar to slip springs, populate any pair of beads in close spatial proximity, but they are fully immobile. To study the effect of trapped entanglements, cross-linked beads can be chosen to be excluded from migration and relocation dynamics. A case where all chains are end-linked is studied. Thus, slip springs can migrate along their network strands but cannot leave them, which is meant to mimic trapped entanglements known from experiments and network theories[118].

Macromolecules

pubs.acs.org/Macromolecules Article

Different Stages of Polymer-Chain Collapse Following Solvent Quenching—Scaling Relations from Dissipative Particle Dynamics Simulations

Jurek Schneider,* Melissa K. Meinel, Han Dittmar, and Florian Müller-Plathe*

Cite This: *Macromolecules* 2020, 53, 8889–8900 Read Online

ACCESS | Metrics & More | Article Recommendations | Supporting Information

ABSTRACT: We study the collapse of a linear bead-spring chain under a sudden quench in solvent conditions using explicit-solvent dissipative particle dynamics. We investigate the collapse stages of our $50 \leq N \leq 1000$ bead chains by studying local structures identified by an extended clustering algorithm. We find evidence for the three early stages proposed by Halperin and Goldbart [*Phys. Rev. E* 2000, **61**, 565−573]. Their apparent scaling with the chain length is $\propto N^0$, $N^{0.82(6)}$, and $N^{1.04(2)}$. These values are similar to the predicted ones, and deviations likely stem from the approximations made. The scaling of the overall collapse time with the chain length $\tau_c \propto N^{0.94(2)}$, the decay of the squared radius of gyration $(R_g^2(0) - R_g^2(t)) \propto t^{1.09(1)}$, and the growth of blobs along the chain $\langle S_n \rangle \propto t^1$ are all found to be approximately linear.

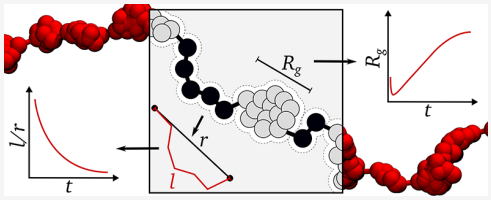

INTRODUCTION

The collapse of a linear polymer chain under a sudden quench in solvent conditions has been a subject of scientific interest for a long time.[1] After the pioneering theoretical work by de Gennes[2] in 1985, many studies approached this problem by either theoretical models, computer simulations, or, rarely, experiments. Investigation of the coil-to-globule transition of homopolymers has been recognized as an important first step in understanding more complex biological processes such as protein folding[3] and the formation of crumpled chromatin structures.[4] More recently, the development of flash nanoprecipitation[5,6] has motivated further studies on polymer collapse and precipitation.[7−9]

The first collapse process was suggested by de Gennes to describe a dissolved polymer chain quenched below its θ temperature. He proposed an initial, fast collapse into a "sausage-like" state followed by slow crumpling until the final, globular structure is reached.[2] De Gennes predicted the scaling of the collapse time with the chain length N in the two regimes as $\propto N^2$ and $\propto N^{0.33}$, respectively. In 1988, Grosberg et al.[10] reviewed this work and proposed a single-stage collapse for chains shorter than their entanglement length. Otherwise, they expected a collapse into a fractal globule ($\propto N^2$), just to reorient and knot in a reptation-like fashion ($\propto N^3$) afterward. The authors later expanded this model to add a third stage of interchain knotting for multichain systems.[11] The model of de Gennes was later refined by Klushin[12] and Abrams,[13] who incorporated a solvent-induced capillary instability and predicted the formation of blobs and an intermediate structure resembling a "necklace". They estimated the characteristic collapse times to scale as $\propto N^{0.93}$ and $\propto N^{0.83}$, respectively.

From 1995 on, Dawson and coworkers described a three-stage collapse mechanism in a series of publications.[14−18] According to their lattice Monte Carlo and Langevin equation based simulations, monomeric units would first form blobs along the polymer's backbone. In later stages, the chain would coarsen until all beads were part of a blob and eventually form a compact globule. Blob formation, coarsening, and relaxation were found to scale as $\propto N^{0.1}$, $\propto N^{1.5}$, and $\propto N^1$ if hydrodynamics were considered.[17] Experimental works using dynamic light scattering[19−21] and fluorescence labeling techniques[22] confirmed a two-stage collapse mechanism of different polymers. Since the fast formation of blobs was not detectable by their means, these works supported the early models of de Gennes and the Dawson group.

A different mechanism was proposed by Ostrovsky and Bar-Yam,[23−25] who observed an end-driven collapse mechanism in their two- and three-dimensional lattice Monte Carlo simulations. They described a formation of blobs on the chain ends, which smoothly grew upon aggregation with neighboring beads, until a metastable dumbbell structure was reached. Eventually, both blobs merged into the final nanoparticle. Their overall collapse time scaled as $\propto N^1$ in the absence of hydrodynamics. Notably, this scaling was not found to be affected by the presence or absence of the chains' excluded volume.[23]

Received: June 4, 2020
Revised: September 16, 2020
Published: October 5, 2020

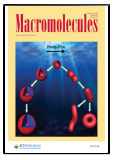

Finally, a sophisticated theoretical model for a flexible chain brought from above- to below-θ conditions was described by Halperin and Goldbart.[26] They argued the first stage to be similar to Dawson's model, where monomeric units would first cluster into blobs. In the second stage, slack polymer connecting the blobs, so-called "bridges", was absorbed by blobs. Bridges would thus straighten, while the overall chain structure remained undisturbed. In analogy to Klushin's work, the resulting conformation was described as a pearl necklace, where blobs are connected by straight bridges. Using free-energy-based arguments, Halperin and Goldbart derived the characteristic times of their collapse stages to scale as $\propto N^0$, $N^{0.2}$, and $N^{1.2}$, respectively.

Despite some experimental studies, the most important tool to approach the fast collapse of chains in an infinite solution has always been computer simulations. However, most studies have focused on fundamental or technical questions such as the influence of hydrodynamics or the necessity of an explicit solvent. By now, hydrodynamic interactions are known to accelerate the collapse in most cases,[27,28] even though their influence can be more complex for special initial configurations such as precollapsed chains.[29] The use of an explicit-solvent model was found to favor a smooth collapse, rather than trapping, of the chain in metastable states[30−33] and was reported to be important for a correct scaling behavior in very poor solvent.[34] Despite the broad interest in the collapse pathway, fewer studies have examined the scaling behavior. In the absence of hydrodynamic interactions, different authors derived a scaling of the characteristic collapse time as approximately $\tau_c \propto N^{1.67}$ from lattice Monte Carlo,[14,35] Gaussian self-consistent field,[17] and Langevin equation[36] based studies. Investigations incorporating hydrodynamic interactions, on the other hand, have not yet reached an agreement for the characteristic collapse time.[37] More sophisticated studies using stochastic rotational dynamics,[38] Brownian dynamics,[28] and dissipative particle dynamics[39] (DPD) do, however, favor an approximately linear scaling.

Apart from the works of Dawson and co-workers, studies focusing on the scaling of different collapse stages are surprisingly sparse. A study of Halperin and Goldbart's pathway was conducted in 2011 when Guo et al.[39] utilized DPD simulations to investigate different stages. By tracing the number of solvent particles in vicinity to the collapsing chain, they were able to identify three stages and provided apparent scaling laws of $\propto N^0$ and $N^{0.99(11)}$ for the first and third one, respectively. Here, we use a similar system to study the formation and scaling behavior of local structures in long bead-spring polymer chains. Dissipative particle dynamics allows us to perform explicit-solvent simulations of chains of up to 1000 beads quenched from above- to below-θ conditions. The potential of DPD beads to comprise multiple monomers[40] facilitates a further coarsening. We present an extended clustering algorithm to identify local structures, such as blobs and bridges, which we find to provide a more intuitive access to the duration and scaling of different collapse stages than global properties. In a first section, we describe the observed collapse pathway and derive global properties to compare our systems to the literature, namely, the scaling exponent of the overall collapse time, $\tau_c \propto N^{\gamma}$, and the decay exponent α of the chain radius of gyration, $(R_g^2(t) - R_g^2(0)) \propto -t^{\alpha}$. We secondly focus on the development of blobs and bridges during the chain collapse. We thereby extract scaling laws for all three early collapse stages and discuss their compliance with Halperin and Goldbart's predictions. In a last section, we examine the growth of blob sizes, $S_n(t) \propto t^z$, which has recently been found to be rather delicate for longer chains.[41,42]

METHODS

Model. Our simulations were performed using dissipative particle dynamics (DPD) simulations, a technique introduced by Hoogerbrugge and Koelman[43] in 1992 and critically reviewed and refined by Warren and different co-workers.[44,45] In this work, we follow the methodology of Groot and Warren (ref 45). DPD particle interactions consist of a stochastic part, a friction part, and a coarse-grained, soft-core conservative potential. Explicit-solvent DPD has been used for various applications on isolated chains and polymer solutions, some of them featuring single-chain collapse[4,8,39] or the precipitation of polymer solutions, so-called flash nanoprecipitation.[46−49] It is noteworthy that explicit-solvent DPD simulations fully include hydrodynamics due to their momentum-conserving nature, which is expected to be crucial for a realistic model system.[31,33]

We use a standard bead-spring chain model[50] where bonded DPD particles interact via a weak Hookean spring on top of the nonbonded interactions (eq 1).

$$\mathbf{F}_{ij}^{B} = -k\mathbf{r}_{ij} \tag{1}$$

The linear chain is initially dissolved in a sea of monomer particles with identical interactions between polymer−polymer (PP), polymer−solvent (PS), and solvent−solvent (SS) beads. In the literature, the Flory exponent for athermal DPD solvents ranged between 2ν = 1.04 and 1.19 for this and very similar models[50−55] but is generally considered to be closer to good-solvent, rather than θ-solvent, conditions.[56]

After equilibration, we model a solvent-to-nonsolvent exchange by making all polymer−solvent interaction parameters a_{PS} three times as repulsive. In our tests, we did not find a strong influence of the quench depth on the overall collapse behavior. This is consistent with previous findings where different choices of a_{PS} only affected prefactors rather than scaling coefficients.[39]

We use reduced units: Time, length, mass, and energy are given in terms of t_{DPD}, $l_{DPD} = r_c$, m_{DPD}, and $\varepsilon_{DPD} = k_BT$, respectively. DPD parameters are taken from the work of Groot and Warren (ref 45) for a system with a number density of 3 r_c^{-3}. Consequently, the conservative repulsion coefficient for "like" interactions, i.e., interactions between solvent and polymer as well as all beads of equal species, is $a = 25\ k_BTr_c^{-1}$. "Repulsive" interactions between polymer and nonsolvent have an interaction coefficient of $75\ k_BTr_c^{-1}$. The force constant of the Hookean spring between bonded beads is $k = 4\ k_BTr_c^{-2}$, and the integration step width is $\Delta t = 0.06\ t_{DPD}$. This paper focuses on the scaling behavior of our model. We thus refrain from a direct comparison with experimental data or atomistic simulations. If need be, our chain model can be mapped onto polystyrene as we suggested in an earlier work.[49]

Our simulations feature one single chain of length N = 50, 75, 100, 250, 500, 750, or 1000 in a cubic box surrounded by monomer DPD beads representing the solvent. The length L of the box is chosen with respect to the chains' root-mean-square radius of gyration to keep a consistent ratio of $L/\langle R_g^2\rangle^{0.5} \approx 4$. This has been shown to allow good-solvent scaling of dynamic properties without the need to apply hydrodynamic corrections.[51,52,57] At the same time, this box size is large enough to prevent finite-size effects. For chain sizes of 50, 75, 100, 250, 500, 750, and 1000 beads, the box lengths are 14, 18, 20, 36, 52, 66, and 78 r_c, respectively. The number of solvent beads is chosen to produce a number density of 3 r_c^{-3}. Equilibration runs are performed for 5×10^5 time steps (30000 t_{DPD}, $N \leq 750$) and 7.5×10^5 time steps (45000 t_{DPD}, N = 1000), which is longer than the chains' longest relaxation times. After the quench into nonsolvent conditions, simulations are continued for 3000 ($N \leq 250$), 4000 (N = 500), 5000 (N = 750), and 6000 (N = 1000) time steps (180, 240, 300, and 360 t_{DPD}). In all cases, simulation times are longer than the longest collapse times.

https://dx.doi.org/10.1021/acs.macromol.0c01315
Macromolecules 2020, 53, 8889−8900

One set of simulations for every chain length consists of 100 independent runs. If not stated otherwise, averaged values over all 100 realizations are presented. Errors denote the standard deviation of the mean or, in case of a fitted property, the fitting error.

For the sake of brevity, units will be omitted from here on. If not denoted otherwise, simulation time is given in t_{DPD}.

Cluster Analysis. Our analysis is based on the idea that DPD beads form "blobs" and "bridges" along the collapsing chain. Blobs are an aggregation of beads to larger structures and expected to be initially formed along the chain's backbone. Bridges connect blobs along the chain's principal structure. In the following section, we lay out our algorithm to identify those structures. It is crucial to differentiate between the constructed properties "blobs" and "bridges", compact "clusters" as identified by cluster analysis, and "beads" as regular DPD monomers.

The identification of blobs and bridges is based on a simple density-based cluster analysis: Here, a cluster describes a number of beads in spatial proximity to each other. A bead is part of a cluster if it is closer than the clustering distance $r_{cc} = 1$ to any bead in the respective cluster. We exclude bonded beads from this cluster definition: Regardless of their distance, bonded beads can only be part of the same cluster if they are "connected" by other cluster members. We did, however, not find a significant difference in the resulting scaling laws if this is neglected or a different cluster criterion (e.g., 0.85 or 1.45, two relevant distances in the radial distribution function of a monomeric liquid[49]) is chosen.

Once clusters are identified, they are separated into either blobs or bridges. In a first step, all clusters with a number of beads $n_b \geq 5$ are declared as blobs and all with $n_b < 5$ are bridges. Second, the definition of bridges is refined: As bridges should connect blobs, bridge-type clusters on chain ends are discarded.

Four relevant special cases are shown in Figure 1. Here, bridges are illustrated black and labeled with letters, while blobs are shown in gray and labeled with numbers. Spatial proximity around beads is hinted by the dashed circles. As shown in Figure 1a, neighbored bridge-type clusters are always counted as part of the same bridge. Naturally, two bridges cannot be direct neighbors but must end in blob-type structures. In our interpretation of a blob, all contained beads should be consecutive chain segments. However, multiple blobs can be parts of the same cluster if they are close enough. This is illustrated in Figure 1b where blobs **1** and **3** are merged by the clustering algorithm. For our analysis, these clusters are split into two independent blobs, both containing only consecutive beads. Another pitfall for the algorithm is the drift-out of a number of beads from a blob. This is displayed in Figure 1c,d. If the size of a cluster drifted out of a blob is above 4, they count as an independent blob. Smaller clusters, however, can either be identified as bridges (Figure 1c) or part of a different blob (Figure 1d). In the first case, the bridge would start and end in the same blob. It is thus discarded, and the respective beads are added to the original blob. In the case shown in Figure 1d, the drifted beads are removed from blob **2** and added to blob **1**. The criterion of a blob consisting of consecutive beads only is thus fulfilled.

Considering all mentioned scenarios, the identification of blobs and bridges allows for the derivation and discussion of local structures, rather than the complete chain.

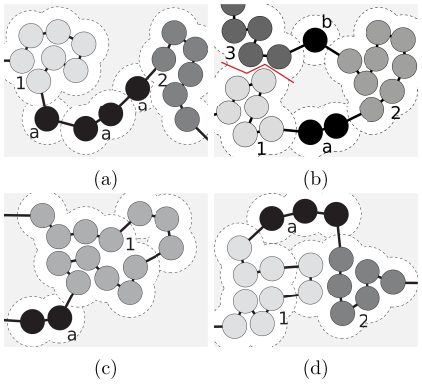

Figure 1. Critical events when subdividing a chain into "blobs" and "bridges": (a) neighbored bridge-type clusters are part of the same bridge, (b) blobs that are part of the same cluster but do not consist of consecutive beads are divided, (c) and (d) beads drifting out of a blob to form a new cluster or join an existing one are considered part of their original blob. Blobs are dense structures along a chain's backbone, displayed in gray, and identified by numbers. Bridges are connecting blobs, illustrated in black, and labeled with letters. For a detailed explanation, see the text.

RESULTS AND DISCUSSION

Equilibrium Properties. The properties of all polymer chains dissolved in a good solvent are derived from additional runs performed for 10^5 time steps after the equilibration. The equilibrium properties of collapsed chains are measured from the last frames of the collapse runs, after the squared spatial distance showed no change for a sufficient time. We examine the scaling of the mean square radius of gyration $\langle R_g^2 \rangle$ with the chain length N as $\langle R_g^2 \rangle \propto (N-1)^{2\nu}$. Scaling exponents are fitted as $2\nu = 1.176(13)$ and $0.669(1)$ for interaction parameters of $a_{PS} = 25$ and 75, respectively. The exponent for the athermal solvent coincides with the expected value for good-solvent conditions[58] and is very close to 1.19, the result reported for our chain model by Nardai and Zifferer.[56] The globules display poor-solvent scaling.[59]

Similar results are obtained by investigating the mean squared spatial distance $\langle R^2 \rangle = \langle (\vec{r}_j - \vec{r}_i)^2 \rangle$ of two beads i and j as a function of their segmental distance $n = |j - i|$. $\langle R^2(n) \rangle$ is presented in Figure 2 for $N = 1000$ and averaged over all runs and all possible pairs per chain. Equilibrium values are shown with dashed lines. Continuous lines mark the squared spatial distance at various stages of the chain collapse, which will be discussed further below. In the coiled state, fitting of shorter segments provides $\langle R^2 \rangle \propto n^{1.163(1)}$ for $n \in [1,100]$, which matches our previous observations. For the equilibrium globule, sub-Gaussian scaling of $\propto n^{0.927(10)}$ is found for $n \in [1,10]$, while long segment lengths scale as $\propto n^{0.143(1)}$. The negative scaling exponent exhibited by the longest chain

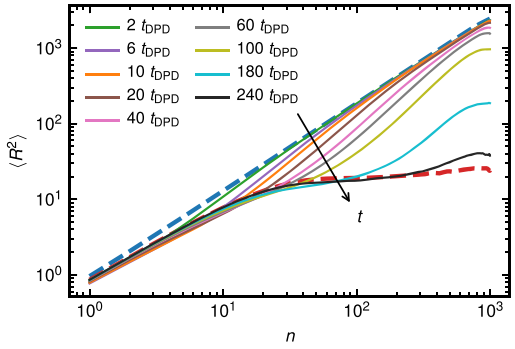

Figure 2. Mean squared spatial distance averaged over all $N = 1000$ systems. Shown is the distance $\langle R^2 \rangle = \langle (\vec{r}_j - \vec{r}_i)^2 \rangle$ of two beads i and j as a function of their segmental distance $n = |j - i|$. Equilibrium curves for good-solvent (blue, $a_{PS} = 25$) and nonsolvent conditions (red, $a_{PS} = 75$) are indicated by bold, dashed lines. Continuous lines show the spatial distance at different times after the quench. The indicated times refer to the time after exchanging solvent for nonsolvent.

https://dx.doi.org/10.1021/acs.macromol.0c01315
Macromolecules 2020, 53, 8889−8900

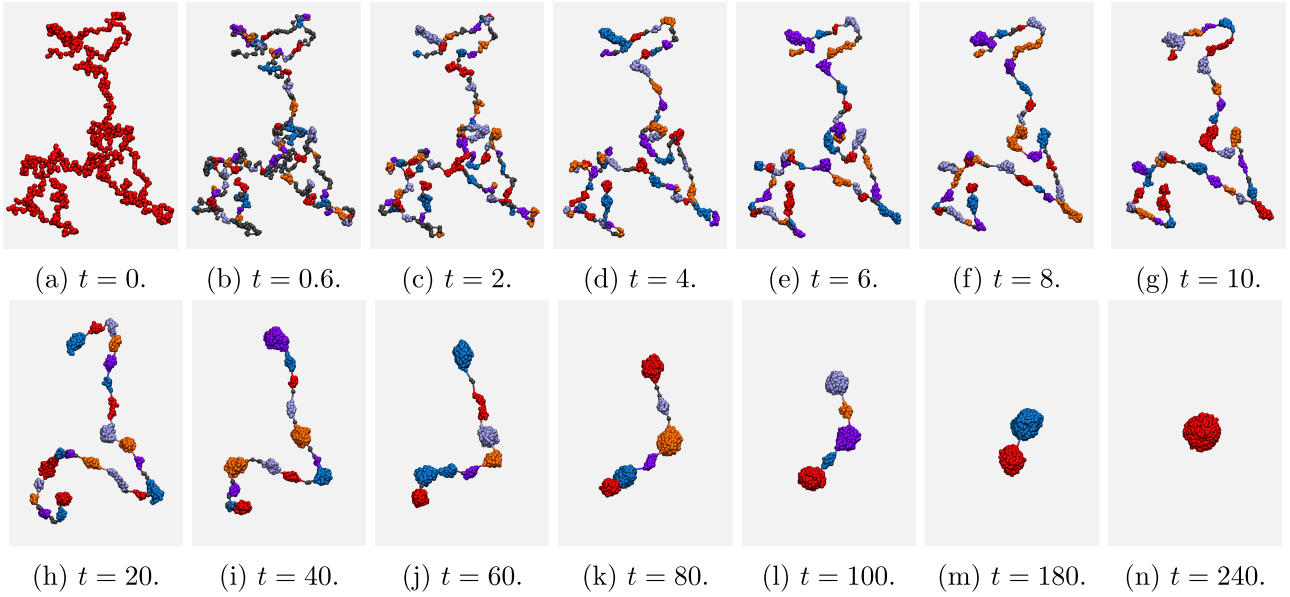

Figure 3. Snapshots of the collapse of a selected $N = 1000$ chain in a nonsolvent with $a_{PS} = 75$. Solvent molecules are not shown. Snapshots are recorded at different times ((a)−(n)) after a quench at $t = 0$ using the VMD software:[61] (a) $t = 0$, (b) $t = 0.6$, (c) $t = 2$, (d) $t = 4$, (e) $t = 6$, (f) $t = 8$, (g) $t = 10$, (h) $t = 20$, (i) $t = 40$, (j) $t = 60$, (k) $t = 80$, (l) $t = 100$, (m) $t = 180$, and (n) $t = 240$. The colors indicate different clusters identified after a cluster analysis with a cluster criterion of 1. Bridges, i.e., clusters with $n \leq 4$, are shown in dark gray.

segments is most likely an artifact of their relatively poor self-averaging. On short scales, Gaussian behavior is expected as central beads in a globule effectively experience a melt-like environment. The reduction of the expected value of 1 is likely due to the finite size of the globule. A similar scaling exponent of ≈0.8 has been reported by Petrov et al.[60] for the local scale of their collapsed, 2×10^4-bead DPD chains. However, their local scaling parameter showed a strong influence on the choice of the fitting boundaries. On the global scale, the squared spatial distance approached a constant value ($\propto n^0$).[60] We note that our globular chains with $N < 1000$ show a behavior similar to the $N = 1000$ systems, with a faster transition to the terminal plateau. In the athermal systems, plots of $\langle R^2(n)\rangle$ for $N < 1000$ are overlapping almost perfectly with the curve presented for $N = 1000$.

Collapse Pathway. A chain quenched from good-solvent to nonsolvent conditions immediately undergoes a coil-to-globule transition. Snapshots of this process are shown in Figure 3 for a selected $N = 1000$ chain with a squared radius of gyration particularly close to the average $\langle R_g^2\rangle$. The collapse appears to follow the three-stage picture described by Halperin and Goldbart[26] and later observed in different other works.[4,29,39,62,63] Here, we briefly describe their proposed pathway, which starts with the formation of blobs along the chain. This "pearling stage" is clearly detected in our system in the first snapshots ($t = 0 - 2$): Polymer beads retract to the backbone of the chain and form small blobs, which are also commonly called "pearls" or "globules". In the second stage, bridges between pearls are stretched as monomer beads transfer from them to neighboring blobs.[26] This "bridge-stretching" stage is difficult to detect by visual means and will be discussed later. Around $t = 20$, a distinct "pearl necklace" structure is formed, which is characterized by medium-sized blobs of ≈50 beads (for $N = 1000$) that are connected by stretched bridges.[12,26] This structure collapses to a dumbbell-like configuration and eventually forms a single, uniform globule. The dumbbell formation was subject to multiple studies by Ostrovsky and different co-workers,[23−25] who argue it to be caused by an end-driven collapse of the chain due to the higher mobility of the chain ends.[24] As dumbbell formation and final aggregation happen on similar timescales, it is however unclear whether they are part of the same or two different collapse stages.[39] We note that some snapshots shown in Figure 3 exhibit very stretched bonds, which is an artifact of the relatively soft Hookean springs employed. However, this affects only a minor fraction of bonds at any time, and characteristic collapse properties are still in very good agreement with literature data,[28] which utilized finitely extensible bonds (see below).

The phenomenological collapse is best understood by a direct comparison of the snapshots (Figure 3) with the change in the squared spatial distance over time (Figure 2, continuous lines). We note that the data presented in Figure 2 are averaged over all runs since individual runs show a surprisingly small deviation from the average at any given time step. The spatial distance confirms a multiscale process: A deviation from the initial good-solvent conditions (blue, dashed line) first occurs for short chain segments ($n \lesssim 50$), i.e., on a local scale. Meanwhile, the chain's backbone, i.e., its global structure, remains unchanged. The formation of blobs is accompanied by the transition to a local sub-Gaussian scaling, which appears to be fully developed around 6 t_{DPD}. As the collapse progresses, longer segments become gradually more affected. Consistent with the snapshots, backbone deformation begins around 20 − 40 t_{DPD}. A relaxation of short segments is observed for late collapse stages as a melt-like environment develops inside the globules. Similar observations for the squared spatial distance have been made by Chertovich and Kos[4] and Petrov et al.[60] However, their systems did not allow chain crossing, which resulted in the temporary formation of a crumpled globule. The latter was characterized by a distinct $\langle R^2\rangle \propto n^{1/3}$ scaling.[4] A crumpled globule is not to be confused with a fractal globule

https://dx.doi.org/10.1021/acs.macromol.0c01315
Macromolecules 2020, 53, 8889−8900

($\propto n^{2/3}$), a self-similar structure proposed by Grosberg et al.[10] that was, to our knowledge, never found in simulations.[60,64−66] Both crumpled and fractal globules can only equilibrate in a reptation-like fashion, which is commonly understood as an additional stage in single-chain collapse.[17] In our system, chain crossing is not prohibited. While this does not allow a correct description of the terminal equilibration *inside* the globule, it has been found that the presence or absence of an excluded volume does not alter the preceding stages of the collapse.[23] In previous works,[8,49] we tried to restore potential effects of chain crossing in precipitating single- and multichain systems using slip-springs.[67,68] We did not find significant changes in the collapse pathway detectable by, for example, the chains' radii of gyration.

The collapse behavior of single chains is commonly discussed in terms of three characteristic exponents: the scaling of the characteristic collapse time with the chain length $\tau_c \propto N^{\gamma}$, the early-stage change of the radius of gyration over time $(R_g^2(0) - R_g^2(t)) \propto t^{\alpha}$, and the growth of blobs formed during the chain collapse, $\langle S \rangle \propto t^{z}$. The exponents γ, α, and z are known to be sensitive to the presence or absence of hydrodynamic interactions and the treatment of solvent particles. An overview over different predicted and derived scaling exponents is given by Pham et al.[28] In this section, we discuss the exponents accessible from the chains' radius of gyration, α and γ. The growth exponent z is investigated further below.

The mean square radius of gyration $\langle R_g^2 \rangle$ of collapsing chains of different lengths is depicted in Figure 4. The gray line

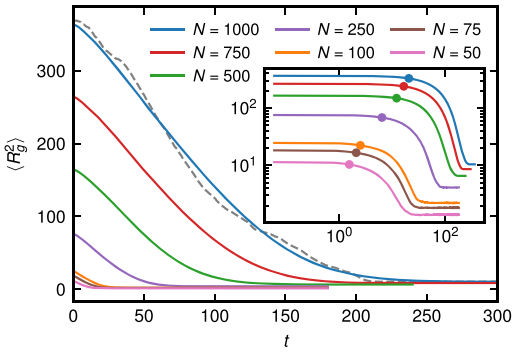

Figure 4. Mean square radius of gyration $\langle R_g^2 \rangle$ of collapsing chains of different lengths N. The quench of a_{PS} = 25 to 75 is performed at t = 0. Colored lines are averaged over a set of 100 independent runs. The gray, dashed line represents the single N = 1000 chain also shown in Figure 3. The inset is a logarithmic presentation of $\langle R_g^2(t) \rangle$. Symbols denote the times where the chains' collapse progressed by 10% (see text).

indicates the decay of a selected N = 1000 chain, which was also chosen for the snapshots in Figure 3. All chains collapse smoothly. We do not observe trapping in local minima along their collapse path, which was occasionally found in early simulation works[28,31,34,69] and has been addressed to the combination of high quenches and an implicit solvent model.[31,32,34] We derive the characteristic collapse time τ_c as the time when a chain's collapse has progressed by 99% (eq 2), which is one of the several established criteria.[28] The scaling of τ_c with the chain length N is described by γ (eq 3), while the initial decay of $\langle R_g^2 \rangle$ is governed by the apparent power-law exponent α (eq 4).

$$R_g(\tau_c) = 0.01[\langle R_g \rangle(0) - \langle R_g \rangle(\infty)] + \langle R_g \rangle(\infty) \quad (2)$$

$$\tau_c \propto N^{\gamma} \quad (3)$$

$$\langle R_g^2(t) \rangle = \langle R_g^2(0) \rangle - At^{\alpha} \quad (4)$$

At this point, we want to draw the reader's attention to the terminal decay of $\langle R_g^2(t) \rangle$. In Figure 4, averaged data converge toward the globules' equilibrium values slowly. In contrast, the R_g^2 of a single chain (gray line) maintains its trend over the whole range of the collapse, which becomes even more apparent for its square root R_g (not shown). We thus suspect the terminal progress of $\langle R_g^2(t) \rangle$ to be an artifact due to the averaging over many chains. Consequently, we attempt to derive the coefficients α and γ from single-chain properties. To evaluate α, we investigate $R_g^2(0) - R_g^2(t)$ as a function of time. A corresponding presentation (not shown, see, e.g., ref 28) emphasizes a power-law dependence. However, a direct derivation of α is impeded by a plateau of $\langle R_g^2 \rangle$ preceding the collapse, which is best observed in a logarithmic presentation of $\langle R_g^2(t) \rangle$ (Figure 4, inset). This offset corresponds to the short initial collapse stages where the chain's backbone remains mostly undeformed. It ends roughly when $\langle R_g^2(t) \rangle$ decayed by 10% as indicated by symbols in the inset in Figure 4. We will return to this further below. α is thus fitted in the regions where the chain's individual collapse progressed between 10 and 80%, which we identified using an approach similar to eq 2. Results for α are averaged for all runs of one set and shown in Figure 5a. Since α shows no apparent

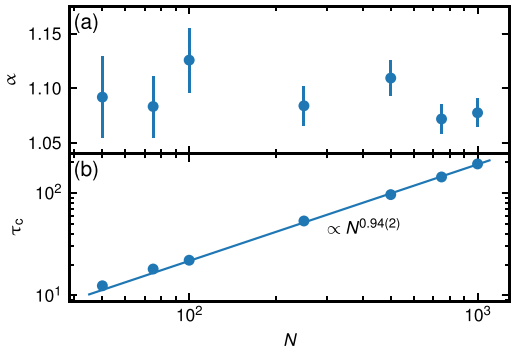

Figure 5. (a) Radius-of-gyration decay exponent α (see eq 4) and (b) characteristic collapse time τ_c (see eq 2) for different chain lengths N. All data points are averaged values of a set of 100 independent runs. α can be averaged over all N to α = 1.09(1). The line is a fit of $\tau_c = A \times N^{\gamma}$ (where A is a constant). Error bars in panel (b) are within the symbol size.

dependence on N, we derive its average value to 1.09(1). Other works describing chain collapse in the presence of hydrodynamic interactions provide similar results: While Gaussian self-consistent field simulations of Kuznetsov et al.[17] yielded $\alpha = 9/11 \approx 0.82$, Pitard[27] reported a value of α = 1 for his Langevin equation studies. Importantly, Brownian dynamics simulations of Pham et al.[28] gave α = 1.05(1). We thus consider our results in line with literature data.

The characteristic collapse time τ_c is derived for every chain following eq 2. Results are given in Figure 5b and Table 1. Theoretical and computational works report a range of values for γ. Simulations of Pitard,[27] Pham et al.,[28] and Guo et al.[39] favored a linear scaling with γ = 1, 1.01(1), and 0.98(9), respectively. Our value of γ = 0.94(2) is in decent agreement

https://dx.doi.org/10.1021/acs.macromol.0c01315
Macromolecules 2020, 53, 8889−8900

Table 1. Characteristic Times τ_p, τ_{bs}, τ_{pn}, and τ_c of the Pearling, Bridge-Stretching, and Pearl-Necklace Stage, and the Overall Chain Collapse[a]

N	τ_p	τ_{bs}	τ_{pn}	τ_c
50	0.24		5.3(5)	12.4(4)
75	0.24		11.4(7)	18.1(5)
100	0.24	2.28(6)	15.8(7)	22.0(7)
250	0.18	4.55(4)	44.6(15)	53.2(14)
500	0.18	7.05(4)	83.7(27)	96.2(25)
750	0.24	10.12(6)	127.2(33)	143.0(32)
1000	0.24	13.56(8)	174.4(42)	191.7(40)
μ	−0.03(5)	0.82(6)	1.04(2)	0.94(2)

[a] μ denotes the best fit of a scaling factor as $\tau_i \propto N^{\mu}$. The errors are the standard deviation of the mean in a set of 100 independent runs for τ_{pn} and τ_c and the fitting error for τ_{bs} and μ.

with these results. It is, however, even closer to the prediction of Klushin[12] (γ = 0.93), whose model is an extension to de Gennes' original work by incorporating hydrodynamics and capillary instability into the collapse picture. Other values for studies incorporating hydrodynamic interactions ranged between 4/5 and 4/3.[13,17,26,69,70] The origin of the discrepancies in literature data is, however, unknown to us.

Stages of the Collapse Process. We employ the density-based clustering algorithm to identify and study different stages of the collapse. The distribution of clusters along a selected N = 1000 chain is shown in Figure 3, with clusters containing less than five beads colored gray. Using the algorithm described in Cluster Analysis, clusters are classified as either "blobs" or "bridges". Our names for the stages follow Halperin and Goldbart's original work.[26]

Pearling. Immediately after the quench from good- to poor-solvent conditions, chain beads in spatial proximity aggregate and form blobs along the chain's backbone. In the picture of Halperin and Goldbart, these blobs are labeled as "pearls", and the first collapse stage is called the pearling stage. The numbers of blobs and bridges (N_{bl} and N_{br}) as a function of time are shown in Figure 6. A sudden increase of the numbers of blobs and bridges is observed in the first steps after the quench followed by a slow decay of both numbers. The highest number of blobs is found around 0.6 t_{DPD}. It appears to be linearly dependent on the chain length: Normalization of N_{bl} with N leads to a collapse of the curves for all N (Figure 6c). This indicates that the formation and development of blobs are local processes. However, a similar collapse of curves could not be achieved for N_{br}. The pearling stage ends when nascent blobs start growing by absorbing polymer beads from neighboring bridges. It is yet difficult to estimate whether this coincides with the time where N_{bl} is maximal, and a slight overlap between the first two stages is expected. For this reason, we employ the root-mean-square radius of gyration of an average blob as a function of time, $\langle R^2_{g,bl}(t)\rangle^{0.5}$ (Figure 7). Continuous, colored lines show the average $\langle R^2_{g,bl}(t)\rangle^{0.5}$ of 100 independent runs. The dashed, gray line indicates the progress for the single N = 1000 chain of Figure 3. Figure 7 shows an initial compaction of blobs as they form. We take the position of the minimum, i.e., the time where initial globules are most compact, as the end of the pearling stage and its characteristic time. This time is found between 0.18 and 0.24 t_{DPD} for all chain lengths (Table 1), which is slightly prior to the time where the maximum number of blobs is observed. Regarding our integration step width of 0.06, we can confirm the $\tau_p \propto N^0$

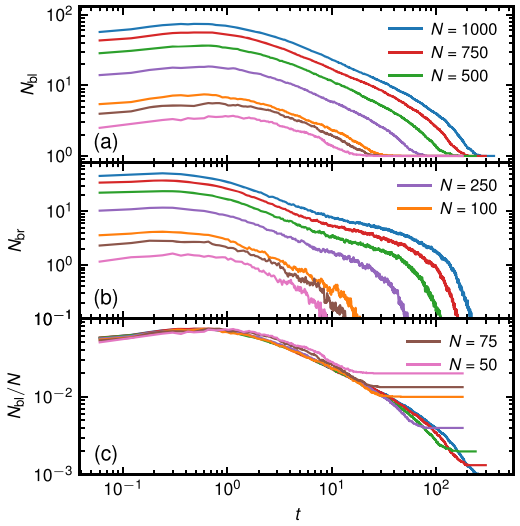

Figure 6. Number of blobs (N_{bl}, (a)) and bridges (N_{br}, (b)) for chains of different lengths N as a function of time. Also shown is the normalized number of blobs (N_{bl}/N, (c)). The definition of blobs and bridges can be found in the section Cluster Analysis. All lines show the average over 100 independent runs after a quench from a_{PS} = 25 to a_{PS} = 75 at t = 0.

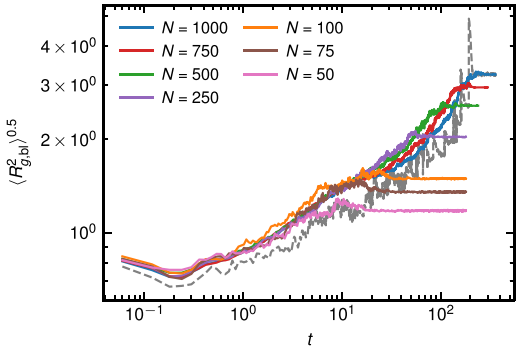

Figure 7. Root-mean-square radius of gyration $\langle R^2_{g,bl}(t)\rangle^{0.5}$ of all blobs as a function of time for different chain lengths N. The definition of blobs and bridges can be found in the section Cluster Analysis. Colored lines show the average over 100 independent runs after a quench from a_{PS} = 25 to a_{PS} = 75 at t = 0. The gray, dashed line indicates the selected N = 1000 chain of Figure 3.

= const. scaling predicted by Halperin and Goldbart and others.[17] Slightly lower values (≈0.1 t_{DPD}) are reported for the DPD simulations of Guo et al.,[39] which is probably due to their somewhat different chain model. Both models do, however, agree in their $\propto N^0$ scaling. The dynamics of the pearling stage can be approached by studying the beads' non-Gaussian motion. The non-Gaussian parameter[71] shows a distinct heterogeneous behavior around 0.18 − 0.66 t_{DPD} for all chain lengths. This is likely a consequence of some beads being part of a blob formed in their close vicinity, while others have to displace further and are thus more exposed to nonsolvent. At early times, the non-Gaussian parameter is fully independent of the chain length. More details can be found in the Supporting Information.

We want to emphasize that pearling takes place very rapidly and locally, with every blob consisting of only 9−10 beads at τ_p irrespective of the chain length. This makes the initial stage

https://dx.doi.org/10.1021/acs.macromol.0c01315
Macromolecules 2020, 53, 8889−8900

barely detectable by other means. It is particularly impossible to visually distinguish between the mean squared spatial distance of the equilibrium coil and the quenched chain at τ_p.

Bridge-Stretching. After the initial stage, a high number of small blobs exist along the otherwise undeformed chain. Following the Halperin−Goldbart pathway, the snapshots of our simulations show a decreasing number of bridges as blobs grow in size (Figure 3). This trend can also be observed in Figures 6 and 7. To quantify the bridge deformation, we introduce the following descriptors: The quantities $r_{1n,br}$ and l_{br} are defined as a bridge's end-to-end distance, i.e., the distance between the two beads where both bridge ends are anchored, and its contour length, i.e., the sum of all bond vectors. The ratio $s_{br} = l_{br}/r_{1n,br}$ is the bridge's stretch factor. An example for the $N = 1000$ system is shown in Figure 8a. The average

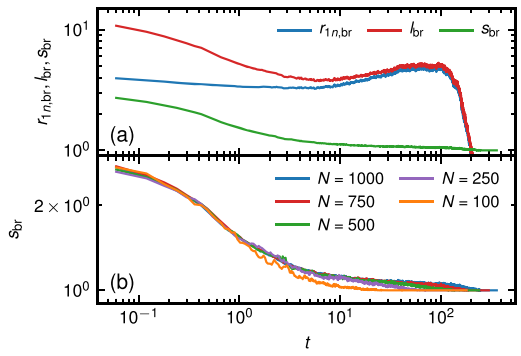

Figure 8. Descriptors of bridge conformations. (a) Comparison of the bridge's end-to-end distance $r_{1n,br}$, the sum of all bond lengths l_{br}, and the stretch factor $s_{br} = l_{br}/r_{1n,br}$ as a function of time. (b) Stretch factor s_{br} as a function of time for different chain lengths. All quantities are averaged over 100 independent runs.

bridge's end-to-end distance stays approximately constant over the first $\approx 10 t_{DPD}$, which supports the assumption of mostly immobile blobs. At the same time, the contraction of bridges decreases their contour length by roughly a factor of 2. As bridge beads are absorbed by blobs, the stretch factor decreases toward its minimum value of 1, which indicates a linear bridge. In later stages of the chain collapse ($10\ t_{DPD} < t < 100\ t_{DPD}$), both $r_{1n,br}$ and l_{br} increase again as bond deformation allows the linear bridges to stretch slightly further. Their ratio, on the other hand, remains mostly unaffected by this.

The bridges' stretch factors are shown for different chain lengths in Figure 8b. As a self-averaged property, the statistical quality of s_{br} depends on the chain length. For this reason, we omit chains with $N < 100$ in this section. Visual inspection of the stretch factor suggests a dependency on the chain length for timescales above $t = 1\ t_{DPD}$. Interestingly, the continuous decay of s_{br} begins immediately and extends to $\approx 100\ t_{DPD}$ for the longest chain length. This indicates that a clear differentiation between different collapse stages might be difficult. In fact, we find that the decay toward $s_{br} = 1$ is best fitted by three exponentials (eq 5). From this fit, we extract characteristic times of three different modes and define the overall characteristic bridge-stretching time τ_{bs} accordingly (eq 6).

$$f(t) = 1 + \sum_{i=1}^{3} a_i \exp\left(-\frac{t}{\tau_i}\right) \tag{5}$$

$$\tau_{bs} = \sum_{i=1}^{3} a_i \tau_i \tag{6}$$

The resulting values τ_{bs} are provided in Table 1 and Figure 9. The latter also shows the characteristic times of the modes τ_i

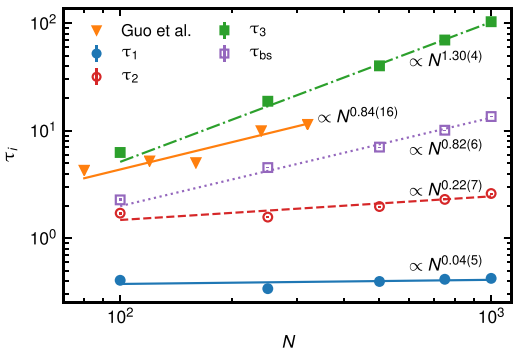

Figure 9. Modes extracted from the stretching of bridges. Shown are the three characteristic times τ_i derived by fitting eq 5 to s_{br} (Figure 8b), as well as the bridge-stretching time τ_{bs} (eq 6). Data from Guo et al. were extracted from ref 39 (see also ref 72). The lines indicate the best fit of the respective set as $\tau_i \propto N^{\mu}$. Error bars are within the symbol sizes.

and of the second collapse stage reported by Guo et al.[72] The scaling of the τ_i and the bridge-stretching time τ_{bs} with the chain length N allows two interesting insights. First, the value of $\tau_{bs} = 13.56(8)$ for $N = 1000$ meets the visually estimated onset of backbone deformation in both the mean squared spatial distance and the snapshots (Figures 2 and 3). τ_{bs} also bears a strong resemblance to the estimated end times of the plateau in $\langle R_g^2(t)\rangle$: Earlier, we estimated this offset to end after the collapse progressed by 10% (symbols in the inset of Figure 4). The respective times were 1.56, 2.10, 2.52, 6.42, 12.12, 16.56, and 20.64 t_{DPD} for $N = 50 - 1000$, which is close to the observed τ_{bs}. Notably, their $\propto N^{0.85(3)}$ scaling is very similar to our observation of $\tau_{bs} \propto N^{0.82(6)}$. The characteristic bridge-stretching time, even though being derived from local structures, can thus also be approached from a global viewpoint. Moreover, $\tau_{bs} \propto N^{0.82(6)}$ is in excellent agreement with *our* fit of the data reported by Guo et al. ($\propto N^{0.84(16)}$), which have the same order of magnitude. On the other hand, our scaling of the bridge-stretching stage deviates from Halperin and Goldbart's suggested behavior of $\tau_{bs} \propto N^{0.2}$.

Second, we find that the scaling of our *modes contributing to bridge-stretching* ($\tau_1 \propto N^{0.04(5)}$, $\tau_2 \propto N^{0.22(7)}$, and $\tau_3 \propto N^{1.30(4)}$) are in striking resemblance to the scaling of *different collapse stages* proposed by Halperin and Goldbart[26] of $\tau_p \propto N^0$, $\tau_{bs} \propto N^{0.2}$, and $\tau_{pn} \propto N^{1.2}$. To interpret this similarity, it is crucial to realize that their scaling predictions often assume one dominating mechanism per stage. The discussion of the second stage is based on the model of a collapsing chain with fixed ends − therefore, a pure $\propto N^{0.2}$ scaling implies that the chain shrinks only after all short-scale processes are terminated. The $\tau_{pn} \propto N^{1.2}$ scaling of the third stage, on the other hand, is traced to the dominance of the stretched bridges' dissipative contribution over two other dissipation mechanisms during the collapse of the pearl necklace. To our understanding, their scaling predictions thus apply to mechanisms rather than collapse stages. In our attempt to fit the stretching of the bridges, we detect contributions of all three important

https://dx.doi.org/10.1021/acs.macromol.0c01315
Macromolecules 2020, 53, 8889−8900

mechanisms − formation of blobs by squeezing out the surrounding solvent beads, growth of blobs by sucking in beads of bridges, and displacement of beads due to the chain's deformation − inseparably acting as bridges are stretched. The characteristic time of the bridge-stretching stage appears to be the weighted sum of the processes' characteristic times.

Collapse of the Pearl Necklace. The bridge-stretching regime terminates in a characteristic pearl necklace structure (Figure 3h).[12,26] While local segments are fully collapsed, the chain's primitive path is still mostly undeformed (see Figure 2). The chain cannot further collapse without blobs displacing.[26] Upon collapse of the pearl necklace, blobs merge, with their root-mean-square radius of gyration (Figure 7, gray line) repeatedly increasing in an abrupt fashion. This is always followed by a smooth decay, which indicates the formation of prolate structures smoothly assembling into a spherical shape. As indicated by the mean squared spatial distance (Figure 2), the latter happens upon relaxation of short chain segments. We note that both mechanisms depend on the chain model employed: Simulations of semiflexible chains suggest a formation of more cylindrical intermediate structures,[62,73] while a restriction of bond crossing favors the formation of crumpled structures.[4] After a succession of blob coalescences, the last two blobs form a dumbbell-like structure and eventually merge into a single blob. This is succeeded by internal processes that potentially include reptation-like relaxation not captured by the DPD model.[11,14] We define the characteristic time of the collapse of the pearl necklace as the point where the number of blobs becomes 1. This time τ_{pn} is derived for every individual run, and the average values are given in Table 1. We find an apparent scaling of $\tau_{pn} \propto N^{1.04(2)}$, which is close to the exponent of 0.99(11) reported by Guo et al.[39] Halperin and Goldbart[26] considered three major dissipation mechanisms contributing to the collapse of the pearl necklace: the hydrodynamic flow of solvent around the blobs (with a characteristic time $\tau \propto N^{0.8}$), the contribution of stretched bridges ($\propto N^{1.2}$), and the motion of blobs ($\propto N^{1.07}$). While the bridge dissipation is suggested to be the dominating mode for sufficiently strong quenches, lower quenches favor the hydrodynamic contribution.[26] Our scaling exponent, however, rather supports the motion of blobs as the dominant process. On the other hand, we deem it likely that our scaling exponent stems from multiple underlying mechanisms rather than a single, dominating one.

Summation of all three now-derived characteristic times is an alternative way to derive the overall collapse time.[39] We find that this accumulated characteristic time is very similar to the collapse time τ_c, which was derived earlier from the chains' $\langle R_g^2 \rangle^{0.5}$. Accordingly, it scales as $(\tau_p + \tau_{bs} + \tau_{pn}) \propto N^{1.01(3)}$, which confirms the dominance of the pearl necklace stage as well as the linear relation between N and τ_c.

Growth of the Blob Size. We finally discuss the growth of blobs along the chain during the collapse. We consider the number-averaged blob size $\langle S_n \rangle$ as a function of time, as shown in Figure 10 in a linear and logarithmic presentation. Visual inspection of the linear plot indicates an approximately linear behavior for $N \leq 250$. Indeed, a scaling exponent of $z = 0.984(2)$ is obtained for a fit of $\langle S(t) \rangle = At^z$ for $N = 250$ and $t \in [10,50]$, where A is a constant. Literature values differ for systems incorporating hydrodynamic interactions: While scaling predictions of Klushin[12] and Kikuchi et al.[70] suggested sublinear scaling of $z = 0.8$ and 0.75, respectively, Pham et al.[28] and Guo et al.[39] reported a linear growth with $z = 1.08$ and 0.95 for their Brownian dynamics and DPD simulations. However, they only investigated chain lengths up to $N = 128$ and 320. In our simulations, we find the growth of blobs to be less intuitive for longer chains. For $N = 1000$, we observe multiple regions with scaling coefficients strongly depending on the choice of the fitting region. For example, fitting of $\langle S(t) \rangle = At^z$ yields $z = 0.744(2)$, 1.141(2), and 1.453(4) for $t \in [10,50]$, $t \in [50,100]$, and $t \in [150,200]$, respectively. The inconsistent behavior is further emphasized in the logarithmic presentation (inset in Figure 10). With increasing chain length, the regions following a $\propto t^z$ behavior become less pronounced. On short timescales, a scaling of $z \approx 2/3$ is indicated (black line), a value occasionally observed in systems without hydrodynamic interactions.[28,74] The logarithmic presentation also reveals an overlap of all data in the pearling and bridge-stretching stages irrespective of N. This is in line with previous findings for the normalized number of blobs (Figure 6c), and it stresses that the growth mechanism is indeed independent of the chain length during early collapse stages.[74] However, the collapse of curves is visibly weaker for $\langle S_n(t) \rangle$ than for N_{bl}/N, which is possibly due to a certain polydispersity in the blob sizes. In any case, the overlap does not hold over the whole range of the collapse of the pearl necklace.

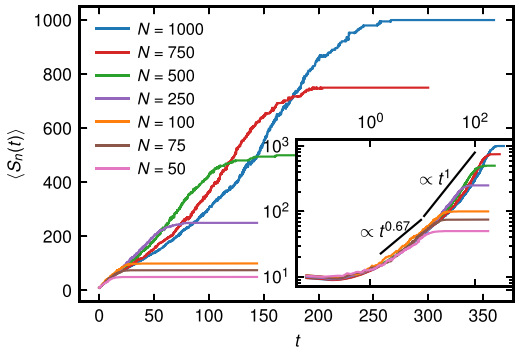

Figure 10. Number-averaged blob size $\langle S_n(t) \rangle$ (in number of beads) for chains of different chain lengths N as a function of time. All lines are the average over 100 independent runs. The inset shows a logarithmic presentation of $\langle S_n(t) \rangle$. The black lines in the inset indicate the slopes for $t^{0.67}$ and t^1 scaling.

A different approach to the growth of blobs along a collapsing chain has been recently proposed by Majumder and co-workers.[41,42] They attributed the nonlinearity as well as the inadequate overlap between curves for different N in their kinetic Monte Carlo systems to two factors: First, offsets in time and cluster size, t_0 and S_0, are assumed to impede the identification of a power-law scaling. To account for this, Majumder et al. described the blob size evolution as

$$\langle S_n(t) \rangle = S_0 + A(t - t_0)^z \tag{7}$$

Second, they identify finite-size effects for $\langle S_n \rangle \approx N$, i.e., for the last collapse steps. Both effects are considered in their finite-size scaling analysis, a method originally developed to describe behavior close to a critical point such as a phase transition.[75] The method revolves around a convenient definition of a scaling function $Y(y)$ and a scaling variable y. Following ref 42, we introduce $Y(y)$ into eq 7:

$$\langle S_n(t) \rangle - S_0 = A(t - t_0)^z = (N - S_0)Y(y) \tag{8}$$

https://dx.doi.org/10.1021/acs.macromol.0c01315
Macromolecules 2020, 53, 8889−8900

$$Y(y) = \frac{\langle S_n(t)\rangle - S_0}{N - S_0} \tag{9}$$

The scaling variable is chosen as

$$y = \frac{(N - S_0)^{1/z}}{t - t_0} \tag{10}$$

Thus, in the finite-size limit ($t \to \infty$, $\langle S_n(t)\rangle \to N$), $y \to 0$ and $Y(y) \to 1$ apply. Importantly, the expected behavior of the scaling function in the finite-size unaffected regime is

$$Y(y) = \frac{\langle S_n(t)\rangle - S_0}{N - S_0} = \frac{A(t - t_0)^z}{N - S_0} = Ay^{-z} \tag{11}$$

In the finite-size scaling analysis, the scaling coefficient z and the offset time t_0 are input parameters. For an adequate set of parameters and a data set well-described by the scaling function, curves for chains of all lengths collapse into a master curve. Furthermore, this curve is expected to show the respective $\propto y^{-z}$ behavior in the finite-size unaffected regime. We follow the suggestion of Majumder and Janke[41] and use the terminal condition of the pearling stage as a choice for t_0 and S_0, i.e., $t_0 = 0.24$ and $S_0 = \langle S_n(t_0)\rangle$. Values of $z = 0.67$ and $z = 1$ are chosen from the behavior indicated in Figure 10. The application of the finite-size scaling analysis to our data is shown in Figure 11. It is clear that both aforementioned

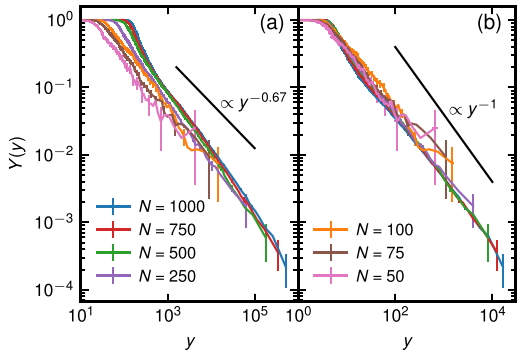

Figure 11. Results of the finite-size scaling analysis for $z = 0.67$ (a) and 1 (b). The scaling function $Y(y)$ and scaling variable y are derived from the growth of the number-averaged blob sizes (see text). The black lines indicate the expected scaling. Error bars are shown for every fifth value. Note that, at low y, they hardly exceed the line width.

criteria are well met for $z = 1$ (Figure 11b). We observe a collapse of data for all chain lengths, which is especially true in the finite-size regime where $\langle S_n(t)\rangle \approx N$ and thus $Y(y) \approx 1$. For earlier times (high values of y), a distinct $Y(y) \propto y^{-1}$ behavior is observed. Both features are striking compared to the $z = 0.67$ assumption (Figure 11a), where no overlap of data is achieved. This becomes most apparent in the finite-size regime, where data sets diverge far more than their error bars. Additionally, the decay is significantly steeper than the expected $y^{-0.67}$ behavior, which indicates that the true scaling is not met.[42] To investigate the scaling, we employ an alternative presentation of Figure 11 with a scaled y-axis of $Y(y) \times y^z$ for values of $z = 0.67$,0.9,1.0, and 1.1 (Figure S2, Supporting Information). Here, $\propto y^{-z}$ scaling is indicated by a horizontal course, which we find to be the case for $z = 1.0$. Multiple conclusions can be drawn from these observations: First, the cluster growth can indeed be described as $\langle S_n(t)\rangle \propto t$. While this behavior has been found for shorter chains, we confirm it for chain lengths up to $N = 1000$, even though the effects of fewer, larger blobs become prevalent for $N \geq 500$. Second, the y^{-1} scaling for short times (high values of y) endorses the choice of t_0. We tested different values for t_0 and found $t = 0.24$ to be the shortest possible time retaining this behavior. Given that these values were originally found to be the point in time where blobs are most compact, we can now confirm this to be the transition point between blob formation and growth. Third, our results of z and the scaling of the collapse time, $\tau_c \propto N^\gamma$, hold for a relation sometimes made in scaling arguments.[14,70] If blobs grow constantly over the whole collapse process, a simple assumption is $\langle S_n(\tau_c)\rangle \propto \tau_c^z \approx N \Rightarrow 1/z \approx \gamma$. Our results of $\gamma = 0.94(2)$ and $z \approx 1$ support this relation.

CONCLUSIONS

We investigated the collapse pathway and scaling behavior of explicit-solvent DPD bead-spring chains with lengths up to 1000 beads when suddenly brought into poor-solvent conditions. To our knowledge, these are the so far longest chains studied under a quench that fulfill all our requirements of an explicit solvent and initial good-solvent scaling. An extended clustering algorithm was used to identify local structures along the collapsing chains, so-called blobs and bridges. Blobs are aggregations of DPD beads along the chain's original backbone, and bridges are slack segments connecting them. We found that descriptors commonly used in single-chain collapse agreed well with other explicit-solvent models: In our systems, the exponents γ and α for the scaling of the characteristic collapse time ($\tau_c \propto N^\gamma$) and the initial decay of the mean square radius of gyration $R_g^2(0) - R_g^2(t) \propto t^\alpha$ were $\gamma = 0.94(2)$ and $\alpha = 1.09(1)$. A linear behavior ($z \approx 1$) was also found for the growth of blob sizes over time ($\langle S_n\rangle \propto t^z$). The latter was, however, strongly affected by finite-size effects for low blob numbers ($\langle S_n(t)\rangle \approx N$) and long chains ($N \geq 500$) in the last collapse stage and could only be confirmed after employing a finite-size scaling analysis that has been recently suggested in an implicit-solvent study.[42]

Our simulations corroborate the three-stage pathway proposed by Halperin and Goldbart.[26] Blobs are initially formed by local contraction of beads in the pearling stage. In the bridge-stretching stage, blobs grow while swallowing beads from neighboring bridges, which causes them to stretch. Last, the characteristic structure thereby formed, known as a pearl necklace, collapses as blobs merge to eventually form a single globule. We did not study internal rearrangements, equilibration, and knotting *inside* the final globule, which is viewed as a potential fourth stage but cannot be properly modeled by our soft-core model. By quantifying blob- and bridge-related properties of local structures, namely, their number and size, the radius of gyration of blobs, and the stretchedness of bridges, we found characteristic times for each stage of the collapse (Table 1). The respective times show an apparent power-law scaling with the chain lengths as $\tau_p \propto N^0$ (pearling), $\tau_{bs} \propto N^{0.82(6)}$ (bridge-stretching), and $\tau_{pn} \propto N^{1.04(2)}$ (pearl necklace coalescence). Differences from the scaling proposed by Halperin and Goldbart are attributed to the approximations made in their model: By analyzing the bridges' stretching factor, we found relevant contributions of different dissipative mechanisms, as opposed to a single, dominant one.

In summary, we presented an alternative route to comprehend the development of local structures in single-

https://dx.doi.org/10.1021/acs.macromol.0c01315
Macromolecules 2020, 53, 8889−8900

chain collapse to contribute to the understanding of dynamical processes in collapsing homopolymers. We believe that our approach will be useful in future studies of related systems, such as quenched heteropolymers,[76] stiff chains,[4] or hydrogels.[77]

■ ASSOCIATED CONTENT

Supporting Information

The Supporting Information is available free of charge at https://pubs.acs.org/doi/10.1021/acs.macromol.0c01315.

Presentation and brief discussion of the non-Gaussian parameter; alternative presentation of Figure 11 scaled by y^z for different exponents z = 0.67,0.9,1.0, and 1.1 (PDF)

■ AUTHOR INFORMATION

Corresponding Authors

Jurek Schneider − *Eduard-Zintl-Institut für Anorganische und Physikalische Chemie and Profile Area Thermofluids and Interfaces, Technische Universität Darmstadt, D-64287 Darmstadt, Germany;* orcid.org/0000-0002-0286-1678; Email: j.schneider@theo.chemie.tu-darmstadt.de

Florian Müller-Plathe − *Eduard-Zintl-Institut für Anorganische und Physikalische Chemie and Profile Area Thermofluids and Interfaces, Technische Universität Darmstadt, D-64287 Darmstadt, Germany;* orcid.org/0000-0002-9111-7786; Email: f.mueller-plathe@theo.chemie.tu-darmstadt.de

Authors

Melissa K. Meinel − *Eduard-Zintl-Institut für Anorganische und Physikalische Chemie and Profile Area Thermofluids and Interfaces, Technische Universität Darmstadt, D-64287 Darmstadt, Germany;* orcid.org/0000-0001-7369-3627

Han Dittmar − *Eduard-Zintl-Institut für Anorganische und Physikalische Chemie and Profile Area Thermofluids and Interfaces, Technische Universität Darmstadt, D-64287 Darmstadt, Germany*

Complete contact information is available at: https://pubs.acs.org/10.1021/acs.macromol.0c01315

Notes

The authors declare no competing financial interest.

■ ACKNOWLEDGMENTS

This work has in part been funded by the Deutsche Forschungsgemeinschaft. Some simulations were performed on the Lichtenberg high-performance computer of the TU Darmstadt.

■ REFERENCES

(1) Williams, C.; Brochard, F.; Frisch, H. L. Polymer collapse. *Annu. Rev. Phys. Chem.* **1981**, *32*, 433−451.

(2) de Gennes, P.-G. Kinetics of collapse for a flexible coil. *J. Phys., Lett.* **1985**, *46*, 639−642.

(3) Pollack, L.; Tate, M. W.; Finnefrock, A. C.; Kalidas, C.; Trotter, S.; Darnton, N. C.; Lurio, L.; Austin, R. H.; Batt, C. A.; Gruner, S. M.; Mochrie, S. G. J. Time resolved collapse of a folding protein observed with small angle X-ray scattering. *Phys. Rev. Lett.* **2001**, *86*, 4962−4965.

(4) Chertovich, A.; Kos, P. Crumpled globule formation during collapse of a long flexible and semiflexible polymer in poor solvent. *J. Chem. Phys.* **2014**, *141*, 134903.

(5) Johnson, B. K.; Prud'homme, R. K. Flash nanoprecipitation of organic actives and block copolymers using a confined impinging jets mixer. *Aust. J. Chem.* **2003**, *56*, 1021−1024.

(6) Johnson, B. K.; Prud'homme, R. K. Chemical processing and micromixing in confined impinging jets. *AIChE J.* **2003**, *49*, 2264−2282.

(7) Nikoubashman, A.; Lee, V. E.; Sosa, C.; Prud'homme, R. K.; Priestley, R. D.; Panagiotopoulos, A. Z. Directed assembly of soft colloids through rapid solvent exchange. *ACS Nano* **2016**, *10*, 1425−1433.

(8) Schneider, J.; Panagiotopoulos, A. Z.; Müller-Plathe, F. Polymer chain collapse upon rapid solvent exchange: Slip-spring dissipative particle dynamics simulations with an explicit-solvent model. *J. Phys. Chem. C* **2017**, *121*, 27664−27673.

(9) Morozova, T. I.; Nikoubashman, A. Coil−globule collapse of polystyrene chains in tetrahydrofuran−water mixtures. *J. Phys. Chem. B* **2018**, *122*, 2130−2137.

(10) Grosberg, A. Y.; Nechaev, S. K.; Shakhnovich, E. I. The role of topological constraints in the kinetics of collapse of macromolecules. *J. Phys.* **1988**, *49*, 2095−2100.

(11) Grosberg, A. Y.; Kuznetsov, D. V. Single-chain collapse or precipitation? Kinetic diagram of the states of a polymer solution. *Macromolecules* **1993**, *26*, 4249−4251.

(12) Klushin, L. I. Kinetics of a homopolymer collapse: Beyond the Rouse−Zimm scaling. *J. Chem. Phys.* **1998**, *108*, 7917−7920.

(13) Abrams, C. F.; Lee, N.-K.; Obukhov, S. P. Collapse dynamics of a polymer chain: Theory and simulation. *Europhys. Lett.* **2002**, *59*, 391−397.

(14) Kuznetsov, Y. A.; Timoshenko, E. G.; Dawson, K. A. Kinetics at the collapse transition of homopolymers and random copolymers. *J. Chem. Phys.* **1995**, *103*, 4807−4818.

(15) Timoshenko, E. G.; Dawson, K. A. Equilibrium properties of polymers from the Langevin equation: Gaussian self-consistent approach. *Phys. Rev. E* **1995**, *51*, 492−498.

(16) Timoshenko, E. G.; Kuznetsov, Y. A.; Dawson, K. A. Kinetics at the collapse transition Gaussian self-consistent approach. *J. Chem. Phys.* **1995**, *102*, 1816−1823.

(17) Kuznetsov, Y. A.; Timoshenko, E. G.; Dawson, K. A. Kinetic laws at the collapse transition of a homopolymer. *J. Chem. Phys.* **1996**, *104*, 3338−3347.

(18) Timoshenko, E. G.; Kuznetsov, Y. A.; Dawson, K. A. Kinetics of a Gaussian random copolymer as a prototype for protein folding. *Phys. Rev. E* **1996**, *54*, 4071−4086.

(19) Yu, J.; Wang, Z.; Chu, B. Kinetic study of coil-to-globule transition. *Macromolecules* **1992**, *25*, 1618−1620.

(20) Chu, B.; Ying, Q.; Grosberg, A. Y. Two-stage kinetics of single-chain collapse. Polystyrene in cyclohexane. *Macromolecules* **1995**, *28*, 180−189.

(21) Zhu, P. W.; Napper, D. H. The longer time collapse kinetics of interfacial poly(N-isopropylacrylamide) in water. *J. Chem. Phys.* **1997**, *106*, 6492−6498.

(22) Xu, J.; Zhu, Z.; Luo, S.; Wu, C.; Liu, S. First observation of two-stage collapsing kinetics of a single synthetic polymer chain. *Phys. Rev. Lett.* **2006**, *96*, No. 027802.

(23) Ostrovsky, B.; Bar-Yam, Y. Irreversible polymer collapse in 2 and 3 dimensions. *Europhys. Lett.* **1994**, *25*, 409−414.

(24) Ostrovsky, B.; Bar-Yam, Y. Motion of polymer ends in homopolymer and heteropolymer collapse. *Biophys. J.* **1995**, *68*, 1694−1698.

(25) Crooks, G. E.; Ostrovsky, B.; Bar-Yam, Y. Mesostructure of polymer collapse and fractal smoothing. *Phys. Rev. E* **1999**, *60*, 4559−4563.

(26) Halperin, A.; Goldbart, P. M. Early stages of homopolymer collapse. *Phys. Rev. E* **2000**, *61*, 565−573.

(27) Pitard, E. Influence of hydrodynamics on the dynamics of a homopolymer. *Eur. Phys. J. B* **1999**, *7*, 665−673.

(28) Pham, T. T.; Bajaj, M.; Prakash, J. R. Brownian dynamics simulation of polymer collapse in a poor solvent: Influence of implicit hydrodynamic interactions. *Soft Matter* **2008**, *4*, 1196−1207.

(29) Kamata, K.; Araki, T.; Tanaka, H. Hydrodynamic selection of the kinetic pathway of a polymer coil-globule transition. *Phys. Rev. Lett.* **2009**, *102*, 108303.
(30) Polson, J. M.; Zuckermann, M. J. Simulation of heteropolymer collapse with an explicit solvent in two dimensions. *J. Chem. Phys.* **2000**, *113*, 1283−1293.
(31) Chang, R.; Yethiraj, A. Solvent effects on the collapse dynamics of polymers. *J. Chem. Phys.* **2001**, *114*, 7688−7699.
(32) Polson, J. M.; Zuckermann, M. J. Simulation of short-chain polymer collapse with an explicit solvent. *J. Chem. Phys.* **2002**, *116*, 7244−7254.
(33) Reddy, G.; Yethiraj, A. Implicit and explicit solvent models for the simulation of dilute polymer solutions. *Macromolecules* **2006**, *39*, 8536−8542.
(34) Jentzsch, C.; Werner, M.; Sommer, J.-U. Single polymer chains in poor solvent: Using the bond fluctuation method with explicit solvent. *J. Chem. Phys.* **2013**, *138*, No. 094902.
(35) Christiansen, H.; Majumder, S.; Janke, W. Coarsening and aging of lattice polymers: Influence of bond fluctuations. *J. Chem. Phys.* **2017**, *147*, No. 094902.
(36) Pitard, E.; Orland, H. Dynamics of the swelling or collapse of a homopolymer. *Europhys. Lett.* **1998**, *41*, 467−472.
(37) Majumder, S.; Christiansen, H.; Janke, W. Scaling laws during collapse of a homopolymer: Lattice versus off-lattice. *J. Phys.: Conf. Ser.* **2018**, *955*, No. 012008.
(38) Lee, S. H.; Kapral, R. Mesoscopic description of solvent effects on polymer dynamics. *J. Chem. Phys.* **2006**, *124*, 214901.
(39) Guo, J.; Liang, H.; Wang, Z.-G. Coil-to-globule transition by dissipative particle dynamics simulation. *J. Chem. Phys.* **2011**, *134*, 244904.
(40) Masubuchi, Y.; Langeloth, M.; Böhm, M. C.; Inoue, T.; Müller-Plathe, F. A multichain slip-spring dissipative particle dynamics simulation method for entangled polymer solutions. *Macromolecules* **2016**, *49*, 9186−9191.
(41) Majumder, S.; Janke, W. Cluster coarsening during polymer collapse: Finite-size scaling analysis. *EPL* **2015**, *110*, 58001.
(42) Majumder, S.; Zierenberg, J.; Janke, W. Kinetics of polymer collapse: Effect of temperature on cluster growth and aging. *Soft Matter* **2017**, *13*, 1276−1290.
(43) Hoogerbrugge, P. J.; Koelman, J. M. V. A. Simulating microscopic hydrodynamic phenomena with dissipative particle dynamics. *Europhys. Lett.* **1992**, *19*, 155.
(44) Español, P.; Warren, P. Statistical mechanics of dissipative particle dynamics. *Europhys. Lett.* **1995**, *30*, 191.
(45) Groot, R. D.; Warren, P. B. Dissipative particle dynamics: Bridging the gap between atomistic and mesoscopic simulation. *J. Chem. Phys.* **1997**, *107*, 4423−4435.
(46) Spaeth, J. R.; Kevrekidis, I. G.; Panagiotopoulos, A. Z. A comparison of implicit- and explicit-solvent simulations of self-assembly in block copolymer and solute systems. *J. Chem. Phys.* **2011**, *134*, 164902.
(47) Spaeth, J. R.; Dale, T.; Kevrekidis, I. G.; Panagiotopoulos, A. Z. Coarse-graining of chain models in dissipative particle dynamics simulations. *Ind. Eng. Chem. Res.* **2011**, *50*, 69−77.
(48) Spaeth, J. R.; Kevrekidis, I. G.; Panagiotopoulos, A. Z. Dissipative particle dynamics simulations of polymer-protected nanoparticle self-assembly. *J. Chem. Phys.* **2011**, *135*, 184903.
(49) Schneider, J.; Süss, L. D.; Müller-Plathe, F. The influence of entanglements on the dynamics of flash nanoprecipitation: A slip-spring dissipative-particle-dynamics investigation. *J. Chem. Eng. Data* **2020**, *65*, 1264−1272.
(50) Spenley, N. A. Scaling laws for polymers in dissipative particle dynamics. *Europhys. Lett.* **2000**, *49*, 534.
(51) Kong, Y.; Manke, C. W.; Madden, W. G.; Schlijper, A. G. Effect of solvent quality on the conformation and relaxation of polymers via dissipative particle dynamics. *J. Chem. Phys.* **1997**, *107*, 592−602.
(52) Schlijper, A. G.; Hoogerbrugge, P. J.; Manke, C. W. Computer simulation of dilute polymer solutions with the dissipative particle dynamics method. *J. Rheol.* **1995**, *39*, 567−579.
(53) Symeonidis, V.; Karniadakis, G. E.; Caswell, B. Dissipative particle dynamics simulations of polymer chains: scaling laws and shearing response compared to DNA experiments. *Phys. Rev. Lett.* **2005**, *95*, No. 076001.
(54) Ilnytskyi, J. M.; Holovatch, Y. How does the scaling for the polymer chain in the dissipative particle dynamics hold? *Condens. Matter Phys.* **2007**, *10*, 539−551.
(55) Jiang, W.; Huang, J.; Wang, Y.; Laradji, M. Hydrodynamic interaction in polymer solutions simulated with dissipative particle dynamics. *J. Chem. Phys.* **2007**, *126*, No. 044901.
(56) Nardai, M. M.; Zifferer, G. Simulation of dilute solutions of linear and star-branched polymers by dissipative particle dynamics. *J. Chem. Phys.* **2009**, *131*, 124903.
(57) Pierleoni, C.; Ryckaert, J.-P. Molecular dynamics investigation of dynamic scaling for dilute polymer solutions in good solvent conditions. *J. Chem. Phys.* **1992**, *96*, 8539−8551.
(58) de Gennes, P.-G. Exponents for the excluded volume problem as derived by the Wilson method. *Phys. Lett. A* **1972**, *38*, 339−340.
(59) de Gennes, P.-G. *Scaling concepts in polymer physics*; Cornell University Press: Ithaca, 1979.
(60) Petrov, A.; Kos, P.; Chertovich, A. Kinetic mechanisms of crumpled globule formation. *Soft Matter* **2020**, 2045−2054.
(61) Humphrey, W.; Dalke, A.; Schulten, K. VMD: Visual molecular dynamics. *J. Mol. Graphics* **1996**, *14*, 33−38.
(62) Lappala, A.; Terentjev, E. M. "Raindrop" coalescence of polymer chains during coil−globule transition. *Macromolecules* **2013**, *46*, 1239−1247.
(63) Majumder, S.; Hansmann, U. H. E.; Janke, W. Pearl-necklace-like local ordering drives polypeptide collapse. *Macromolecules* **2019**, *52*, 5491−5498.
(64) Bunin, G.; Kardar, M. Coalescence model for crumpled globules formed in polymer collapse. *Phys. Rev. Lett.* **2015**, *115*, No. 088303.
(65) Imakaev, M. V.; Tchourine, K. M.; Nechaev, S. K.; Mirny, L. A. Effects of topological constraints on globular polymers. *Soft Matter* **2015**, *11*, 665−671.
(66) Schram, R. D.; Barkema, G. T.; Schiessel, H. On the stability of fractal globules. *J. Chem. Phys.* **2013**, *138*, 224901.
(67) Langeloth, M.; Masubuchi, Y.; Böhm, M. C.; Müller-Plathe, F. Recovering the reptation dynamics of polymer melts in dissipative particle dynamics simulations via slip-springs. *J. Chem. Phys.* **2013**, *138*, 104907.
(68) Langeloth, M.; Masubuchi, Y.; Böhm, M. C.; Müller-Plathe, F. Reptation and constraint release dynamics in bidisperse polymer melts. *J. Chem. Phys.* **2014**, *141*, 194904.
(69) Kikuchi, N.; Gent, A.; Yeomans, J. M. Polymer collapse in the presence of hydrodynamic interactions. *Eur. Phys. J. E: Soft Matter Biol. Phys.* **2002**, *9*, 63−66.
(70) Kikuchi, N.; Ryder, J. F.; Pooley, C. M.; Yeomans, J. M. Kinetics of the polymer collapse transition: The role of hydrodynamics. *Phys. Rev. E* **2005**, *71*, No. 061804.
(71) Aichele, M.; Gebremichael, Y.; Starr, F. W.; Baschnagel, J.; Glotzer, S. C. Polymer-specific effects of bulk relaxation and stringlike correlated motion in the dynamics of a supercooled polymer melt. *J. Chem. Phys.* **2003**, *119*, 5290.
(72) For stage two, Guo et al. (ref 39) stated that their data did not allow them to obtain a meaningful scaling exponent for $\tau_{bs} \propto N^{\mu}$. They did, however, report a scaling with the quench depth ξ as $\tau_{bs} \propto \xi^{-0.32(2)}$, where ξ follows, to our understanding, the relation $\xi = 0.0370 \times (a_{PS} - a_{PS}^{\theta})$. $a_{PS}^{\theta} = 27.0$ is the repulsion parameter for θ conditions for their chain model. Although the authors did not provide data for our $a_{PS} = 75$ system, these two relations allow us to rescale their values of τ_{bs} to our environment.
(73) Ivanov, V. A.; Martemyanova, J. A.; Rodionova, A. S.; Stukan, M. R. Computer simulation of stiff-chain polymers. *Polym. Sci. Ser. C* **2013**, *55*, 4−22.
(74) Byrne, A.; Kiernan, P.; Green, D.; Dawson, K. A. Kinetics of homopolymer collapse. *J. Chem. Phys.* **1995**, *102*, 573−577.

https://dx.doi.org/10.1021/acs.macromol.0c01315
Macromolecules 2020, 53, 8889−8900

(75) Privman, V. *Finite size scaling and numerical simulation of statistical systems*; World Scientific: Singapore, 1990, DOI: 10.1142/1011.
(76) Pham, T. T.; Dünweg, B.; Prakash, J. R. Collapse dynamics of copolymers in a poor solvent: Influence of hydrodynamic interactions and chain sequence. *Macromolecules* **2010**, *43*, 10084−10095.
(77) Kamerlin, N.; Elvingson, C. Collapse dynamics of core−shell nanogels. *Macromolecules* **2016**, *49*, 5740−5749.

https://dx.doi.org/10.1021/acs.macromol.0c01315
Macromolecules 2020, 53, 8889−8900

Journal of chemical & engineering data

Article

Cite This: *J. Chem. Eng. Data* 2020, 65, 1264–1272

pubs.acs.org/jced

The Influence of Entanglements on the Dynamics of Flash Nanoprecipitation: A Slip-Spring Dissipative-Particle-Dynamics Investigation

Jurek Schneider,* Leonard D. Süss, and Florian Müller-Plathe*

Eduard-Zintl-Institut für Anorganische und Physikalische Chemie and Profile Area Thermofluids and Interfaces, Technische Universität Darmstadt, Alarich-Weiss-Straße 8, D-64287 Darmstadt, Germany

ABSTRACT: We study the precipitation of polymer solutions using explicit-solvent dissipative particle dynamics. We investigate the influence of slip springs as an incarnation of entanglements on the aggregation dynamics. In a set of simulations, the precipitation of a 1% solution of chains of lengths of 75, 100, 150, and 200 beads is analyzed as 50% of the solvent is suddenly exchanged for antisolvent. We find that the aggregation includes a network-like stage where most polymers are entirely globular and bridged by some elongated chains. Effects of entanglements on this structure are investigated by imposing different numbers of slip springs onto the precipitating chains. We find the influence of these entanglements or the chain length on the collapse time and structure of the formed nanoparticles to be very limited.

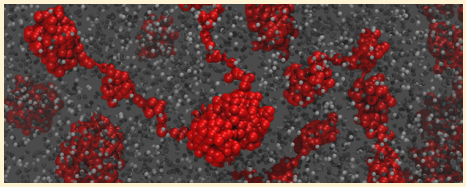

INTRODUCTION

For the past two decades, the production of colloids has been intensively studied both by experiments and simulations. Notions of how they can be produced in a controlled fashion are still being challenged today. A promising and by now well-established approach is the production of kinetically frozen nanoparticles by rapid mixing of a polymer solution with an antisolvent, that is, a fluid miscible with the solvent but immiscible with the polymer.[1−3] Developed in 2003 by Johnson and Prud'homme,[4] "Flash Nanoprecipitation" (FNP) evolved into a convenient tool to target various applications:[5−7] Scalability as well as excellent and independent control over particle size and composition allowed the production of structured particles from both homopolymer blends and copolymers. Target systems were, for example, patchy,[8] core−shell and Janus,[9,10] or internally structured particles.[11] Computational studies frequently assisted experiments to understand relations between experimental parameters and aggregation behavior.[11−13] However, purely theoretical and computational studies also became a well-established tool to explore the collapse dynamics and the self-assembly of dissolved, isolated chains as well as polymer solutions.[14−18] A first study by Spaeth et al. investigated the influence of solvent particles comparing implicit-solvent Brownian dynamics and explicit-solvent dissipative particle dynamics (DPD) simulations in which solvent particles were suddenly exchanged by antisolvent particles.[19] They stated the need for an explicit-solvent system and stressed the suitability of DPD to show correct diffusion behavior of growing nanoparticles.[19] In a second study, they used their DPD model to investigate the role of experimental parameters such as the mixing time, solute solubility, and different compositions on the precipitation of polymer-protected nanoparticles. The transition from solvent to antisolvent happened by a gradual worsening of *all* polymer−solvent interactions.[20] This approach has been used in simulations ever since: Questions studied were, for example, the influence of surface charges on the direct assembly of colloids,[12] the self-assembly of homopolymer blends into Janus particles[21] and patchy particles,[22] and the self-assembly of nanoparticles in binary polymer blends.[23]

In a first study,[24] we employed a slightly different technique to investigate single-chain collapse under rapid solvent exchange: We exchanged 50% of the solvent particles by antisolvent instantaneously *outside* a defined volume around the polymer chain. We found the dynamics of the polymer chain collapse to be mainly governed by the distance that the antisolvent has to diffuse toward the chain. We also detected solvent trapping and the formation of a solvent-rich layer around the collapsed globule, which was later confirmed by atomistic simulations.[25] We could, however, not detect any influence of self-entanglement of a single chain on its collapse dynamics.

In the present study, we extend our earlier work to explore precipitation dynamics of polymer solutions of many polymer chains. We use the bead−spring DPD model with explicit solvent and slip springs developed previously in our group[26,27] to simulate large systems of up to 1.1×10^6 particles. Slip springs are widely used to restore entanglement effects in simulations suffering from bond crossing due to soft-core interactions.[28−32] They were previously applied to simulations of mono- and bidisperse polymer melts[26,27] and polymer solutions.[33] Here, we use them to study steric interactions of

Special Issue: Hans Hasse

Received: July 12, 2019
Accepted: September 30, 2019
Published: October 14, 2019

collapsing chains and try to answer the following question: How is precipitation of polymer solutions influenced by entanglements, that is, slip springs we impose onto our system? This paper outlines our methods to simulate slip spring DPD and solvent-to-antisolvent exchange. We present results for the precipitation of polymer solution systems entangled to different degrees, and the behavior of slip springs in the rapidly changing environment.

METHODS

Model. Simulations were performed using dissipative particle dynamics (DPD) simulations.[34−36] The methodology used in this work follows ref 36 of Groot and Warren. Details can be found in section Simulation Details. DPD uses solely pairwise interactions consisting of a stochastic part, a friction part, and a coarse-grained, soft-core conservative potential. Simple DPD models have been used for a variety of applications, including nonequilibrium studies of single-chain collapse[24] and flash nanoprecipitation.[19,20]

As an effect of the soft-core potential, polymer chains are allowed to cross each other, which prevents them from following entangled dynamics in polymer melts or dense solutions as described by, for example, de Gennes.[37] Hard-core molecular models such as the Kremer-Grest model[38] show reptation, but have long simulation times. Instead, we restore entanglements to DPD using slip springs, that is, artificial, mobile bonds. We follow the work of Langeloth et al.,[26,27] in which slip springs connect different, nonbonded beads, and migrate along the chains following a Metropolis Monte Carlo (MC) algorithm. Alternating blocks of DPD and MC allow a slip-spring mobility high enough to let them migrate even during fast chain collapse.[24] For more information, see the section Simulation Details or the original work in ref 26. Flash nanoprecipitation is initiated by instantaneously exchanging 50% of the solvent for the antisolvent at a mixing time of 0. This is in contrast to previous works, where usually the solvent quality of *all* solvent particles was changed either instantaneously[19] or gradually over time.[20,12,21] Because effects such as solvent trapping and the formation of a solvent layer are known to play a role during the collapse,[24,25] we would like all three species to remain present in the system. Solvent and antisolvent are modeled as nonconnected beads of the same size as monomer beads. Polymer−antisolvent interactions are twice as repulsive as solvent−solvent interactions, polymer−solvent and solvent−antisolvent interactions.

The bead−spring chain model is that of Langeloth et al.[26,27] and Masubuchi et al.[33] It was used for solvent exchange simulations in an earlier work.[24] Polymer chains of four different chain length were simulated with various numbers of slip springs. Slip springs as well as bonded interactions are treated as harmonic bonds (eq 1).

$$\mathbf{F}_{ij}^{\mathrm{B,SS}} = -k\mathbf{r}_{ij} \tag{1}$$

As slip springs are not allowed to attach to solvent- or antisolvent beads, their number must be chosen in consideration of the polymer concentration. The theoretical, concentration-dependent total number of slip springs $N_{\mathrm{SS}}^{\mathrm{theo}}(\varphi)$ can be derived from the respective value in polymer melts ($N_{\mathrm{SS}}^{\mathrm{theo}}(\varphi = 1)$) as

$$N_{\mathrm{SS}}^{\mathrm{theo}}(\varphi) = N_{\mathrm{SS}}^{\mathrm{theo}}(1)\varphi^{1+\alpha} \tag{2}$$

where α is a dilution exponent between 1.0 and 1.3.[39−41] In this work, however, solvent-to-antisolvent exchange inevitably leads to a collapse of all polymer chains; this makes bond crossing an event occurring more frequently as the simulation progresses. For this reason, we run simulations with different slip spring numbers for every system. The number of slip springs is kept constant during the precipitation process. Slip springs can, however, become inactive, as discussed in the section Results and Discussion. An alternative approach would be the use of a concentration-dependent slip spring number.[29,33] Creation and destruction of these slip springs in models proposed by , for example, Uneyama and Masubuchi[29] depend on a "chemical potential" associated with the slip spring density. We refrain from going down this path as we find the interpretation of a chemical potential of (already artificial) slip springs not straightforward. Instead, we believe that a fixed number of slip springs eases the interpretation of their role in the precipitation process, which is the purpose of this work.

Simulation Details. Reduced units were used in all simulations: $l_{\mathrm{DPD}} = r_c$ and t_{DPD} were chosen as units of length- and time scale; energy and mass are defined by $\epsilon_{\mathrm{DPD}} = k_{\mathrm{B}}T$ and m_{DPD}. All these units are set to unity. DPD parameters were extracted from ref 36 for a system with a number density of 3 r_c^{-3}. "Like" and "repulsive" conservative interaction coefficients were set to 25 $k_{\mathrm{B}}Tr_c^{-1}$ and 50 $k_{\mathrm{B}}Tr_c^{-1}$, respectively. While staying consistent with earlier works in our group, this choice of parameters is still reasonably close to the nongeneric model used by Spaeth et al.[20] who proposed a = 25 $k_{\mathrm{B}}Tr_c^{-1}$ and 54 $k_{\mathrm{B}}Tr_c^{-1}$ for simulations of polystyrene undergoing FNP when transferred from a good to a poor solvent. The first value was generally used to describe like interactions, the second one chosen to match the critical micelle concentration of polystyrene in water.[20] The spring constant for both bonded and slip spring interactions was chosen to be $k = 2\ k_{\mathrm{B}}Tr_c^{-2}$. The integration step width was $\Delta t = 0.06\ t_{\mathrm{DPD}}$.

A total number of 1 119 744 beads were simulated in a $(72\ r_c)^3$ box. For chains of length N = 75, 100, 150, and 200 beads, the numbers of molecules were 150, 112, 75, and 56, respectively. All systems had a polymer concentration of 1%, which matches other FNP simulations by Spaeth et al. but is still one order of magnitude above experimental concentrations.[20] The theoretical number of slip springs can be derived from eq 2. We choose α = 1.3 following the suggestion for ϑ-solvents by Colby et al.[42] $N_{\mathrm{SS}}^{\mathrm{theo}}(1)$ is one tenth of the total number of beads in our system.[26,27] For a simulation box containing 1 119 744 beads, the theoretical, total number of slip springs in an unperturbed polymer solution with φ = 0.01 is derived to $N_{\mathrm{SS}}^{\mathrm{theo}}$ = 3. In this work, we employ higher slip spring numbers of N_{SS} = 0, 10, 100, 250, and 500 for each chain length. A discussion of how especially the higher slip spring numbers affect the chains under the initial solvent conditions can be found in the section Results and Discussion. For every combination of slip springs and chain length, a set of five simulations was carried out.

The slip spring mobility was controlled by a Metropolis MC algorithm. Every block of 500 DPD steps was followed by one attempt of slip spring relocation and 500 migration attempts. In the relocation procedure, slip springs located on a chain end were given the opportunity to jump to any other chain end. During migration, every slip spring was allowed 500 trials to move one bead along either chain in any direction. The acceptance or rejection of either move was determined by the

DOI: 10.1021/acs.jced.9b00679
J. Chem. Eng. Data 2020, 65, 1264−1272

energy change using a Metropolis criterion. Notably, the slip spring migration was not bound to any kinetic criterion. Instead, the block length was chosen to match the slip spring's spatial correlation time in MC and DPD sequences. Further details can be found in ref 26.

After 5×10^5 timesteps (30000 t_{DPD}) of equilibration, 50% of all solvent beads were replaced by antisolvent beads *instantaneously* and *randomly*. For all five simulations of each set, collapse runs were performed for a total of 5×10^5 timesteps. Equilibrium properties of the initial solutions were studied by a single run for every combination of N and N_{SS} for 5×10^5 timesteps after equilibration. Statistic errors were calculated as the standard deviation of the mean and are reported as confidence intervals with a confidence level of 95%.

Given the system size and speed of precipitation dynamics, this work does not aim to give a one-to-one comparison to either atomistic simulations or experiments but rather offers a systematic discussion on how entanglements influence precipitation behavior. We nonetheless want to give a short interpretation of the time- and length scales discussed. In an earlier work by Masubuchi et al.,[33] the system of reference for a bead−spring polymer chain similar to ours of 120 beads length was a melt of atactic polystyrene with a molar weight of $M_w = 9.64 \times 10^4$ g/mol. Following this, one DPD bead represents roughly eight monomers, which determines $m_{DPD} \approx 830$ u and $l_{DPD} = r_c \approx 2$ nm. With $\epsilon_{DPD} = k_B T = 4.1 \times 10^{-21}$ J at 298 K, $t_{DPD} = l_{DPD}(m_{DPD}/\epsilon_{DPD})^{0.5} = 36$ ps can be derived.[20] However, DPD simulations are known to show artificially accelerated dynamics; the final value of t_{DPD}^{real} must thus be estimated by comparison with experiments. For example, Spaeth et al.[20] found an acceleration correction of $t_{DPD}^{real} = 55.6\ t_{DPD}$ by fitting their model's diffusion coefficient.

For the sake of brevity, we will omit units from here on. If not stated otherwise, runtimes are always given in t_{DPD} where $0.06\ t_{DPD} = 1$ timestep.

RESULTS AND DISCUSSION

Initial Solvent Conditions. The properties of a $\varphi = 0.01$ solution of bead−spring chains in a monomeric solvent are investigated in equilibrium. Different chains with $N = 75$, 100, 150, and 200 beads and various slip spring numbers of $N_{SS} = 0$, 10, 100, 250, and 500 are examined. Figure 1 shows the scaling of the mean squared radii of gyration $\langle R_g^2 \rangle$ for different numbers of slip springs with the number of bonds per chain. Fitting toward $\langle R_g^2 \rangle \propto (N-1)^{\nu}$ revealed scaling exponents of $\nu = 1.077(4)$ for 0 and 1.035(11) for 500 slip springs, where the uncertainty denotes the standard deviation error of the fit. For our athermal model, ν ranges between 1.04 and 1.19 in the literature.[43−49] Here, the majority suggests good solvent conditions rather than the ϑ conditions indicated by our fit.[49] Given that the scaling exponent in DPD is debated to be very sensible to, for example, insufficient statistics,[47] but also the box size,[48] and our data set consists of merely four different chain lengths, we do not want to commit to the observed ϑ behavior. After all, the precise solvent quality in the initial state is expected to be of little influence in the scope of this work.

In our model, slip springs introduce purely attractive interactions between chain beads. Their application without further correction is thus expected to cause side effects, most notably a decreased pressure and a contraction of chains[33] and thus an intrinsically decreased solvent quality.[28] Earlier works with our model did report a slight change in pressure but could not detect any influence of slip springs on the chain's static

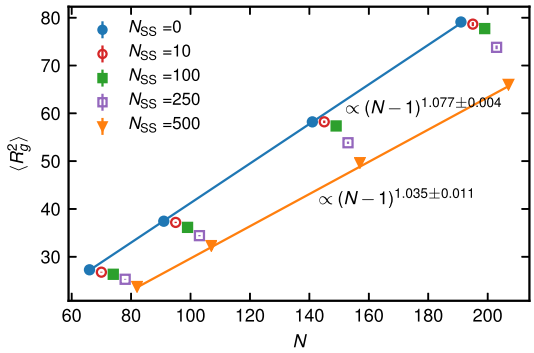

Figure 1. Mean squared radius of gyration $\langle R_g^2 \rangle$ of chains of lengths N with different numbers of slip springs in a solvent of monomer beads. The lines indicate the scaling exponent of $(N-1)$ for systems without slip springs (blue) and with 500 slip springs (orange). Symbols are plotted with a horizontal offset of −8, −4, 0, 4, 8 for N_{SS} = 0, 10, 100, 250, 500, respectively. In all cases, error bars are smaller than the symbol size.

properties in a melt[26] or a dense solution.[33] Similar observation were made with other slip spring models.[50] In these works, the number of polymer beads per slip spring was up to 10, compared to 22.5 in our $N_{SS} = 500$ simulations.[26] While the influence on the system pressure was noticeable, intermolecular slip springs could still compensate for the contraction introduced by intramolecular ones.[26] Here, we observe the opposite behavior: While the pressure is not influenced by the number of slip springs to any detectable degree, Figure 1 exhibits a clear contraction when high slip spring numbers (compared to the theoretical value derived by eq 2, $N_{SS} \geq 250$) are in use. Simulations with $N_{SS} = 10$ and 100, on the other hand, are not significantly affected. The contractions can be countered by a compensating mean potential.[28] This is, however, known to increase the simulation time.[50] We investigated different alternatives in a small model system where a single chain of $N = 100$ beads was dissolved in a monomeric solvent and contracted by five slip springs. This corresponds to 20 beads per slip spring, which is slightly more contracting compared to the maximum value of 22.5 in our recent systems. A simple decrease of the slip spring constant by up to 200% increased the radius of gyration by 13.5% but was not potent enough to restore the slip-spring-free value. At the same time, desired entanglement effects were unacceptably weakened. A second attempt was to increase the polymer−polymer interaction cutoff and thus inflate the chain. In this case, an increment of 2.5% of r_c was found sufficient to restore the original, slip-spring-free radius of gyration. However, this approach requires a reparametrization of polymer−polymer friction coefficients.[51,52] We eventually decided to restrict the number of slip springs to a level where consequences are manageable. We believe that the contraction in the initial state of our simulations is weak enough to not significantly alter possible trends introduced by slip springs during precipitation.

The type of slip springs is analyzed in the equilibrated initial solution as well as the final stages of the collapse. Table 1 shows the number of springs connecting beads of the same chain ("intra") and of different chains ("inter") as well as those connecting beads already regularly bonded ("neigh."). The latter also count as intrachain slip springs. Data are extracted from the $N_{SS} = 500$ runs. For the initial solution ("sol."), the vast majority of all slip springs connects beads of the same

DOI: 10.1021/acs.jced.9b00679
J. Chem. Eng. Data 2020, 65, 1264−1272

Table 1. Numbers of Slip Springs Connecting Beads of the Same Chain ($N_{SS,intra}$), Different Chains ($N_{SS,inter}$), and Neighboring Beads ($N_{SS,neigh}$), and the Average Inter-Slip-Spring Distance N_e.[a]

N		$N_{SS,intra}$	$N_{SS,inter}$	$N_{SS,neigh}$	N_e
75	sol.	478.7(6)	21.3(6)	175.4(20)	7.6(1)
	coll.	125.3(11)	374.7(11)	31.7(9)	9.2(1)
100	sol.	482.6(5)	17.4(5)	165.0(17)	8.8(1)
	coll.	122.2(6)	377.8(6)	30.1(8)	10.0(1)
150	sol.	484.5(4)	15.5(4)	155.6(15)	11.0(1)
	coll.	178.5(16)	321.5(16)	35.3(11)	10.8(1)
200	sol.	489.5(4)	10.5(4)	168.2(18)	12.4(1)
	coll.	240.2(17)	259.8(17)	43.0(12)	11.2(1)

[a]N_e is not to be confused with the number of slip springs (see text). Numbers were extracted from simulations of different chains in an equilibrated solution ("sol.") and as snapshots at the end of our collapse simulations ("coll."). All systems included a total of 500 slip springs.

chain. The ratio of intra- to interchain slip springs also increases with increasing chain length (and, thus, with decreasing number of molecules). Additionally, roughly one-third of all springs are between neighboring beads, that is, lying on top of a real bond. Given the distribution of chains in an athermal solvent, it is not surprising that potential partners for slip spring migration and relocation are part of the same chain. This observation is confirmed by Masubuchi et al.[33] who report an increasing number of intrachain springs with decreasing φ. During migration along one chain, intrachain slip springs naturally seek the potential minimum of a zero-bond length. However, the move $\{i, (j = i + 1)\} \rightarrow \{i, i\}$ (for a slip spring connecting beads i and j) is forbidden in our algorithm,[26] which leads to an accumulation of slip springs between bonded beads. In this specific scenario, slip springs are deactivated and not contributing to the total bead−bead interaction in order to avoid unnaturally stiff bonds. Slip springs are nonetheless found to be mobile and able to escape this reservoir. Figure 1 shows that despite including around 30 times the slip spring value derived by eq 2, solutions with N_{SS} = 100 barely show any contraction, which we attribute to the high amount of inactive slip springs. Table 1 also displays the slip spring distribution under poor solvent conditions. Although the collapsed structures are not yet fully equilibrated (discussed below), it is obvious that most slip springs become active as more beads are available in the globular state, which also manifests itself in the increasing number of interchain slip springs. A discussion of the slip spring redistribution as the chains precipitate is provided below.

Table 1 is completed by the inter-slip-spring distance N_e in the system. It is derived as the average number of monomers between two slip springs on the same chain. Slip springs connecting neighboring beads are excluded. In melts, N_e is directly imposed onto the system as the ratio of the total number of beads and N_{SS} divided by two.[26] The collapsed structures with N_{SS} = 500 and the N = 200 show this ideal distribution of slip springs: For 500 slip springs on 56 × 200 = 11200 polymer beads, N_e = 11.2 is expected and confirmed in Table 1. The N = 200 chains show an expected behavior: In solution, a low number of slip springs is "active", leading to a higher-than-expected value for N_e. After precipitation, the slip spring mobility increases and N_e approaches the expected value. This observation is also true for precipitated shorter chains. However, N_e decreases with decreasing N in solutions. This is likely a statistical issue: The higher the number of molecules in the system, the smaller is the number of chains with more than one slip spring. Thus, the number of chains suited for the computation of N_e decreases, while the influence of slip springs connecting second or third-neighbored beads becomes stronger.

Calculation of N_e also gives access to the length scale of entanglements. r_e is derived in the same way as N_e but incorporates the spatial (instead of the segmental) distance between the respective beads. For the initial solutions, systems with N_{SS} = 500 beads have r_e = 2.2, 2.5, 2.8, and 3.0 for N = 75, 100, 150, and 200, respectively. Globular systems show r_e = 2.7, 2.7, 2.8, and 2.6. All distances have a confidence interval of ±0.1. Since this is below the size of both the initially dissolved chains and the resulting clusters, we assume the model to be capable of capturing potential effects of entanglement on the precipitation process.

We also analyzed the characteristic times of the initial and final state. Since the globule state in our simulations is not equilibrated, our time scales for it are taken from simulations of polymer melts, performed in the same fashion as described in ref 26. The Rouse times τ_R are derived as half the end-to-end vector relaxation times of the polymer chains.[53] Rouse times for systems without slip springs are roughly $\tau_R \approx$ 280, 470, 840, and 1800 t_{DPD} in the initial state and 480, 840, 1900, and 4100 t_{DPD} in the melt (as a model of the final state) for N = 75, 100, 150, and 200. This is in good agreement with the value of ∼2100 t_{DPD} reported by Masubuchi et al. for a melt of N = 120 chains.[33] Reptation times are derived for the final state only, as reptation does not play a role for the initially small local polymer concentrations.[33] Assuming melt-like behavior, the reptation or disentanglement times are estimated as $\tau_d = 6\tau_R \frac{N}{N_e}$.[53] If the expected value of N_e = 11.2 is used, the reptation times derive to $\tau_d \approx 19.3 \times 10^3$, 45.0×10^3, 152.7×10^3, and 439.3×10^3 t_{DPD} for N = 75, 100, 150, and 200, respectively. Notably, these values are for the systems containing 500 slip springs. Reptation times for other systems are expected to be smaller. All derived Rouse- and reptation times act on similar scales as the collapse- and aggregation behavior discussed below.

Aggregation Dynamics. Starting from the equilibrated solution, we perform an instantaneous solvent-to-antisolvent exchange where 50% of all solvent beads are randomly chosen to adapt antisolvent properties. Snapshots are shown in Figure 2 for 56 200-bead chains with different numbers of slip springs. The root mean squared radius of gyration $\langle R_g^2 \rangle^{0.5}$ during the precipitation is shown in Figure 3, averaged over multiple runs and all chains in each system. Both Figures 2 and 3 show a fast reaction of the chains when exposed to antisolvent: 60 t_{DPD} (1000 timesteps) after the collapse, chains are visibly contracted perpendicular to their contour vector. At the same time, $\langle R_g^2 \rangle^{0.5}$ is still only starting to decrease (see Figure 3, N = 200). At 300 t_{DPD} (5000 timesteps), most chains are fully globular. However, a few elongated chains stretch between separated globules, forming a temporary network-like state. (For a detailed snapshot, see the table-of-content graphic.) These connecting chains are fully retracted at 1200 t_{DPD} (20000 timesteps), when a high number of mostly small globules are dispersed in the system. At this globular stage, $\langle R_g^2 \rangle^{0.5}$ reaches its minimum value. In later stages of the precipitation, globules coagulate and form larger nanoparticles

DOI: 10.1021/acs.jced.9b00679
J. Chem. Eng. Data 2020, 65, 1264−1272

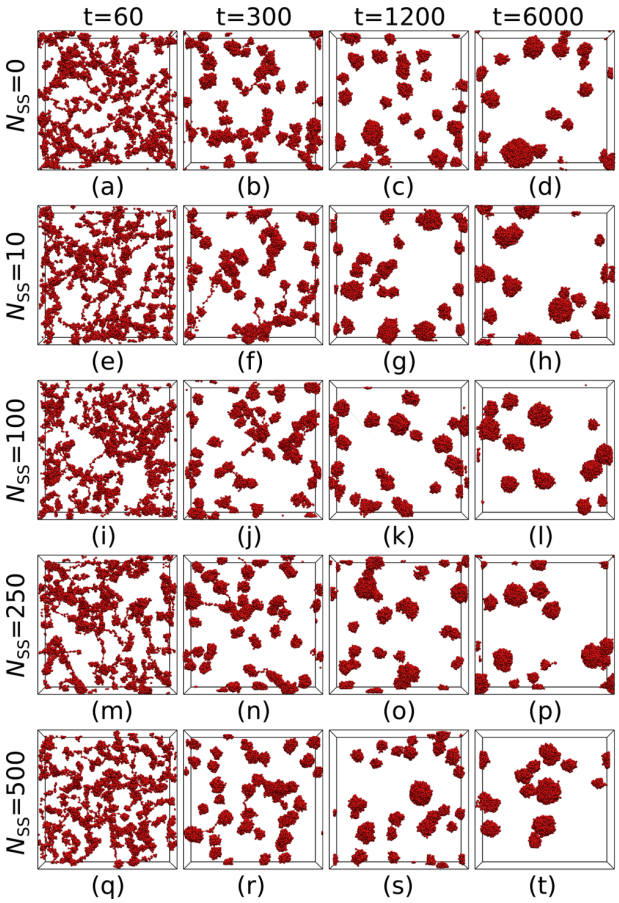

Figure 2. Snapshots of the precipitation of a solution of 56 chains (N = 200) with N_{SS} = 0 (a–d), 10 (e–h), 100 (i–l), 250 (m–p), and 500 (q–t). Solvent molecules are not shown. Snapshots are taken at 0, 300, 1200, and 6000 t_{DPD} after the solvent-to-antisolvent exchange using the VMD software.[54]

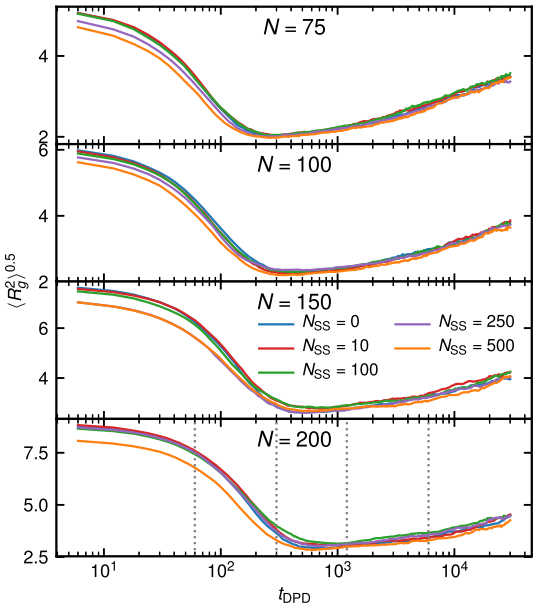

Figure 3. Root mean squared radius of gyration $\langle R_g^2 \rangle^{0.5}$ for chains of different lengths N with different slip spring numbers N_{SS}. At t = 0, 50% of the solvent beads are exchanged for antisolvent. Dotted gray lines for N = 200 indicate the times when the snapshots displayed in Figure 2 are taken.

(6000 t_{DPD}, 100 000 timesteps). In this process, the chains' average radii of gyration increase again as surrounding polymer beads act as a ϑ-solvent.[45] The equilibrium state in simulations of flash nanoprecipitation is known to be a single nanoparticle.[12] This state is not reached within the simulation time of 30 000 t_{DPD} nor in selected runs performed for up to 90 000 t_{DPD}, where still two or three nanoparticles exist. Beside the difference in the magnitude of $\langle R_g^2 \rangle^{0.5}$, only minor influences of the chain size are visible in Figure 3: First, the minimum of $\langle R_g^2 \rangle^{0.5}(t)$ is shifted to longer times with N. This can be explained by the increased collapse time for longer chains. Second, longer chains should form fewer, larger, and thus spatially more separated globules which leads to a slower formation of aggregates. This is hinted by the slightly delayed relaxation for $t \geq 1000$ t_{DPD} when, for example, comparing N = 75 and N = 200 bead systems.

The formation of globules is further investigated by performing a density-based cluster analysis:[55] A bead is considered part of a "cluster" if it is closer than the cluster criterion r_{cc} to any other bead in the cluster. Two clusters are thus recognized as separate if they are not closer than r_{cc}. Following Spaeth et al.,[20] we first choose r_{cc} = 0.85, which is where the radial distribution function of a monomeric liquid with a_{ij} = 25 has its first maximum. Note that beads of the same chain are not necessarily part of one cluster: For all unperturbed systems, the histogram of bond lengths has its maximum around 0.95 with a mean of 1.23. Stretched bonds are thus not uncommon. In fact, a very small number of elongated chains in the network-like stage (see Figure 2, t = 300) exhibit bond lengths up to almost 4 r_c, which we consider an artifact due to the softness of our Hookean springs. The results of the r_{cc} = 0.85 cluster analysis is shown in Figure 4. The number of clusters N_{Cl} starts at its maximum value of several thousand clusters before rapidly decreasing as first globules are formed. A distinct two-regime precipitation behavior is shown for all bead- and slip-spring numbers and will here be discussed for the N = 200 simulations. In the first region, all chains collapse into smaller "blobs". Chains are still stretched out but clusters form along their contours. In this region, N_{Cl} scales logarithmically as $\propto -1959 \log_{10}(t)$, or linearly with the logarithm of time. This "linear regime" ends around the time of the first snapshot (Figure 2), 60 t_{DPD}. A second linear regime of N_{Cl} with $\log_{10}(t)$ is observed starting around 1000 t_{DPD} when all chains are collapsed into globules. The number of clusters now only decreases when two globules merge into a larger particle. This is visualized at 1200 and 6000 t_{DPD} in Figure 2. In this regime, a distinct $N_{Cl} \propto -83.2 \log_{10}(t)$ scaling is observed. The transition time between both regimes is found at 202 t_{DPD} as the crossover time of two linear fits. In this crossover section, the snapshots taken at 60, 300, and 1200 t_{DPD} reveal an interesting behavior: After the contraction toward the chain's principal axis, we expected them to collapse into globules of one or very few molecules which would merge together afterward. However, while most chains do so, some polymers stay stretched and exposed to antisolvent as they span between two globules. This network-like state is assumed to cause the broad width of the crossover region. Eventually, chains retreat from one of two globules and join the other. The question of how the lifespan

DOI: 10.1021/acs.jced.9b00679
J. Chem. Eng. Data 2020, 65, 1264–1272

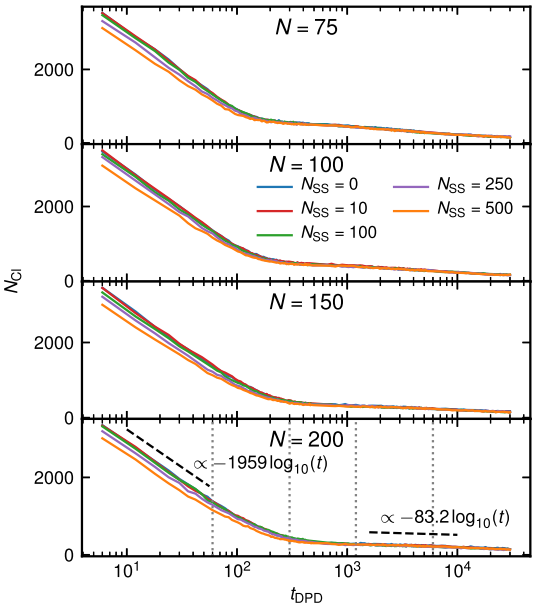

Figure 4. Number of cluster N_{Cl} as a function of time for different chain sizes N and slip spring numbers N_{SS}. At t = 0, 50% of the solvent beads are exchanged by antisolvent. The cluster criterion was chosen to be 0.85. Dotted gray lines for N = 200 indicate the times when the snapshots displayed in Figure 2 are taken.

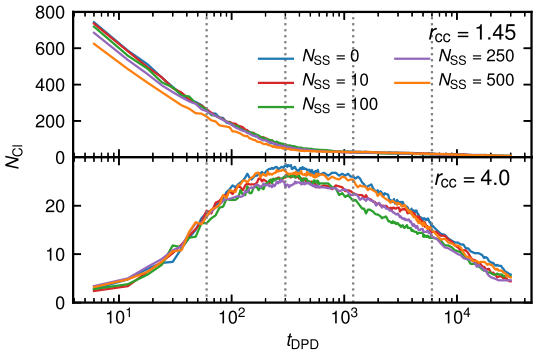

Figure 5. Number of clusters N_{Cl} as a function of time for different slip spring numbers N_{SS} and two different cluster criteria of r_{cc} = 1.45 and 4.0. All chains are of length 200. At t = 0, 50% of the solvent beads are exchanged by antisolvent. Dotted gray lines for N = 200 indicate the times when the snapshots displayed in Figure 2 are taken.

of this network-like state is influenced by slip springs (which effectively decrease the chain mobility) is addressed below. Interestingly, both the absolute number of clusters at a given time and their evolution seems to be roughly independent of the chain length, with only the crossover time between both regimes slightly increasing with N. The independence of the aggregation dynamics from the chain length could be explained by the diffusion limited aggregation (DLA) model. This model has been successfully used to describe early aggregation behavior in other simulations of flash nanoprecipitation.[18] However, the DLA model suggests a $N_{Cl} \propto t^{-1}$ scaling rather than our logarithmic scaling. As yet, we can only conclude that our long and overlapping chains create a system too complex to be fully described by such a simple model.

The previously discussed cluster analysis only covers the formation and destruction of clusters generated with a very short cluster criterion of r_{cc} = 0.85. As mentioned, a chain can thus contribute to several different clusters as bonds stretched beyond 0.85 commonly exist. We consequently perform two other cluster analyses with criteria of r_{cc} = 1.45 and r_{cc} = 4. The first value marks the distance where the radial distribution function of a monomeric fluid crosses equilibrium density after the first depletion. This is considered to be a distance long enough to respect moderately stretched bonds but short enough so that two polymer beads cannot be separated by a solvent- or antisolvent particle. The value of r_{cc} = 4 is an arbitrary distance larger than any bond in the system; it is thus ensured that all beads of one molecule must be part of the same cluster. By employing a cluster criterion this high, we access information about the spatial separation of whole chains rather than aggregation of monomer blobs. Results of both analyses can be found in Figure 5 for the system containing chains of 200 beads length. Matching previous results, different chain lengths were not found to strongly influence the outcome and are therefore omitted for the sake of brevity.

The absolute numbers of clusters shown in Figure 5 are expectedly lower than for r_{cc} = 0.85. At 30 000 t_{DPD}, the averaged cluster numbers for the (N = 200, N_{SS} = 0) systems are 202.6 for r_{cc} = 0.85 and 13.0 and 9.4 for 1.45 and 4.0, respectively. Both of the latter analyses thus reflect the numbers of "real" clusters and nanoparticles better compared to r_{cc} = 0.85. For r_{cc} = 1.45, the overall picture is however not different from the one previously described. The slopes for the first and second linear regime of $\log_{10}(t)$ for the (N = 200, N_{SS} = 0) system are −457.9 and −16.8, respectively. With the transition between both regimes again found at 202 t_{DPD}, it is clear that the same mechanism drives the formation of two linear regimes. In the case of r_{cc} = 4.0, the initial stages of the precipitation process show a very low number of clusters. In both the initially dissolved and following network-like state, chains are distributed in the simulation cell which causes the low number of spatially separated structures. As chains retract during collapse and the network-like state vanishes, the amount of these structures increases to a point where a maximum number of separated globules is distributed in the cell. This is still smaller than the number of chains (56). Therefore, the average chain does not collapse in isolation, but simultaneously joins at least a second one to form a first aggregate. The maximum is positioned in the transition regime previously described and marks the time when cluster numbers can only be reduced further by diffusion-dependent aggregation. After this regime, the same linear decay of N_{Cl} with $\log_{10}(t)$ is found.

We last investigate the size of the clusters formed. This is done by counting the beads per cluster for every cluster observed by the r_{cc} = 1.45 and 4.0 analyses at certain timesteps for one run with N = 200 bead chains and different N_{SS}. Histograms of the cluster sizes are displayed in Figure 6 (r_{cc} = 1.45) and Figure 7 (r_{cc} = 4.0). As the difference between different slip-spring numbers is negligible, only the systems with N_{SS} = 0 and 500 are shown.

For the r_{cc} = 1.45 analysis, a majority of the initial clusters consist of very few beads, while only a small number of clusters starts with sizes up to 300. A consistent behavior is observed for all values of N_{SS}: a depletion of small clusters is accompanied by the formation of larger blobs. In the beginning of the network-link stage after roughly 300 t_{DPD}, mostly clusters of sizes well below 10 or above 100 exist. While larger clusters describe globules, smaller ones are assumed to be part of a stretched chain with bond lengths above 1.45. In the

DOI: 10.1021/acs.jced.9b00679
J. Chem. Eng. Data 2020, 65, 1264−1272

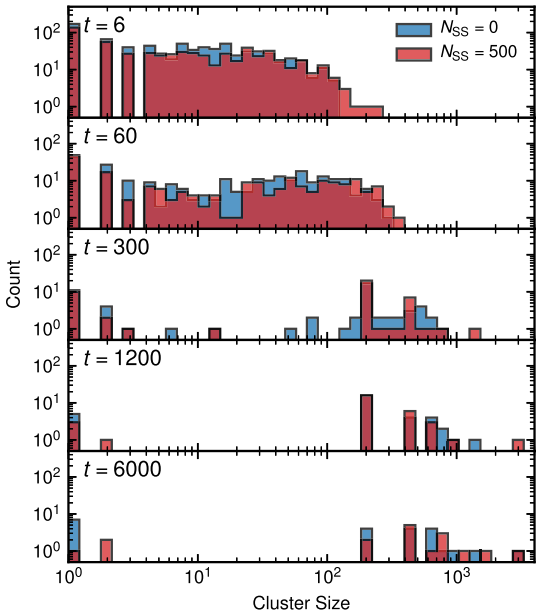

Figure 6. Cluster size histogram of a 200-bead chain after a cluster analysis with r_{cc} = 1.45 at different times of the precipitation process. At t = 0, 50% of the solvent beads are exchanged by antisolvent.

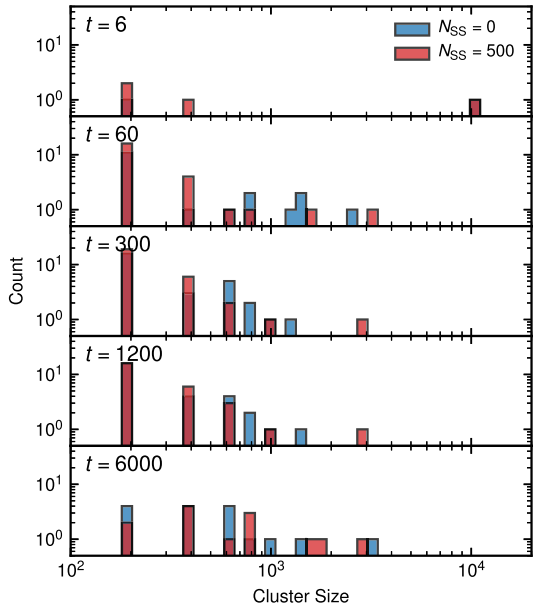

Figure 7. Cluster size histogram of a 200-bead chain after a cluster analysis with r_{cc} = 4.0 at different times of the precipitation process. At t = 0, 50% of the solvent beads are exchanged by antisolvent.

following globular stage, most clusters are of a size of hundreds or thousands of beads (with few clusters of every size) while single-bead clusters are comparably rare. If a cluster criterion of 4.0 is used, systems for all N_{SS} start with mostly one cluster containing all or most beads. As discussed, this is due to the initial distribution of the dissolved chains. As the precipitation progresses, chains become spatially separated. Figure 7 gives a clear view of how globules of 200 beads, that is, one chain, dominate the globular state until they slowly merge into larger particles.

Influence of Slip Springs on the Aggregation Dynamics. After elucidation of the precipitation process, we turn to examining the role and behavior of slip springs on the observations made. Starting from Table 1, slip spring types in both solution and the preliminary collapsed state are known. Figure 8 shows the evolution of slip-spring types for one

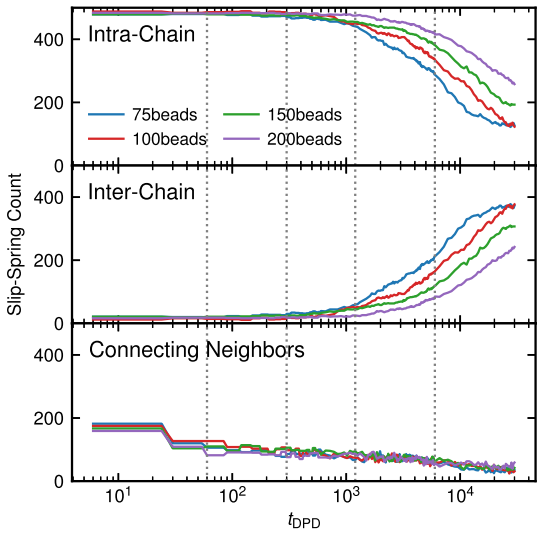

Figure 8. Number of slip springs connecting beads of the same chain (intra), different chains (inter), and neighboring beads as a function of time. All systems include a total of 500 slip springs. At t = 0, 50% of the solvent beads are exchanged by antisolvent. Dotted gray lines indicate the times when the snapshots displayed in Figure 2 are taken.

selected run of every chain length with N_{SS} = 500 as chains collapse. In this process, inactive slip springs leave their reservoir between bonded beads and become active, until eventually most slip springs are available to the system. An interesting question is whether slip springs influence the lifetime of the network-like structure observed around 300 t_{DPD}. It was discussed above that chains spanning between different globules eventually retract to minimize their surface exposed to antisolvent: here, we want to address the question of how chain ends can entangle *inside* the globules and delay the retraction process. The transition of an intra- to an inter-slip-spring dominated system takes place at later stages of the precipitation (Figure 8). It is clear that this requires different chains to be in close vicinity to each other. Interestingly, we observe a large contribution of interchain springs only in the globular stage starting around 1200 t_{DPD} but not in the network-like stage. At this point, we need to emphasize that this behavior exhibits no strong dependency on the slip spring mobility. To probe systems with higher and lower mobilities, we performed runs of the (N = 200, N_{SS} = 500) system with 500 MC steps every 50 and 5000 DPD steps. We found the transition of the intra- to inter-slip-spring dominated systems to be accelerated for the 50/500 scheme and delayed for the 5000/500 scheme, compared to our regular 500/500 pattern. The differences are, however, pronounced only considerably after the network-like stage. Consequently, no influence on the collapse dynamics was found. This is in agreement with an earlier work, where we observed no influence upon changing the 500/500 scheme to a 50/5000 scheme in simulations of 1 and 10 slip springs on a single, rapidly collapsing N = 100 chain.[24]

DOI: 10.1021/acs.jced.9b00679
J. Chem. Eng. Data 2020, 65, 1264−1272

Comparing the snapshots given in Figure 2 as well as the radii of gyration and the results of the cluster analyses (Figures 3−7), the most distinct difference is observed between N_{SS} = 500 and all other slip spring numbers. In the case of $\langle R_g^2 \rangle$, this is clearly due to the precontraction of chains in the initial solvent. This already discussed phenomenon becomes negligible after entering the globular stage. In the case of the cluster analyses, the influence of the precontraction is less clear and fully vanished after the onset of the second linear regime. For all previously discussed figures, the precontraction remains the only measured influence of a higher N_{SS} on the precipitation process. We thus conclude that the precipitation process observed in our model systems is not altered by the presence of slip springs and that entanglement effects can be neglected in experiments such as flash nanoprecipitation.

■ CONCLUSIONS

We evaluated the influence of slip springs on the precipitation of a solution of polymer chains using a simple and fast DPD bead−spring model. We observed an interesting aggregation behavior of our rather long chains after solvent-to-antisolvent exchange. Our simulations initially showed chains uniformly distributed through the whole volume of the simulation box. As they precipitated, polymer solutions initially formed a large number of small blobs that were sometimes connected by bridging chains. These elongated chains were highly exposed to antisolvent and quickly retracted from one of the globules to join the other. After retraction of the bridging chains, the large number of globules continued to coagulate over time into a small number of aggregates. Our working hypothesis was that in the network-like state, bridging chains could be entangled in the globules they were connecting. Mimicking these entanglements, the presence or absence of slip springs should alter the precipitation dynamics. In our results, we did not see any influence of varying slip spring numbers on the dynamics nor the resulting globules and nanoparticles formed. We conclude that, for the chain lengths and polymer concentration addressed, the role of entanglements in dilute polymer solutions is negligible during flash nanoprecipitation.

■ AUTHOR INFORMATION

Corresponding Authors

*E-mail: j.schneider@theo.chemie.tu-darmstadt.de.
*E-mail: f.mueller-plathe@theo.chemie.tu-darmstadt.de.

ORCID

Jurek Schneider: 0000-0002-0286-1678
Florian Müller-Plathe: 0000-0002-9111-7786

Notes

The authors declare no competing financial interest.

■ ACKNOWLEDGMENTS

Simulations were performed on the Lichtenberg high performance computer of the TU Darmstadt. J.S. and F.M.-P. thank Professor Athanassios Panagiotopoulos for his hospitality at Princeton University and for many fruitful discussions on the topic.

■ REFERENCES

(1) Saad, W. S.; Prud'homme, R. K. Principles of nanoparticle formation by flash nanoprecipitation. *Nano Today* **2016**, *11*, 212−227.
(2) Fessi, H.; Puisieux, F.; Devissaguet, J. P.; Ammoury, N.; Benita, S. Nanocapsule formation by interfacial polymer deposition following solvent displacement. *Int. J. Pharm.* **1989**, *55*, R1−R4.
(3) Bilati, U.; Allémann, E.; Doelker, E. Development of a nanoprecipitation method intended for the entrapment of hydrophilic drugs into nanoparticles. *Eur. J. Pharm. Sci.* **2005**, *24*, 67−75.
(4) Johnson, B. K.; Prud'homme, R. K. Chemical processing and micromixing in confined impinging jets. *AIChE J.* **2003**, *49*, 2264−2282.
(5) Johnson, B. K.; Prud'homme, R. K. Flash nanoprecipitation of organic actives and block copolymers using a confined impinging jets mixer. *Aust. J. Chem.* **2003**, *56*, 1021−1024.
(6) Liu, Y.; Cheng, C.; Liu, Y.; Prud'homme, R. K.; Fox, R. O. Mixing in a multi-inlet vortex mixer (MIVM) for flash nanoprecipitation. *Chem. Eng. Sci.* **2008**, *63*, 2829−2842.
(7) Zhang, C.; Pansare, V. J.; Prud'homme, R. K.; Priestley, R. D. Flash nanoprecipitation of polystyrene nanoparticles. *Soft Matter* **2012**, *8*, 86−93.
(8) Sosa, C.; Lee, V. E.; Grundy, L. S.; Burroughs, M. J.; Liu, R.; Prud'homme, R. K.; Priestley, R. D. Combining precipitation and vitrification to control the number of surface patches on polymer nanocolloids. *Langmuir* **2017**, *33*, 5835−5842.
(9) Lee, V. E.; Sosa, C.; Liu, R.; Prud'homme, R. K.; Priestley, R. D. Scalable platform for structured and hybrid soft nanocolloids by continuous precipitation in a confined environment. *Langmuir* **2017**, *33*, 3444−3449.
(10) Sosa, C.; Liu, R.; Tang, C.; Qu, F.; Niu, S.; Bazant, M. Z.; Prud'homme, R. K.; Priestley, R. D. Soft multifaced and patchy colloids by constrained volume self-assembly. *Macromolecules* **2016**, *49*, 3580−3585.
(11) Grundy, L. S.; Lee, V. E.; Li, N.; Sosa, C.; Mulhearn, W. D.; Liu, R.; Register, R. A.; Nikoubashman, A.; Prud'homme, R. K.; Panagiotopoulos, A. Z.; Priestley, R. D. Rapid production of internally structured colloids by flash nanoprecipitation of block copolymer blends. *ACS Nano* **2018**, *12*, 4660−4668.
(12) Nikoubashman, A.; Lee, V. E.; Sosa, C.; Prud'homme, R. K.; Priestley, R. D.; Panagiotopoulos, A. Z. Directed assembly of soft colloids through rapid solvent exchange. *ACS Nano* **2016**, *10*, 1425−1433.
(13) Morozova, T. I.; Lee, V. E.; Panagiotopoulos, A. Z.; Prud'homme, R. K.; Priestley, R. D.; Nikoubashman, A. On the stability of polymeric nanoparticles fabricated through rapid solvent mixing. *Langmuir* **2019**, *35*, 709−717.
(14) de Gennes, P. G. Kinetics of collapse for a flexible coil. *J. Phys., Lett.* **1985**, *46*, 639−642.
(15) Chen, T.; Hynninen, A.-P.; Prud'homme, R. K.; Kevrekidis, I. G.; Panagiotopoulos, A. Z. Coarse-grained simulations of rapid assembly kinetics for polystyrene-b-poly(ethylene oxide) copolymers in aqueous solutions. *J. Phys. Chem. B* **2008**, *112*, 16357−16366.
(16) Chen, T.; D'Addio, S. M.; Kennedy, M. T.; Swietlow, A.; Kevrekidis, I. G.; Panagiotopoulos, A. Z.; Prud'homme, R. K. Protected peptide nanoparticles: experiments and brownian dynamics simulations of the energetics of assembly. *Nano Lett.* **2009**, *9*, 2218−2222.
(17) Chang, R.; Yethiraj, A. Solvent effects on the collapse dynamics of polymers. *J. Chem. Phys.* **2001**, *114*, 7688−7699.
(18) Li, N.; Nikoubashman, A.; Panagiotopoulos, A. Z. Multi-scale simulations of polymeric nanoparticle aggregation during rapid solvent exchange. *J. Chem. Phys.* **2018**, *149*, 084904.
(19) Spaeth, J. R.; Kevrekidis, I. G.; Panagiotopoulos, A. Z. A comparison of implicit- and explicit-solvent simulations of self-assembly in block copolymer and solute systems. *J. Chem. Phys.* **2011**, *134*, 164902.
(20) Spaeth, J. R.; Kevrekidis, I. G.; Panagiotopoulos, A. Z. Dissipative particle dynamics simulations of polymer-protected nanoparticle self-assembly. *J. Chem. Phys.* **2011**, *135*, 184903.
(21) Li, N.; Panagiotopoulos, A. Z.; Nikoubashman, A. Structured nanoparticles from the self-assembly of polymer blends through rapid solvent exchange. *Langmuir* **2017**, *33*, 6021−6028.

DOI: 10.1021/acs.jced.9b00679
J. Chem. Eng. Data 2020, 65, 1264−1272

(22) Li, N.; Nikoubashman, A.; Panagiotopoulos, A. Z. Controlled production of patchy particles from the combined effects of nanoprecipitation and vitrification. *Soft Matter* **2017**, *13*, 8433−8441.
(23) Li, N.; Nikoubashman, A.; Panagiotopoulos, A. Z. Self-assembly of polymer blends and nanoparticles through rapid solvent exchange. *Langmuir* **2019**, *35*, 3780−3789.
(24) Schneider, J.; Panagiotopoulos, A. Z.; Müller-Plathe, F. Polymer chain collapse upon rapid solvent exchange: Slip-spring dissipative particle dynamics simulations with an explicit-solvent model. *J. Phys. Chem. C* **2017**, *121*, 27664−27673.
(25) Morozova, T. I.; Nikoubashman, A. Coil−globule collapse of polystyrene chains in tetrahydrofuran−water mixtures. *J. Phys. Chem. B* **2018**, *122*, 2130−2137.
(26) Langeloth, M.; Masubuchi, Y.; Böhm, M. C.; Müller-Plathe, F. Recovering the reptation dynamics of polymer melts in dissipative particle dynamics simulations via slip-springs. *J. Chem. Phys.* **2013**, *138*, 104907.
(27) Langeloth, M.; Masubuchi, Y.; Böhm, M. C.; Müller-Plathe, F. Reptation and constraint release dynamics in bidisperse polymer melts. *J. Chem. Phys.* **2014**, *141*, 194904.
(28) Chappa, V. C.; Morse, D. C.; Zippelius, A.; Müller, M. Translationally invariant slip-spring model for entangled polymer dynamics. *Phys. Rev. Lett.* **2012**, *109*, 148302.
(29) Uneyama, T.; Masubuchi, Y. Multi-chain slip-spring model for entangled polymer dynamics. *J. Chem. Phys.* **2012**, *137*, 154902.
(30) Ramírez-Hernández, A.; Detcheverry, F. A.; Peters, B. L.; Chappa, V. C.; Schweizer, K. S.; Müller, M.; de Pablo, J. J. Dynamical simulations of coarse grain polymeric systems: rouse and entangled dynamics. *Macromolecules* **2013**, *46*, 6287−6299.
(31) Ramírez-Hernández, A.; Peters, B. L.; Andreev, M.; Schieber, J. D.; de Pablo, J. J. A multichain polymer slip-spring model with fluctuating number of entanglements for linear and nonlinear rheology. *J. Chem. Phys.* **2015**, *143*, 243147.
(32) Vogiatzis, G. G.; Megariotis, G.; Theodorou, D. N. Equation of state based slip spring model for entangled polymer dynamics. *Macromolecules* **2017**, *50*, 3004−3029.
(33) Masubuchi, Y.; Langeloth, M.; Böhm, M. C.; Inoue, T.; Müller-Plathe, F. A multichain slip-spring dissipative particle dynamics simulation method for entangled polymer solutions. *Macromolecules* **2016**, *49*, 9186−9191.
(34) Hoogerbrugge, P. J.; Koelman, J. M. V. A. Simulating microscopic hydrodynamic phenomena with dissipative particle dynamics. *Europhys. Lett.* **1992**, *19*, 155.
(35) Español, P.; Warren, P. Statistical mechanics of dissipative particle dynamics. *Europhys. Lett.* **1995**, *30*, 191.
(36) Groot, R. D.; Warren, P. B. Dissipative particle dynamics: Bridging the gap between atomistic and mesoscopic simulation. *J. Chem. Phys.* **1997**, *107*, 4423.
(37) de Gennes, P. G. Reptation of a polymer chain in the presence of fixed obstacles. *J. Chem. Phys.* **1971**, *55*, 572−579.
(38) Kremer, K.; Grest, G. S. Dynamics of entangled linear polymer melts: A molecular-dynamics simulation. *J. Chem. Phys.* **1990**, *92*, 5057−5086.
(39) Watanabe, H.; Ishida, S.; Matsumiya, Y.; Inoue, T. Viscoelastic and dielectric behavior of entangled blends of linear polyisoprenes having widely separated molecular weights: test of tube dilation picture. *Macromolecules* **2004**, *37*, 1937−1951.
(40) van Ruymbeke, E.; Masubuchi, Y.; Watanabe, H. Effective value of the dynamic dilution exponent in bidisperse linear polymers: From 1 to 4/3. *Macromolecules* **2012**, *45*, 2085−2098.
(41) van Ruymbeke, E.; Shchetnikava, V.; Matsumiya, Y.; Watanabe, H. Dynamic dilution effect in binary blends of linear polymers with well-separated molecular weights. *Macromolecules* **2014**, *47*, 7653−7665.
(42) Colby, R. H.; Rubinstein, M.; Viovy, J. L. Chain entanglement in polymer melts and solutions. *Macromolecules* **1992**, *25*, 996−998.
(43) Kong, Y.; Manke, C. W.; Madden, W. G.; Schlijper, A. G. Effect of solvent quality on the conformation and relaxation of polymers via dissipative particle dynamics. *J. Chem. Phys.* **1997**, *107*, 592−602.
(44) Schlijper, A. G.; Hoogerbrugge, P. J.; Manke, C. W. Computer simulation of dilute polymer solutions with the dissipative particle dynamics method. *J. Rheol.* **1995**, *39*, 567−579.
(45) Spenley, N. A. Scaling laws for polymers in dissipative particle dynamics. *Europhys. Lett.* **2000**, *49*, 534.
(46) Symeonidis, V.; Em Karniadakis, G.; Caswell, B. Dissipative particle dynamics simulations of polymer chains: scaling laws and shearing response compared to DNA experiments. *Phys. Rev. Lett.* **2005**, *95*, 076001.
(47) Ilnytskyi, J. M.; Holovatch, Y. How does the scaling for the polymer chain in the dissipative particle dynamics hold? *Condens. Matter Phys.* **2007**, *10*, 539.
(48) Jiang, W.; Huang, J.; Wang, Y.; Laradji, M. Hydrodynamic interaction in polymer solutions simulated with dissipative particle dynamics. *J. Chem. Phys.* **2007**, *126*, 044901.
(49) Nardai, M. M.; Zifferer, G. Simulation of dilute solutions of linear and star-branched polymers by dissipative particle dynamics. *J. Chem. Phys.* **2009**, *131*, 124903.
(50) Megariotis, G.; Vogiatzis, G. G.; Sgouros, A. P.; Theodorou, D. N. Slip spring-based mesoscopic simulations of polymer networks: methodology and the corresponding computational code. *Polymers* **2018**, *10*, 1156.
(51) Spaeth, J. R.; Dale, T.; Kevrekidis, I. G.; Panagiotopoulos, A. Z. Coarse-graining of chain models in dissipative particle dynamics simulations. *Ind. Eng. Chem. Res.* **2011**, *50*, 69−77.
(52) Backer, J. A.; Lowe, C. P.; Hoefsloot, H. C. J.; Iedema, P. D. Combined length scales in dissipative particle dynamics. *J. Chem. Phys.* **2005**, *123*, 114905.
(53) Rubinstein, M.; Colby, R. H. *Polymer Physics*; Oxford University Press: New York, 2003.
(54) Humphrey, W.; Dalke, A.; Schulten, K. VMD: Visual molecular dynamics. *J. Mol. Graphics* **1996**, *14*, 33−38.
(55) Ester, M.; Kriegel, H.-P.; Sander, J.; Xiaowei, X. *Proceedings of the Second International Conference on Knowledge Discovery and Data Mining (KDD-96)*; AAAI Press, 1996; pp 226−231.

DOI: 10.1021/acs.jced.9b00679
J. Chem. Eng. Data 2020, 65, 1264−1272

Macromolecules

pubs.acs.org/Macromolecules Article

Simulation of Elastomers by Slip-Spring Dissipative Particle Dynamics

Jurek Schneider,* Frank Fleck, Hossein Ali Karimi-Varzaneh, and Florian Müller-Plathe*

Cite This: *Macromolecules* 2021, 54, 5155–5166 Read Online

ACCESS | Metrics & More | Article Recommendations

ABSTRACT: We study elastomeric networks using dissipative-particle-dynamics simulations. This soft-core method gives access to mesoscopic time and length scales and is potentially capable to study complex systems such as network defects and gels, but the unmodified method underestimates topological interactions and can only model phantom networks. In this work, we study the capability of slip springs to recover topological effects of network strands. We show that slip springs with a restricted mobility restore the topological contributions of trapped entanglements. Uniaxial strain experiments give access to the cross-link and entanglement contribution to the shear modulus of a slip-spring model network. We find these contributions to coincide with those reported for comparable hard-core Kremer−Grest networks (Gula et al. *Macromolecules* **2020,** *53,* 6907−6927). For network strands longer than the chains' entanglement length, the contribution of slip springs to the shear modulus equals the plateau modulus of the un-cross-linked precursor melt. However, a constant number of slip springs overestimates the shear modulus for high cross-link densities. To probe their applicability, we successfully compare our simulations with experimental polyisoprene rubbers: a network obtained by parameter-free cross-linking of a simulated polyisoprene melt reproduces the viscoelastic moduli of experimental rubbers.

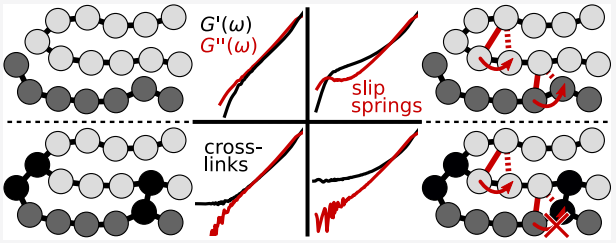

INTRODUCTION

Computer simulations have aided the research of polymer networks, gels, and rubbers for more than 30 years. Contrary to many experiments, they offer an insight into the underlying network structures and address the still recent challenge of relating them to bulk properties.[1] Early network simulations almost exclusively employed the Kremer−Grest model,[2] a generic bead-spring model of hard-core Lennard-Jones beads and finitely extensible springs. Kremer, Grest, and co-workers investigated static and dynamic network properties[3−12] as well as their cross-linking dynamics[13,14] and provided tests of the existing network theories.[7] One of their key findings was the importance of topological interactions and especially entanglements of network strands. The latter were shown to increase a network's shear modulus well above the predictions from classical network theories[6−8,11] even for strands shorter than their entanglement length.[5]

In network theories, the role of entanglements has been debated for a long time. The first network models, the affine[15,16] and phantom[17−19] network models, described chains as phantom-like, noninteracting strands that were coupled either affinely or not at all to a deforming background. Subsequent models incorporated topological interactions as restrictions of the fluctuations of network nodes and strands. It is, by now, accepted that the entanglement contribution to a network's shear modulus can greatly exceed the pure cross-link contribution.[20,21] For a discussion of the development of different network models, we refer to the corresponding literature,[22−24] but note that most of the modern ones are based on Edwards' tube model.[25,26] This model describes a single network strand as confined by a quasi-harmonic potential perpendicular to its primitive path. It is similar in spirit to its predecessor, the slip-link model,[21] where strand fluctuations are restricted by sliding junctions called slip links.

In simulations, structural defects and slow relaxation often necessitate large time and length scales, something that is extremely challenging in molecular dynamics simulations.[27] Coarse-grained and mesoscopic simulation techniques are capable of accessing these scales but usually have the disadvantage of employing soft-core potentials.[28] As a result, polymer chains and network strands may cross each other, which prevents these methods from correctly sampling related physical phenomena such as reptation[29] and in-tube relaxation.[26] Moreover, network shear moduli fail to show a contribution of trapped entanglements, that is, entanglements of immobile network strands unable to resolve by relaxation.[5]

Received: March 12, 2021
Revised: April 23, 2021
Published: May 20, 2021

https://doi.org/10.1021/acs.macromol.1c00567
Macromolecules 2021, 54, 5155−5166

Different approaches have addressed this shortcoming. For example, the mesoscopic dissipative particle dynamics (DPD) simulation method[30] was successfully employed to study general network structures[31,32] and the mechanical behavior of filled elastomer composites.[33−35] In these simulations, topological constraints were added via a segmental repulsion potential[36−38] or additional excluded-volume interactions.[39] Both methods introduce additional, steeper repulsions which work well in reproducing entangled dynamics but also necessitate the use of shorter time steps, or, put differently, with a given number of time steps, a smaller part of phase space is covered.

In polymer melts, an alternative route to restore entanglement effects into coarse-grained soft-core simulations at low computational costs evolved around the concept of slip links and slip springs. Their development until 2014 is laid out in a review by Masubuchi.[40] The first single-chain slip-link[41−44] and slip-spring[45] models are based on the tube- and slip-link network models. Their central picture describes a single chain reptating along its primitive path, held in place by slip links. In a multichain slip-link approach, Masubuchi et al.[46] proposed the primitive-chain network (PCN) model: here, pairs of Brownian, noninteracting chains were connected by slip links. Polymer chains were able to slide through their confining links, which reproduced their reptative motion and linear and nonlinear rheological properties. In 2012, Uneyama and Masubuchi[47] combined the PCN model and Likhtman's single-chain slip-spring model[45] into a successful multichain slip-spring method: here, the Brownian chains interacted via a number of artificial springs. These springs were allowed to migrate along the chains and followed their own dynamics of migration, creation, and destruction, which implied a sophisticated method in between conventional molecular dynamics simulations and single-chain models. Similar slip-spring mechanisms were adopted by different groups[48−50] and implemented into other coarse-grained methods suffering from the same shortcomings, such as DPD[51,52] and the hybrid particle field method.[53] Recently, the Brownian dynamics, DPD, and hybrid-particle-field slip-spring implementations were utilized for dynamical and hierarchical multiscale models.[54−56]

Given their popularity in soft-matter simulations, the applications of slip-link and slip-spring methods to networks have been surprisingly sparse. Shortly after its invention, Oberdisse and co-workers[57,58] extended the PCN model by a formalism for cross-links. In their description, a network consisted of nodes that were either tetrafunctional cross-links or slip links. Two nodes were separated by strands of a variable number of monomers, and slip links were allowed to exchange monomers between both adjacent strands. All chains were ideal, Brownian noninteracting chains besides cross-links and slip springs. This model successfully restored known topological and entanglement effects such as strain thinning and a nonzero shear modulus even for weakly cross-linked systems. However, dynamic properties such as the viscoelastic moduli have not been reported. More recently, Megariotis et al.[59] applied their multichain slip-spring Brownian dynamics method to elastomeric systems. They reported an approximate reproduction of the shear modulus of polyisoprene (PI) rubber by uniaxial strain experiments as well as the linear relaxation moduli of exemplary networks. However, the influence of slip springs was not systematically studied. In a similar extension to their multichain slip-spring model, Masubuchi and Uneyama[60] recently investigated the gelation process of entangled polymer melts but did not further study the resulting network.

Based on an earlier model for polymer melts,[52] here, we present an application of the slip-spring DPD model to study elastomeric networks. The mesoscopic DPD model is very coarse, and thus, mapping of chemical detail is very approximate. Its big advantage, however, is its computational efficiency due the softness of the DPD potential. This allows simulation times and system sizes which would otherwise be unattainable. Another reason for the popularity of DPD is the explicit treatment of hydrodynamic interactions, which facilitates a potential extension to, for example, gels. In this work, however, we focus on the influence of slip springs on a randomly cross-linked network free of dangling ends and their capability to restore different entanglement effects: in the first section, we present and characterize networks with different cross-link densities. Second, we focus on their relaxation dynamics: we study the retardation of strand motion and linear stress relaxation. Using regular DPD simulations as a reference, we can directly compare the influence of slip springs on our networks' viscoelastic moduli. We show that our model is capable of reproducing the frequency-dependent storage and loss moduli of PI rubber after straightforward cross-linking of a mapped DPD melt. Finally, we analyze how the presence of slip springs changes the entanglement contributions to the networks' shear moduli and probe their ability to reproduce the elaborate Kremer−Grest network simulations recently presented by Gula et al.[61]

METHODS

Slip-Spring DPD. We use the DPD simulation technique.[30,62,63] DPD is a mesoscopic method that describes nonbonded bead interactions as the sum of purely pairwise conservative, dissipative, and random forces. The dissipative and random forces are coupled and account for the system's friction and a stochastic contribution; they thus act as a thermostat. The conservative force is usually soft and short-ranged, which allows for large integration steps. Depending on the underlying mapping, a DPD bead may represent a few atoms, chain segments, or even entire domains[33] of soft-matter systems. This flexibility along with the low computational costs gives access to mesoscopic time and length scales, making DPD a popular method for the simulation of polymer melts,[51,52,64] solutions,[65−69] and even elastomeric systems.[31,32,34,35] In this work, we follow the method of Groot and Warren,[63] where the conservative force is purely linear and defined by a repulsion parameter a_{ij} and a cutoff radius r_c. Details can be found in the Simulation Details and ref 63. Our polymer chains are modeled by a standard bead-spring model,[70] where a weak Hookean spring is added onto the nonbonding interactions of bonded beads (eq 1)

$$\mathbf{F}_{ij}^{\mathrm{B,SS,CL}} = -k\mathbf{r}_{ij} \tag{1}$$

Equation 1 applies to permanently bonded beads as well as those connected by slip springs or cross-links, which are introduced below.

As a consequence of the soft bonded and conservative interactions, DPD beads and bonds can cross each other, which results in qualitatively incorrect polymer dynamics for chains longer than their entanglement length. To restore these entanglement dynamics, slip-spring DPD applications have been developed by Chappa et al.[51] and Langeloth et al.[52] In this work, we use the methodology of Langeloth et al., which we briefly present here. For further details, we refer to the original work (ref 52). Initially, a fixed number of slip springs is distributed in the simulation box to connect pairs of spatially close beads. After their initiation, both mounting points of each slip spring attempt a pre-defined number of migration steps, that is, a jump to any direct neighbor of its current anchor bead. Every trial step is accepted or rejected by a Metropolis Monte Carlo (MC) criterion.

https://doi.org/10.1021/acs.macromol.1c00567
Macromolecules 2021, 54, 5155−5166

After a set of migration steps, the slip springs are frozen and act as fixed bonds in a sequence of DPD steps. Before every MC migration block, slip springs located at a chain end perform a single relocation attempt: such a slip spring is deleted and a new slip spring is created at a randomly chosen chain end that is then connected to a random bead within a certain close distance. Again, the potential energy difference between the old and new slip springs is derived, and the relocation is accepted by a Metropolis MC trial. Thus, the number of slip springs is kept constant at all times. To avoid an energetic trapping of slip springs, migration moves are always discarded if they result in both mounting points falling on the same bead. Additionally, slip springs connecting two already bonded beads do not contribute in the DPD steps to avoid artificially strong bonds. They are, however, allowed to migrate. In actual simulations of melts, both these occurrences are very rare. To summarize, alternating execution of DPD and MC blocks allows for a certain slip-spring mobility while recovering entanglement effects like reptation[52] and constraint release[64] dynamics.

To simulate elastomers, cross-links are introduced: they are mounted on two different DPD beads, which we refer to as "cross-linked beads", but are fully immobile. Beside this additional bond, cross-linked beads behave regularly. Similar to existing slip-link and slip-spring implementations for elastomers,[57,59] our cross-linked beads cannot carry slip springs. Any slip-spring migration or relocation attempt to a cross-linked bead is thus rejected.

Cross-Linking. A variety of methods exist to create networks in simulations, such as random cross-linking of chain ends or all beads, and cross-linking of dedicated nodal points with a fixed sub-chain length.[9,31] Ideal networks, that is, networks without unconnected chain ends or loops, are commonly built on a lattice.[7] We follow a cross-linking method recently employed by Gula et al.:[61] starting from an equilibrated melt of linear chains, we first connect all chain ends to a randomly chosen bead of any other chain within a certain distance ($1.1\ r_c$). In this way, we prevent dangling ends, which brings our systems closer to the ideal state assumed by many network theories. It also conveniently prevents unconnected chains at low cross-linking densities. We then continue to cross-link random pairs of beads that are (i) not part of the same chain and (ii) within a defined spatial distance ($1.1\ r_c$) until the desired number of cross-links is achieved. Cross-links are modeled as harmonic springs, identical to regular bonds (eq 1). We note that while our networks do not contain intra-chain cross-links, dangling loops can still be formed on larger scales. Since our networks do not contain free chain ends, slip springs are trapped on the chains they were occupying in the precursor melt at the time of cross-linking. They are, however, allowed to migrate within the limits discussed above.

Simulation Details. We use reduced units. Our scales for time, length, mass, and energy are t_{DPD}, $l_{DPD} = r_c$, m_{DPD}, and $\varepsilon_{DPD} = k_BT$, respectively, where k_B and T are Boltzmann's constant and the temperature. Conversion factors for a comparison to experimental PI melts and rubbers are given in the respective sections. Our choice of DPD parameters follows the original work of Groot and Warren[63] for a bead number density of $3\ r_c^{-3}$. We choose a repulsion parameter of $a = 25\ k_BTr_c^{-1}$ and an integration step width of $\Delta t = 0.06\ t_{DPD}$. The force constant for bonds, slip springs, and cross-links is $k = 2\ k_BTr_c^{-2}$.

Slip-spring simulations follow the work of Langeloth et al.[52] The sequence length for both MC migration and DPD blocks is set to 500 steps, which was originally chosen to match the slip springs' spatial correlation time in both sequences.

Our precursor melts consist of 415 chains of length $N = 100$ in a $(24\ r_c)^3$ box, which results in a density of $\rho = 3.002$. All simulations are performed both without slip springs and with 4150 slip springs, with the latter corresponding to a slip-spring density of $\phi_{SS} = 0.1$, as suggested by Langeloth et al.[52] Melts are equilibrated for at least 5×10^6 time steps ($3 \times 10^5\ t_{DPD}$), which is roughly 10 times the disentanglement time of $\tau_d \approx 2.6 \times 10^4\ t_{DPD}$ found for $N = 100$ chains carrying slip springs. Melt properties are derived from production runs of 10^7 time steps ($6 \times 10^5\ t_{DPD}$).

Cross-linking is performed from the equilibrated melts as described above. The distance criterion for defining a cross-link between two beads is $1.1\ r_c$, which is slightly shorter than the average bond length of $1.21\ r_c$. However, length histograms for bonds, slip springs, and cross-links become indistinguishable after equilibration. Systems contain a total number of 830, 1245, 2490, 4150, and 6225 cross-links and will be referred to by their cross-link densities of $\phi_{cl} = 0.02$, 0.03, 0.06, 0.10, and 0.15, respectively. They correspond to average network strand lengths of 33.0, 19.9, 9.0, 5.2, and 3.4. Networks with $\phi_{cl} = 0.02$ are purely end-linked. Networks are equilibrated for 5×10^6 time steps ($3 \times 10^5\ t_{DPD}$) before production runs of 10^7 time steps ($6 \times 10^5\ t_{DPD}$).

To investigate the behavior of strained networks, we additionally perform uniaxial strain experiments. Here, we initially stretch the z-components of the simulation box and all bead positions of the equilibrated network systems by a factor of $\lambda \in [1.1, 1.2, 1.4, 1.6, 1.8]$. At the same time, x- and y-components are deformed by $\lambda^{-0.5}$ for volume conservation. We note that the inevitability of bond crossing allows us to stretch the systems in a single step, while elongation has to be performed carefully and slowly in hard-core systems.[61] The stretched networks are equilibrated for 5×10^6 time steps ($3 \times 10^5\ t_{DPD}$), and normal stresses are measured in 10^6 additional time steps ($6 \times 10^4\ t_{DPD}$).

For all simulations, system properties are averaged over 10 independent runs for every combination of ϕ_{SS}, ϕ_{cl}, and, for uniaxial strain experiments, λ. Thus, different networks are investigated, which are necessary given the loss of ergodicity in cross-linked systems.[31] If not denoted otherwise, average values are stated. Errors are the standard error of the mean or, in the case of a fitted property, the fitting error. Except for the comparison with other systems, units will be omitted from here on. Simulation time is given in t_{DPD}.

Experiments. For experimental validation, unfilled PI rubber samples are prepared in a mixer using the recipes in Table 1. Two different samples IR_1 and IR_2 with varying amounts of sulfur and the accelerator represent two different network densities. Both are vulcanized up to their respective optimal degree of cross-linking. A dynamic-mechanical analysis is performed on a GABO EPLEXOR in the compression mode. Here, frequency sweeps at varying temperatures are conducted. Using the shifting procedure according to the Williams–Landel–Ferry equation,[71] a corresponding master curve for the storage modulus for both samples is obtained. The effective network density is measured on a Bruker BioSpin 400 MHz spectrometer using the technique of solid-state NMR. In particular, the method of the Hahn spin echo[72] is used to obtain the average molecular weight between respective localizations, that is, chemical cross-links and elastically active entanglements.

Table 1. Recipes to Create PI Rubber Samples IR_1 and IR_2 with Two Different Network Densities[a]

ingredient	IR_1	IR_2
PI	100	100
zinc oxide	2	2
stearic acid	1	1
sulfur	0.65	0.85
CBS[b]	6.5	8.5

[a]Quantities are given in "per hundred rubber" (phr). [b]*N*-Cyclohexyl-2-benzo-thiazole sulfenamide.

RESULTS AND DISCUSSION

Network Properties. Our characterization of cross-linked networks follows the work of Gula et al.[61] We first identify individual cross-links, that is, pairs of cross-linked beads. If two cross-linked beads (which must belong to two different cross-links) are first neighbors, both respective cross-links are formally viewed as part of the same larger cross-link cluster. These clusters are connected by a number of network strands. For high cross-link densities ϕ_{cl}, the formal number of cross-

https://doi.org/10.1021/acs.macromol.1c00567
Macromolecules 2021, 54, 5155–5166

Table 2. Averaged Properties of the Slip-Spring Networks for Different Cross-Link Densities ϕ_{cl}[a]

ϕ_{cl}	$\langle N_s \rangle$	$\langle N_s^{fix} \rangle$	N_{str}^{good}/N_{str}	N_{cl}^{good}/N_{cl}	f	G^{aff}	G^{ph}
0.02	32.98(25)	5.2(9)	0.999(0)	1.000(0)	3.047(2)	0.08731(39)	0.02995(2)
0.03	19.86(13)	4.8(8)	0.998(0)	1.000(0)	3.460(4)	0.14178(61)	0.05964(6)
0.06	9.01(4)	3.8(8)	0.994(0)	1.000(0)	4.090(6)	0.29133(136)	0.14801(11)
0.10	5.21(2)	3.0(5)	0.989(0)	1.000(0)	4.776(7)	0.45559(174)	0.26280(18)
0.15	3.42(1)	2.4(3)	0.977(1)	1.000(0)	5.934(18)	0.59933(466)	0.39277(57)

[a]The properties of networks without slip springs are virtually identical. Shown are the average strand lengths $\langle N_s \rangle$ and $\langle N_s^{fix} \rangle$, the fractions of good network strands and cross-links, N_{str}^{good}/N_{str} and N_{cl}^{good}/N_{cl}, the average cross-link functionality f, and the affine and phantom moduli G^{aff} and G^{ph}. For an explanation of these properties, see the text.

link clusters can thus be lower than the original number of cross-links distributed in the melt. Similarly, their functionality, that is, the number of connected network strands, can exceed a value of 4. For the characterization of network properties, we will only discuss cross-link clusters and use the term "cross-link" equivalently. The identification of these cross-links and network strands allows the characterization of a network's average strand length $\langle N_s \rangle$ and cross-link functionality f. We further classify cross-links and strands by their ability to be elastically active: cross-links are "good" if they are connected to at least two "good" strands. "Good" strands have neither loops nor dangling ends, nor are they connected to a "bad" cross-link.[61] Note that dangling ends and intra-chain loops are forbidden in our networks by construction. The numbers of good strands N_{str}^{good} and cross-links N_{cl}^{good} allow the analytical derivation of the network's shear moduli within the affine and phantom network models (eq 2)[6]

$$G = \frac{k_B T}{V}(N_{str}^{good} - hN_{cl}^{good}) \tag{2}$$

Here, V is the volume of the simulation box and $k_B T = 1$. The cases $h = 0$ and $h = 1$ are the affine and phantom network moduli G^{aff} and G^{ph}.[6] The affine network model describes the strain response of a network where all network nodes are displaced affinely without any strand fluctuations.[23] G^{ph} is the network modulus if nodes are freely fluctuating, and strand interactions are thus fully neglected.[73] The derived values for $\langle N_s \rangle$, f, G^{aff}, and G^{ph} are given in Table 2 along with the ratios of good strands and cross-links. Also shown are the average strand lengths $\langle N_s^{fix} \rangle$ of entanglement networks where slip springs are considered frozen and act as additional cross-links. They are averaged over multiple slip-spring positions. As expected, the end-linked $\phi_{cl} = 0.02$ networks have mostly trifunctional cross-links, while f increases with increasing cross-link density. Similarly, the average strand length and the fraction of good strands decrease with increasing ϕ_{cl}. The latter is due to the formation of loops, which are, however, still very rare. We will return to the derived G^{aff}, G^{ph}, and $\langle N_s^{fix} \rangle$ later.

While the fraction of elastically active strands and cross-links is very high, a minor imperfection is revealed by investigating the networks' strand-length distribution. Figure 1 compares the distribution of network strand lengths N_s with the respective probabilities $P(N_s)$ expected for an exponential distribution[61] (eq 3)

$$P(N_s) = \langle N_s \rangle^{-1} \exp\left(-\frac{N_s}{\langle N_s \rangle}\right) \tag{3}$$

It is clear that the exponential distribution is followed in most cases. However, networks with a low cross-link fraction show a distinct uptick for $N = 98$, which is the longest possible

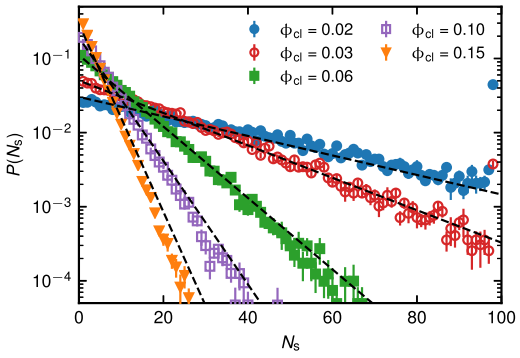

Figure 1. Probability distribution of network strand lengths N_s (symbols) and their expected exponential form (eq 3, dashed lines). The histograms are averaged over 10 different networks carrying slip springs. Networks without slip springs show identical statistics.

strand length for our $N = 100$ chains. This is a finite-chain-length artifact. For comparison, we also constructed networks from (unequilibrated) random-walk melts of chains up to $N = 1500$, which showed a considerable probability for strands with $N_s > 98$ (not shown). These strand lengths are clearly underrepresented in the present networks. However, other properties of the $N = 100$ networks are well met, which is especially true for higher ϕ_{cl}. On the other hand, longer chains require a drastically increased equilibration time for both precursor melts and networks. We thus consider the slightly flawed strand-length distributions a reasonable price to pay.

It is worth noting that the networks discussed up to this point are averaged over 10 different realizations, all of which carry slip springs and are cross-linked from equilibrated slip-spring melts. Static properties of the precursor melts are very weakly affected by the presence of slip springs:[51,52] since slip springs introduce an additional attractive potential, they effectively decrease the system's pressure, which could lead to compression. If inter-particle repulsions are weak, this raises the necessity of a compensating potential,[51] which comes, however, at high computational costs.[59] The strongly repulsive interactions of DPD beads were found to sufficiently cancel this effect.[52,74] Still, the end-to-end distances of the precursor melts show a weak contraction of about 6% when slip springs are included. This effect is, however, small enough to become negligible when cross-links are added too. We find all investigated static network properties (Table 2) to be virtually indistinguishable for networks with and without slip springs. We emphasize that the distributions of bond lengths and end-to-end distances observed in the precursor melts are not altered by cross-links, which is in line with earlier simulation studies.[9,59] However, the reproduction of the respective

https://doi.org/10.1021/acs.macromol.1c00567
Macromolecules 2021, 54, 5155−5166

histograms (not shown) requires averaging over all 10 network realizations due to the absence of ergodicity.[31]

Network Relaxation Dynamics. Restoring the dynamic effects of chain uncrossability, such as reptation, into soft-core models has been the original purpose of slip springs. In this section, we first focus on how dynamic network properties, namely, monomer mean squared displacements (MSDs), linear relaxation moduli, and storage and loss moduli, are affected if slip springs are added to our soft-core networks. We then attempt a comparison of the dynamic moduli to experimental systems to see whether mapping is possible and easily transferable from slip-spring melt simulations.

Influence of Slip Springs on Network Relaxation Dynamics. The MSD of the central bead of DPD chains in melts is shown in Figure 2 with and without slip springs and

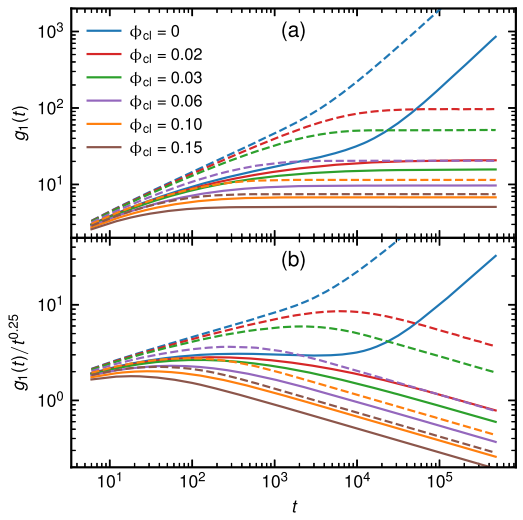

Figure 2. (a) MSD $g_1(t)$ of DPD chains in melts (ϕ_{cl} = 0) and networks with different cross-link densities. The MSD is monitored for the central beads of the melt chains and compared to the same beads after cross-linking. Continuous and dashed lines indicate systems with and without slip springs, respectively. To highlight the $\propto t^{0.25}$ scaling expected for reptating chains in melts, the MSD is shown in a reduced fashion in (b).

compared to the MSD of the same beads after cross-linking ($\phi_{cl} \in [0.02, 0.03, 0.06, 0.10, 0.15]$). As expected, cross-links drastically decrease the beads' mobility. The MSDs of all network systems approach a plateau which decreases with increasing cross-link density. In contrast, beads in the melts (ϕ_{cl} = 0) eventually show free diffusion. The diffusive behavior for DPD melts with and without slip springs is well understood:[52] while soft-core DPD chains without slip springs (dashed, blue lines in Figure 2) show the Rouse-like motion of unentangled chains with $g_1 \propto t^{0.5}$ before assuming free diffusion, slip springs restore the scaling associated with a reptative motion ($g_1 \propto t^{0.25}$, continuous blue line). This is especially visible in the reduced presentation in Figure 2b. For networks, slip springs reduce the space available to the monomer beads additionally, as indicated by the reduced plateau of $g_1(t)$. This decrease by about 79, 69, 52, 41, and 32% of the unentangled plateau value for ϕ_{cl} = 0.02, 0.03, 0.06, 0.10, and 0.15 indicates that the impact of slip springs is weaker for higher cross-link densities. We note that we effectively observe a suppression of network strand fluctuations, which is one of the oldest interpretations of entanglement effects in networks.[23] Additionally, Figure 2b reveals that the monomers in weakly cross-linked networks (ϕ_{cl} = 0.02, blue lines) closely follow the behavior of those in a melt until network restrictions set in; this is observed for systems both with and without slip springs. A reptation-like scaling regime in networks is known, for example, from hard-core simulations of polyethylene rubber.[75] While this is not yet fully pronounced for slip-spring simulations with ϕ_{cl} = 0.02, we believe that a $g_1(t) \propto t^{0.25}$ behavior would be restored if longer strand lengths could be considered.

The linear relaxation moduli $G(t)$ are derived from stress fluctuations employing the linear-response theory (eq 4), where $\sigma_{\alpha\beta}$ with $\alpha, \beta \in [x, y, z]$ are the off-diagonal elements of the stress tensor (eq 5)[76]

$$G(t) = \frac{V}{3k_BT}\sum_{\alpha\neq\beta}\langle\sigma_{\alpha\beta}(t)\sigma_{\alpha\beta}(0)\rangle \tag{4}$$

$$\sigma_{\alpha\beta} = \frac{1}{V}\left(-\sum_i m_i v_{i\alpha}v_{i\beta} + \frac{1}{2}\sum_{i,j\neq i} r_{ij\alpha}f_{ij\beta}\right) \tag{5}$$

Here, the velocities $v_{i\alpha}$, $v_{i\beta}$ of every bead i contribute as well as all forces f_{ij} between particles i and j at distance r_{ij}. This includes all DPD forces, slip springs, and cross-links. We briefly investigate the individual contributions of nonbonded interactions, bonds, slip springs, cross-links, and their correlations (not shown). For both melts and networks, $G(t)$ is dominated by bond contributions except for very short times. Since slip springs and cross-links are modeled identical to regular bonds, their contributions equal their fractions ϕ_{ss} and ϕ_{cl}. We extract $\sigma_{\alpha\beta}$ every time step and derive $G(t)$ from eq 4, where the autocorrelation is computed using the multi-τ correlator of Ramírez et al.[77] A comparison of our melts and networks is shown in Figure 3. Again, melts with and without

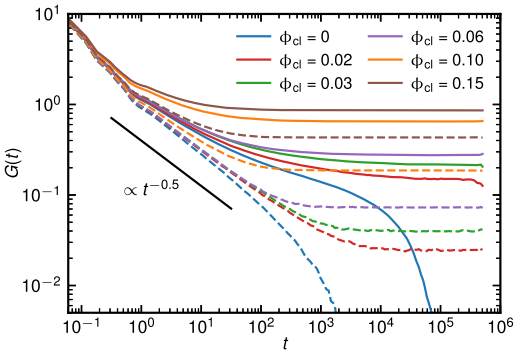

Figure 3. Linear relaxation moduli $G(t)$ of DPD melts (ϕ_{cl} = 0) and networks. Systems with and without slip springs are shown by continuous and dashed lines, respectively. The black line indicates a Rouse-like decay of $\propto t^{-0.5}$.

slip springs show the known behavior:[52,59] while $G(t)$ of the unentangled melt roughly follows a $\propto t^{-0.5}$-decay associated with Rouse-mode relaxation before the terminal exponential decay, the presence of slip springs leads to a clearly visible yet not fully developed entanglement plateau. Cross-linked systems expectedly decay to a nonzero plateau irrespective of the presence or absence of slip springs. In the absence of slip springs, this decay follows a $G(t > 1) \propto t^{-0.5}$ trend, which is

https://doi.org/10.1021/acs.macromol.1c00567
Macromolecules 2021, 54, 5155−5166

visibly suppressed by slip springs. They additionally increase the terminal plateau moduli. In contrast to melts, slip springs thus not only slow the relaxation dynamics of networks but also have an effect on their static properties. We investigate a trial network with $\phi_{cl} = 0.06$ which does contain slip springs but allows them to migrate and relocate as if they populated a melt (not shown). Here, relaxation is still retarded, but the eventually assumed plateau modulus is the one of networks without slip springs. This confirms that the increase in the plateau moduli stems from trapping of slip springs, a mechanism probably analogous to the trapping of entanglements in real systems.[78]

We continue by deriving the storage and loss moduli $G'(\omega)$ and $G''(\omega)$ from the Fourier transform of the relaxation modulus $G(t)$. This is done using the i-Rheo algorithm[76] implemented in the REPTATE rheology toolkit.[79] The different moduli are shown in Figure 4. Clearly, an increase

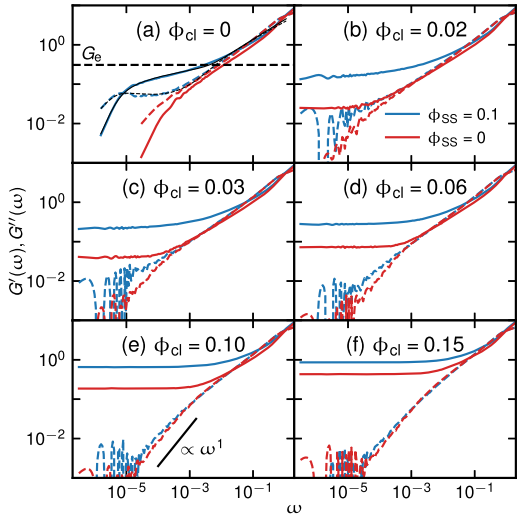

Figure 4. Storage ($G'(\omega)$) and loss moduli ($G''(\omega)$) of DPD melts (a) and networks (b–f) of different cross-link densities ϕ_{cl} with (blue) and without (red) slip springs. Storage and loss moduli are given by continuous and dashed lines, respectively. The thin, black lines in (a) are a fit of the Likhtman–McLeish theory.[80] Also indicated are the entanglement modulus G_e of the slip-spring melt (a) and the low-frequency scaling of the loss moduli (e).

in ϕ_{cl} increases the storage moduli of systems both with and without slip springs, while the loss moduli appear unaffected. Slip-spring systems show a slower relaxation for both G' and G'', which is especially visible in the scaling behavior of the loss modulus: a low-frequency scaling of $G'' \propto \omega^1$ is expected for both relaxed networks and melts[81] and is observed for systems without slip springs (e.g., Figure 4e). For stronger cross-linked networks with slip springs ($\phi_{cl} \geq 0.10$), the loss modulus resembles the one of networks without slip springs. The loss modulus of the slip-spring $\phi_{cl} = 0.02$ network, on the other hand, is closer to the one of the slip-spring melt. To our understanding, the lower exponent of the low-frequency $G''(\omega)$ indicates that the network is not yet relaxed. This is in line with the observation that the storage moduli of the weakly cross-linked slip-spring networks ($\phi_{cl} \leq 0.03$) have apparently not reached a plateau at the lowest observed frequencies. Whether or not slip springs delay the relaxation is likely connected to their mobility. The approached low-frequency storage plateau is higher than that for networks without slip springs. As noted before, this difference decreases with increasing cross-link density. We will return to this when discussing the static network properties.

For later reference, we take an excursus to derive some rheological properties of our precursor melt chains from the storage and loss moduli. Both G' and G'' of the slip-spring melt are well approached by a fit to the Likhtman–McLeish theory[80] (thin, black lines in Figure 4a), which we perform using the REPTATE toolkit. For our melt, this gives $G_e = 0.308(5)$, $N_e = 11.7(1)$, and $\tau_e = 52.6(24)$ for the entanglement modulus, the entanglement length, and the entanglement time, respectively. The best fit is found for a constraint-release coefficient of $c_\nu = 0.01$, which is in line with earlier findings that constraint-release dynamics is of little importance in monodisperse systems.[64] We note that here, G_e and N_e are fitted as independent parameters. Their relation is still under discussion[82] and likely affected by, for example, the functionality of entanglements and the fluctuations imposed on their anchoring points.[82−84] However, the classical theory of rubber elasticity relates them as[25]

$$G_e = \frac{\rho k_B T}{N_e} = \frac{\rho k_B T}{2N_e^{SS}} \tag{6}$$

where ρ is the system's mass density. For entanglements modeled by slip springs as binary topological contacts with an average segmental distance of N_e^{SS}, the relation $N_e = 2N_e^{SS}$ between rheological and topological entanglements has been suggested by Everaers.[85] Inserting the fitting result $G_e = 0.308$ into eq 6 gives $N_e \approx 9.7$ and $N_e^{SS} \approx 4.9$. The measured average distance between two slip springs in our melts is $N_e^{SS} = 4.59(1)$, which is remarkably close to the classical prediction.

Comparison to Experimental Systems. With our networks' storage and loss moduli known, we attempt a mapping to experimental systems. Example networks of PI rubbers are synthesized and characterized as presented in the Methods section. We determine conversion factors for the molecular weight, time, and moduli from rheological data for the $M_w = 33.6$ kg/mol PI melt of Auhl et al.[86] The authors give an entanglement molecular mass of $M_e = 4.82$ kg/mol ($N_e = M_e/M_{isoprene} = 70.8$) with $Z = 7.0$ entanglements per chain. The extracted experimental moduli (at $T = 25$ °C) are shown in Figure 5a. By matching the values of Z, we find this system to correspond to a monodisperse melt of $N = 2N_e^{SS}Z \approx 64$ DPD chains, which we study in a set of 30 independent simulations of 129 chains in a $(14\ r_c)^3$ box. Fitting of the storage and loss moduli to the Likhtman–McLeish theory[80] gives $G_e = 0.560(12)$ MPa, $\tau_e = 11.3(7)$ μs, $M_e = 4.79(5)$ kg/mol ($N_e = 70.3(7)$) for the experimental 33.6 kg/mol melt and $G_e = 0.337(68)$, $\tau_e = 43.9(23)$, $M_e = N_e = 9.1(1)$ for our $N = 64$ DPD melt (in reduced units). Both systems have $Z = 7.0$ entanglements per chain. We note that the fitted properties show slight deviations from those derived for the $N = 100$ DPD chain. They probably come from the fitting procedure. However, matching the number of experimental monomers per DPD bead (N_{DPD}) and the DPD units of molar mass, modulus, and time (M_{DPD}, $G_{DPD} = k_B T/r_c^3$, t_{DPD}) to real units gives eqs 7–9, which yield an excellent overlap between experimental and simulated melts (Figure 5a)

$$N_{DPD} \approx 7.7 \Rightarrow M_{DPD} \approx 0.525 \text{ kg/mol} \tag{7}$$

$$G_{DPD} \approx 1.661 \text{ MPa} \tag{8}$$

https://doi.org/10.1021/acs.macromol.1c00567
Macromolecules 2021, 54, 5155–5166

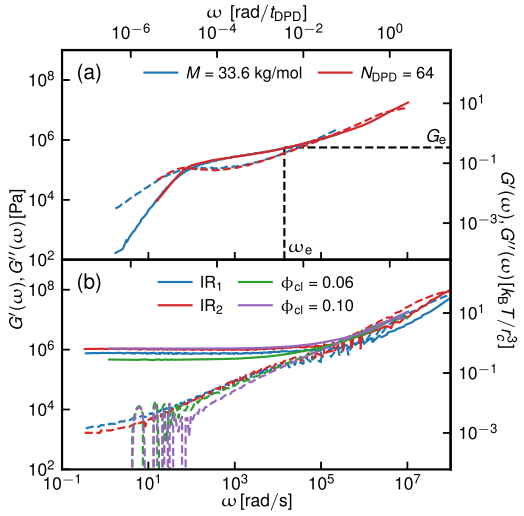

Figure 5. Comparison to experimental storage and loss moduli $G'(\omega)$ and $G''(\omega)$ (continuous and dashed lines, respectively). (a) Slip-spring DPD melts ($N = 64$) are compared to the $M = 33.6$ kg/mol PI melts of Auhl et al.[86] by matching their entanglement length, entanglement modulus G_e, and entanglement time $\tau_e = 2\pi/\omega_e$. (b) The estimated conversion factors are employed to compare slip-spring DPD networks with PI rubbers. The average (converted) strand lengths between cross-links and slip springs are 3.9, 3.3 for experimental IR_1 and IR_2 systems and 3.8(8), 3.0(5) for $\phi_{cl} = 0.06$ and 0.10 DPD networks, respectively (in DPD units).

$$t_{DPD} \approx 2.57 \times 10^{-7}\ \text{s} \tag{9}$$

We note that the same experimental reference system has previously been used by Ramírez-Hernández et al.[87] and Masubuchi and Uneyama[74] to map their multichain slip-spring models. Their chains had $N = 32$ and $N = 84$ beads and thus a different yet roughly comparable coarseness compared to ours. However, the comparison of different models is beyond the scope of this work.

We finally use the derived conversion factors to compare our cross-linked melts to the experimental PI rubbers. The dry (unswollen) rubbers are characterized by solid-state NMR measurements, which yield average strand weights of $\bar{M}_s = 2.058$ and 1.745 kg/mol for the IR_1 and IR_2 systems. Following eq 7, these correspond to roughly 3.9 and 3.3 DPD beads, respectively. Since $\bar{M}_s$ is measured in the dry state, it effectively describes the average network strand between both cross-links and entanglements. We thus compare it to the strands between slip springs and cross-links $\langle N_s^{fix} \rangle$ (Table 2). The storage and loss moduli of the experimental IR_1 and IR_2 rubbers are shown in Figure 5b and next to our $\phi_{cl} = 0.06$, 0.1 slip-spring networks, which have similar strand lengths of $\langle N_s^{fix} \rangle = 3.8(8)$ and 3.0(5), respectively. In the low-frequency regime, the DPD systems indeed reproduce the experimental rubber reasonably well. The plateau moduli of the IR_2 and $\phi_{cl} = 0.1$ systems match remarkably, while the loss modulus decays slightly faster for the DPD simulation. The IR_1 and $\phi_{cl} = 0.06$ systems show slightly different plateau moduli. This is possibly due to the stronger fluctuations in slip-spring positions since the average strand length for the $\phi_{cl} = 0.06$ networks is close to N_e. However, an overall good agreement is reached for all frequencies $\omega \leq \omega_e = 2\pi/\tau_e$. At high frequencies, a strong compression of the simulated $G'(\omega)$ and $G''(\omega)$ curves is visible, an effect often found for coarse-grained models.[28] Our DPD network is thus not able to appropriately separate shorter time scales, which is, however, fully expected for such a simple and coarse model. Considering that a sophisticated match of static moduli and dynamic behavior is not given in simulations without slip springs (compare Figure 4d,e), we conclude that our networks become generally capable of modeling experimental rubbers by the inclusion of slip springs. Finally, we emphasize that the mapping between the experiment and simulation has been done for melt systems; no network parameters entered the procedure. However, this mapping reproduces well the elastic behavior of cross-linked elastomers too.

Contribution of Slip Springs to the Shear Moduli. In slip-spring simulations of polymer melts, a crucial requirement is that static chain properties are not (strongly) affected by the addition of slip springs. In networks, on the other hand, a contribution of entanglements to the static shear modulus G is well known,[24] and the chains' inability to freely cross has been explicitly probed and confirmed to affect G in several simulation studies.[11,67] The slip-link models of Ball et al.[21] and Edwards and Vilgis[25] provide a theoretical description of this influence, which has, in parts, also been observed by Oberdisse et al.[57,58] in their network implementation of the PCN slip-link model. In this section, we study the contribution of entanglements and cross-links in networks with and without slip springs. We access them by performing uniaxial strain experiments where equilibrated networks are deformed by a factor of $\lambda \in [1.1, 1.2, 1.4, 1.6, 1.8]$ in the z-direction and $\lambda^{-0.5}$ in the x- and y-directions. The deformations are in a range where finite extensibility effects are expected to be negligible.[57] Details are given in the Simulation Details.

Restoration of the Entanglement Contribution. In a network uniaxially deformed by a factor of λ in the z-direction, the shear modulus G is accessible via the normal tension σ_N (eq 10)[24,61]

$$\sigma_N = \sigma_{zz} - 0.5(\sigma_{xx} + \sigma_{yy}) = G(\lambda^2 - \lambda^{-1}) \tag{10}$$

One of the oldest and most established models for derivation of the shear modulus G is the Mooney–Rivlin model,[88,89] which assumes a linear λ^{-1}-dependence. Here, the reduced normal tension $\sigma_N/(\lambda^2 - \lambda^{-1})$ is described by the two Mooney–Rivlin coefficients C_1 and C_2 (eq 11)

$$\frac{\sigma_N}{\lambda^2 - \lambda^{-1}} = 2C_1 + \frac{2C_2}{\lambda} \tag{11}$$

The stress response of our networks without and with slip springs is shown in Figure 6a,b, respectively. Generally, the normal tension increases with increasing cross-link density and the addition of slip springs. Systems without slip springs show no clear dependence of $\sigma_N/(\lambda^2 - \lambda^{-1})$ on λ^{-1}. Fits of eq 11 are close to a horizontal line for all these networks. They thus show the stress response of unentangled networks, which is in line with the fact that the interaction of different strands allows unrestricted bond crossing. In contrast, a decrease of the reduced normal tension with increasing deformation is expected for real systems. This is more pronounced for low cross-linked systems where cross-links are not yet the dominant factor. Indeed, the presence of slip springs introduces a weak strain thinning. Slip-link network theories[21,25] attribute this to the larger space accessible for slip links in strained network strands, resulting in stronger strand fluctuations. The shear modulus thus decreases under

https://doi.org/10.1021/acs.macromol.1c00567
Macromolecules 2021, 54, 5155–5166

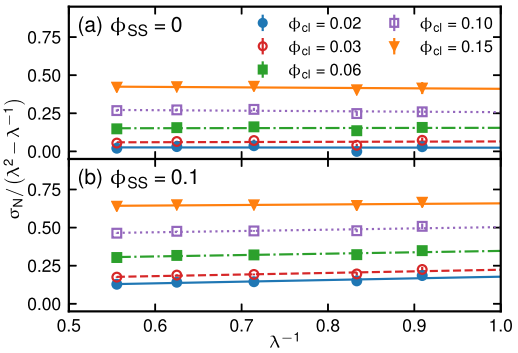

Figure 6. Reduced normal tension $\sigma_N/(\lambda^2 - \lambda^{-1})$ as a function of the inverse z-strain λ^{-1}. The stress response of different networks without (a) and with (b) slip springs is shown. Lines are a fit to the Mooney–Rivlin model (eq 11).

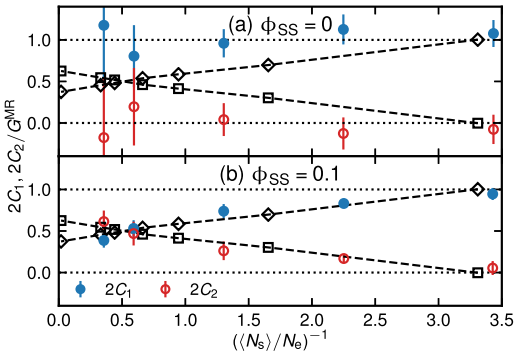

Figure 7. Contribution of the Mooney–Rivlin coefficients C_1 and C_2 to the shear modulus $G^{MR} = 2C_1 + 2C_2$ for networks of different reduced inverse strand lengths $(\langle N_s\rangle/N_e)^{-1}$. $N_e \approx 11.7$ was earlier derived for our $N = 100$ slip-spring DPD chains. Systems without and with slip springs are shown in (a) and (b), respectively. Black diamonds and squares are the values of $2C_1$ and $2C_2$ reported by Gula et al.[61] for their hard-core systems. Dashed lines are linear interpolations of their data. Dotted lines represent $2C_{1,2} = 0$, G^{MR}. The error bars for the end-linked systems without slip springs ((a), $(\langle N_s\rangle/N_e)^{-1} \approx 0.4$, $2C_1 = 1.18(67)$, $2C_2 = -0.18(72)$) are truncated for clarity.

strain. However, the "slippage" commonly employed in these models is independent of the strand elongation, which likely overestimates the strain thinning.[58] Consistent with our findings, the simulations of Oberdisse et al.[57,58] give a rather weak strain thinning for their shorter network strands ($\langle N_s\rangle \approx N_e$).

We further investigate the contribution of the Mooney–Rivlin coefficients C_1 and C_2 to the shear modulus $G^{MR} = 2C_1 + 2C_2$. Many models associate C_1 with both entanglement and cross-link contributions and C_2 with entanglement contributions only.[90] However, their exact share is still debated.[61] In a recent work, Gula et al.[61] present Mooney–Rivlin coefficients for a large network of Kremer–Grest bead-spring chains with a structure similar to ours. It must be noted that their chains have a bending stiffness to represent poly(dimethylsiloxane) chains. However, this stiffness is very weak, making their model practically identical to the original standard model in molecular simulations.[91] Given that the Kremer–Grest model does not allow chain crossing and has successfully been reproduced by slip-spring DPD simulations in the past,[52,64] we utilize their work as a reference system. The contributions of the Mooney–Rivlin coefficients to G^{MR} are shown in Figure 7 as a function of the reciprocal strand length $\langle N_s\rangle^{-1} \propto \phi_{cl}$. The latter is reduced by the entanglement length N_e previously derived for the $N = 100$ melts. For comparison, the data of Gula et al. are shown as black symbols and interpolated by dashed lines. For long strand lengths, they report a modulus dominated by entanglement effects. Correspondingly, C_2 exceeds C_1. As the cross-link density increases, C_1 grows linearly with $\langle N_s\rangle^{-1}$ until $2C_1 \approx G^{MR}$ is reached for short network strands. The authors interpret this as a transfer of entanglement contributions from C_2 to C_1.[61] The DPD networks without slip springs do not show this effect (Figure 7a). As expected for unentangled and phantom networks, C_2 shows very little contribution to G^{MR}. For some strand lengths, a formally negative C_2 coefficient is derived, which is, however, likely of statistical nature. Both C_1 and C_2 are constants within the error bars upon a change of the average strand length. In contrast, slip-spring DPD simulations reproduce the $2C_{1,2}/G^{MR}$ ratios of the hard-core Kremer–Grest simulations (Figure 7b): while $C_1 < C_2$ is found for the end-linked networks, $2C_1 \approx G^{MR}$ and $2C_2 \approx 0$ are determined for $\phi_{cl} = 0.15$. Moreover, our data directly fall onto the intrapolated values of Gula et al. in most cases. This confirms that despite their inability to avoid bond crossing, slip springs are capable of restoring the static effects of trapped entanglements shown by hard-core network strands.

A more direct access to the contributions of entanglements and cross-links to G is suggested by the nonaffine slip-tube model of Rubinstein and Panyukov.[92] It assumes explicit additive contributions of the entanglement modulus G_e^{RP} and the cross-link modulus G_c^{RP} and has been shown to accurately describe stress relaxation in real networks.[93,94] The established approximation to its numerical solution is given by eq 12[92]

$$\frac{\sigma_N}{\lambda^2 - \lambda^{-1}} = G_c^{RP} + \frac{G_e^{RP}}{0.74\lambda + 0.61\lambda^{-1/2} - 0.35} \tag{12}$$

Fitting to the result of our uniaxial strain experiments (Figure 6) gives the moduli presented in Figure 8. The latter are reduced by the earlier derived melt entanglement modulus $G_e = 0.308$. For networks without slip springs (Figure 8a), the

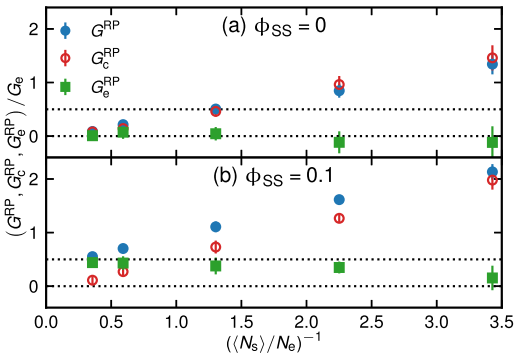

Figure 8. Shear, cross-link, and entanglement moduli G^{RP}, G_c^{RP}, and G_e^{RP} derived by a fit of the nonaffine slip-tube model[92] to uniaxial strain experiments. Systems without and with slip springs are shown in (a) and (b), respectively. All moduli are reduced by the entanglement modulus $G_e = 0.308$ derived earlier for our $N = 100$ slip-spring DPD melt and plotted for different reduced inverse strand lengths $(\langle N_s\rangle/N_e)^{-1}$. Dotted horizontal lines at 0 and 0.5 are to guide the eye (see text).

https://doi.org/10.1021/acs.macromol.1c00567
Macromolecules 2021, 54, 5155–5166

fitted entanglement modulus is 0 within the error bars for all strand lengths. Consequently, the shear modulus $G^{RP} = G_c^{RP} + G_e^{RP}$ is essentially the cross-link contribution. The addition of slip springs introduces a distinct entanglement contribution (Figure 8b), which decreases for higher cross-link densities. This is especially visible for the strongest cross-linked $\phi_{cl} = 0.15$ systems and likely related to the drastically reduced mobility of slip springs. At the same time, the cross-link modulus G_c^{RP} of slip-spring networks is considerably higher than that of comparable networks without slip springs. To our understanding, trapped slip springs thus act as additional cross-links. Whether or not this behavior is physical will be discussed in the next section. For long network strands ($N_s \gtrsim N_e$), G_e^{RP} approaches a value close to $0.5G_e$ (Figure 8b, dotted line). This value is associated with the plateau modulus $G_N^0 = 0.5G_e$ of polymer melts in the slip-link model of Masubuchi et al.[83] Note that in melts, the difference between the plateau and entanglement moduli arises from relaxation mechanisms in contrast to a hypothetical network of "fixed" entanglements. For their multichain slip-spring model, Uneyama and Masubuchi[82] recently derived

$$G_N^0 \approx 0.24 \times \frac{\rho k_B T}{N_e^{SS}} \approx 0.48 \times G_e \tag{13}$$

where the second equality comes from eq 6. We thus identify G_e^{RP} of weakly cross-linked networks as the plateau modulus of the corresponding slip-spring polymer melt. It is worth noting that the cross-link modulus approaches 0 for these systems. This indicates that $G^{RP}(\langle N_s\rangle^{-1} \to 0) \approx G_e^{RP} \approx G_N^0$ is approached for infinitely long strands, a behavior consistent with experimental observations.[95]

Influence of Slip Springs on the Shear Moduli. We last investigate the shear moduli G^{MR} derived in the previous sections. We focus on those extracted using the Mooney–Rivlin model, but note that the Rubinstein–Panyukov model provides very similar results. The shear moduli for systems with and without slip springs are shown in Figure 9. They are compared to the earlier derived affine and phantom network moduli (G^{aff} and G^{ph}, Table 2) as well as those of the hard-core Kremer–Grest simulations of ref 61. Gula et al.[61] also provide the contributions of cross-links only (G_c). The latter were derived by disabling their networks' nonbonded interactions and deforming the resulting phantom chains.[93] The reduced values of G_c (Figure 9, empty, gray triangles) show a close resemblance to our no-slip-spring DPD networks (red circles), which is little surprising given their methodological similarity. Moreover, both data sets coincide with our phantom network prediction. This confirms that DPD networks without slip springs do indeed behave as phantom networks, which is in line with the results of the Rubinstein–Panyukov fit. Consideration of nonbonded interactions shifts the data of Gula et al. by a constant increment of $1.10 \times G/G_e$ while preserving the slope of the phantom networks (full, gray triangles). This is not the case when slip springs are included into the DPD networks (blue circles): First, the reduced quantities G/G_e are significantly lower than those for the Kremer–Grest networks. This is not unexpected as slip springs only restore entanglement effects but are not meant to fully compensate for hard-core nonbonded interactions. Second, the slope of $G(\langle N_s\rangle^{-1})$ displayed by slip-spring DPD networks differs from the one observed for the phantom chains. Fitting the respective data gives $G/G_e \approx 0.41(3) \times (\langle N_s\rangle/N_e)^{-1} -$

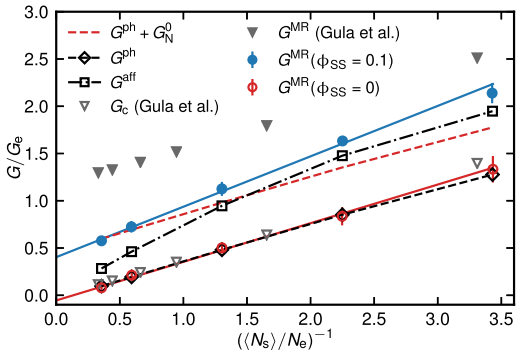

Figure 9. Reduced shear moduli G/G_e as a function of the reduced inverse strand length $(\langle N_s\rangle/N_e)^{-1}$. Shown are the moduli G^{MR} derived from the Mooney–Rivlin fits of our DPD networks without and with slip springs ($\phi_{SS} = 0, 0.1$). Linear fits to these data are shown by the continuous red and blue lines (see text). $G_e = 0.308$ and $N_e = 11.7$ were derived earlier for our $N = 100$ slip-spring melts. Black squares and diamonds are the affine and phantom network moduli of our networks (Table 2). The dashed, red line is a shift of the phantom network prediction by the melt's plateau modulus G_N^0. The Kremer–Grest simulation results of Gula et al.[61] are shown for comparison and reduced by their reported quantities $G_e = 0.226$ MPa and $N_e = 33.1$. They also report the isolated cross-linked moduli G_c (see ref 61).

$0.06(4)$ for $\phi_{SS} = 0$ and $G/G_e \approx 0.53(3) \times (\langle N_s\rangle/N_e)^{-1} + 0.40(4)$ for $\phi_{SS} = 0.1$ (red and blue continuous lines). The change in the slope indicates an overestimation of G^{MR} for strongly cross-linked networks by slip-spring DPD. We recall that for these systems, the Rubinstein–Panyukov fit revealed an increasing action of slip springs as cross-links, rather than as entanglements. The resulting shear moduli even overshoot the predictions of the affine network model (G^{aff}). While this is a known entanglement effect for $\langle N_s\rangle \gtrsim N_e$, the affine network model is considered the upper limit for strongly cross-linked systems.[6] The shear moduli of our strongly cross-linked slip-spring DPD rubbers thus appear to be unphysically high.

We compare our results to the hypothetical case of additive slip-spring and cross-link contributions ($G^{ph} + G_N^0$; red, dashed line in Figure 9). Note that additivity of entanglements and cross-links is commonly assumed but has not been observed by Gula et al. It is, however, given in the slip-link simulations of Oberdisse et al.[58] and ensures the desired conservation of the slope of $G(\langle N_s\rangle^{-1})$. Following our earlier observation, the slip-spring contribution is here assumed to equal the plateau modulus of entangled melts $G_N^0 \approx 0.5G_e$. Comparison with the affine network model highlights that the hypothetical $G^{ph} + G_N^0$ scenario is closer to the expected behavior for short network strands. For $\langle N_s\rangle \gtrsim N_e$, on the other hand, it is reasonably close to our slip-spring networks. Considering that all networks use the same, constant number of slip springs as the precursor melts, we conclude that a straightforward cross-linking produces networks with a reasonable additivity of slip springs and cross-links if the average network strand is not shorter than the melt's entanglement length. For higher degrees of cross-linking, a consistently growing shear modulus likely requires a reduced number of slip springs.

CONCLUSIONS

We presented the extension of our slip-spring DPD simulation method[52] to elastomeric networks. Our networks were constructed from an equilibrated precursor melt. In a first

https://doi.org/10.1021/acs.macromol.1c00567
Macromolecules 2021, 54, 5155–5166

step, all chain ends were connected to close beads of other chains. Remaining cross-links were randomly distributed between pairs of beads belonging to different chains until the desired fraction of cross-links ϕ_{cl} was reached. Our networks were thus free of dangling ends and only contained few loops. A network of regular DPD bead-spring chains is fast to simulate but allows beads and bonds to frequently cross each other. The network strands thus have the mobility and relaxation behavior of Rouse chains but fail to reproduce entanglement dynamics. We found that the almost unrestricted fluctuation of network strands was well described by the phantom network model. Correspondingly, regular DPD networks showed no sign of strain thinning, and their shear modulus G had no detectable entanglement contribution.

Slip-spring networks were created by cross-linking slip-spring DPD melts.[52] Slip springs were allowed to migrate along network strands but could not pass cross-links. Due to our cross-linking procedure, all slip springs were thus trapped on their respective chain segments. We found slip springs to reduce the mobility and fluctuations of network strands (Figure 2) and decelerate network relaxation dynamics if the network strands were not shorter than the entanglement length of the original chains (Figures 3 and 4). The storage and loss moduli of our slip-spring model networks were in good agreement with experimental data of comparable PI rubbers for conversion factors derived from slip-spring melts (Figure 5). Trapped slip springs drastically increased the networks' shear moduli, which we investigated by uniaxial strain experiments. Consistent with earlier findings, slip-spring networks showed a weak strain thinning (Figure 6). A fit to the Mooney−Rivlin model[88,89] gave access to the fitting coefficients $C_{1,2}$ and the shear moduli $G^{MR} = 2C_1 + 2C_2$. The coefficient associated with the entanglement contribution, C_2, was 0 for our slip-spring-free networks. In contrast, slip-spring networks fully restored the contributions of both coefficients to the result of a hard-core reference system[61] (Figure 7). Fitting to the Rubinstein−Panyukov nonaffine slip-tube model[92] confirmed that provided there are long enough network strands, slip springs contribute to the shear modulus with the same plateau modulus as the precursor melt (Figure 8). For higher cross-link densities ϕ_{cl}, on the other hand, the loss in their mobility caused slip springs to increasingly contribute as additional cross-links. Consequently, highly cross-linked slip-spring DPD networks had unphysically high shear moduli (Figure 9). For the model to be transferable over a range of cross-link densities, a prescription for reducing the number of slip springs, as network strands become shorter, would be needed. In their network implementation of the PCN model, Oberdisse et al.[58] employed an additive number of slip links and cross-links. A similar treatment of $\phi_{SS} = \phi_{SS}^{melt} - \phi_{cl}$ could be realized but would necessitate either a precursor melt with too few slip springs or the removal of slip springs upon cross-linking. However, finding a pathway to construct slip-spring networks consistent for high cross-link densities is left for future studies.

To summarize, our slip-spring DPD networks successfully restore the static and dynamic network properties of experiments and hard-core reference systems. For low cross-link densities, the mapping of slip-spring DPD systems to experimental data is consistent upon cross-linking, which gives our method a certain predictive power. Here, the contribution of slip springs to the shear modulus equals the melt's plateau modulus. If the average network strand length falls below the entanglement length of the melt, the reduced slip-spring mobility favors their contribution as additional cross-links. In this case, a more elaborate slip-spring model is needed for transferability over multiple cross-link densities. For low and moderate cross-link densities, the slip-spring DPD method nonetheless offers access to static and dynamic network properties, which makes it a promising tool for the investigation of more complex problems, such as systematic studies of network defects or gels. Equally, it is a computationally cheap model for the simulation of experimental elastomers and elastomer-based materials.

AUTHOR INFORMATION

Corresponding Authors

Jurek Schneider − *Eduard-Zintl-Institut für Anorganische und Physikalische Chemie and Profile Area Thermofluids and Interfaces, Technische Universität Darmstadt, D-64287 Darmstadt, Germany;* orcid.org/0000-0002-0286-1678; Email: j.schneider@theo.chemie.tu-darmstadt.de

Florian Müller-Plathe − *Eduard-Zintl-Institut für Anorganische und Physikalische Chemie and Profile Area Thermofluids and Interfaces, Technische Universität Darmstadt, D-64287 Darmstadt, Germany;* orcid.org/0000-0002-9111-7786; Email: f.mueller-plathe@theo.chemie.tu-darmstadt.de

Authors

Frank Fleck − *Continental Reifen Deutschland GmbH, D-30419 Hannover, Germany*

Hossein Ali Karimi-Varzaneh − *Continental Reifen Deutschland GmbH, D-30419 Hannover, Germany*

Complete contact information is available at: https://pubs.acs.org/10.1021/acs.macromol.1c00567

Notes

The authors declare no competing financial interest.

ACKNOWLEDGMENTS

J.S. is grateful to Zhenghao Wu for many fruitful discussions. This work has in part been funded by the Deutsche Forschungsgemeinschaft (Collaborative Research Center Transregio 146, project A8). Some simulations were performed on the Lichtenberg high-performance computer of the TU Darmstadt.

REFERENCES

(1) Wang, R.; Sing, M. K.; Avery, R. K.; Souza, B. S.; Kim, M.; Olsen, B. D. Classical challenges in the physical chemistry of polymer networks and the design of new materials. *Acc. Chem. Res.* **2016**, *49*, 2786−2795.

(2) Kremer, K.; Grest, G. S. Dynamics of entangled linear polymer melts: A molecular-dynamics simulation. *J. Chem. Phys.* **1990**, *92*, 5057−5086.

(3) Grest, G. S.; Kremer, K. Statistical properties of random cross-linked rubbers. *Macromolecules* **1990**, *23*, 4994−5000.

(4) Grest, G. S.; Kremer, K. Critical properties of crosslinked polymer melts. *J. Phys.* **1990**, *51*, 2829−2842.

(5) Duering, E. R.; Kremer, K.; Grest, G. S. Relaxation of randomly cross-linked polymer melts. *Phys. Rev. Lett.* **1991**, *67*, 3531−3534.

(6) Duering, E. R.; Kremer, K.; Grest, G. S. Dynamics of model networks: the role of the melt entanglement length. *Macromolecules* **1993**, *26*, 3241−3244.

(7) Everaers, R.; Kremer, K. Test of the foundations of classical rubber elasticity. *Macromolecules* **1995**, *28*, 7291−7294.

(8) Everaers, R.; Kremer, K. Topological interactions in model polymer networks. *Phys. Rev. E: Stat. Phys., Plasmas, Fluids, Relat. Interdiscip. Top.* **1996**, *53*, R37−R40.
(9) Duering, E. R.; Kremer, K.; Grest, G. S. Structure and relaxation of end-linked polymer networks. *J. Chem. Phys.* **1994**, *101*, 8169−8192.
(10) Everaers, R.; Kremer, K. Elastic properties of polymer networks. *J. Mol. Model.* **1996**, *2*, 293−299.
(11) Everaers, R. Entanglement effects in defect-free model polymer networks. *New J. Phys.* **1999**, *1*, 12.
(12) Grest, G. S.; Pütz, M.; Everaers, R.; Kremer, K. Stress−strain relation of entangled polymer networks. *J. Non-Cryst. Solids* **2000**, *274*, 139−146.
(13) Grest, G. S.; Kremer, K.; Duering, E. R. Kinetics of end crosslinking in dense polymer melts. *Europhys. Lett.* **1992**, *19*, 195−200.
(14) Grest, G. S.; Kremer, K.; Duering, E. R. Kinetics and relaxation of end crosslinked polymer networks. *Phys. A* **1993**, *194*, 330−337.
(15) Kuhn, W. Dependence of the average transversal on the longitudinal dimensions of statistical coils formed by chain molecules. *J. Polym. Sci.* **1946**, *1*, 380−388.
(16) Wall, F. T.; Flory, P. J. Statistical thermodynamics of rubber elasticity. *J. Chem. Phys.* **1951**, *19*, 1435−1439.
(17) James, H. M. Statistical properties of networks of flexible chains. *J. Chem. Phys.* **1947**, *15*, 651−668.
(18) James, H. M.; Guth, E. Simple presentation of network theory of rubber, with a discussion of other theories. *J. Polym. Sci.* **1949**, *4*, 153−182.
(19) Flory, P. J.; Gordon, M.; Flory, P. J.; McCrum, N. G. Statistical thermodynamics of random networks. *Proc. R. Soc. London, Ser. A* **1976**, *351*, 351−380.
(20) Syed, I. H.; Stratmann, P.; Hempel, G.; Klüppel, M.; Saalwächter, K. Entanglements, defects, and inhomogeneities in nitrile butadiene rubbers: Macroscopic versus microscopic properties. *Macromolecules* **2016**, *49*, 9004−9016.
(21) Ball, R. C.; Doi, M.; Edwards, S. F.; Warner, M. Elasticity of entangled networks. *Polymer* **1981**, *22*, 1010−1018.
(22) Mark, J. E.; Erman, B. *Rubberlike Elasticity: A Molecular Primer*, 2nd ed.; Cambridge University Press: New York, 2007.
(23) Erman, B.; Mark, J. E. *The Science and Technology of Rubber*, 4th ed.; Mark, J. E., Erman, B., Roland, C. M., Eds.; Academic Press: Boston, 2013; pp 167−192.
(24) Rubinstein, M.; Colby, R. H. *Polymer Physics*; Oxford University Press: New York, 2003.
(25) Edwards, S. F.; Vilgis, T. The effect of entanglements in rubber elasticity. *Polymer* **1986**, *27*, 483−492.
(26) Edwards, S. F.; Vilgis, T. A. The tube model theory of rubber elasticity. *Rep. Prog. Phys.* **1988**, *51*, 243−297.
(27) Tsimouri, I. C.; Schwarz, F.; Caseri, W.; Hine, P. J.; Gusev, A. A. Comparative experimental and molecular simulation study of the entropic viscoelasticity of end-Linked polymer networks. *Macromolecules* **2020**, *53*, 5371−5380.
(28) Müller-Plathe, F. Coarse-graining in polymer simulation: From the atomistic to the mesoscopic scale and back. *ChemPhysChem* **2002**, *3*, 754−769.
(29) de Gennes, P. G. Reptation of a polymer chain in the presence of fixed obstacles. *J. Chem. Phys.* **1971**, *55*, 572−579.
(30) Hoogerbrugge, P. J.; Koelman, J. M. V. A. Simulating microscopic hydrodynamic phenomena with dissipative particle dynamics. *Europhys. Lett.* **1992**, *19*, 155.
(31) Lahmar, F. Simulation moléculaire de fondus de polymères et d'élastomères par la méthode de la "Dynamique des Particules Dissipatives". Ph.D. Thesis, Université Paris-Sud, Paris, 2008.
(32) Gavrilov, A. A.; Chertovich, A. V. Computer simulation of random polymer networks: Structure and properties. *Polym. Sci., Ser. A* **2014**, *56*, 90−97.
(33) Long, D.; Sotta, P. Nonlinear and plastic behavior of soft thermoplastic and filled elastomers studied by dissipative particle dynamics. *Macromolecules* **2006**, *39*, 6282−6297.
(34) Gavrilov, A. A.; Chertovich, A. V.; Khalatur, P. G.; Khokhlov, A. R. Effect of nanotube size on the mechanical properties of elastomeric composites. *Soft Matter* **2013**, *9*, 4067.
(35) Gavrilov, A. A.; Chertovich, A. V.; Khalatur, P. G.; Khokhlov, A. R. Study of the mechanisms of filler reinforcement in elastomer nanocomposites. *Macromolecules* **2014**, *47*, 5400−5408.
(36) Pan, G.; Manke, C. W. Developments toward simulation of entangled polymer melts by dissipative particle dynamics (DPD). *Int. J. Mod. Phys. B* **2003**, *17*, 231−235.
(37) Tzoumanekas, C.; Lahmar, F.; Rousseau, B.; Theodorou, D. N. Onset of entanglements revisited. Topological analysis. *Macromolecules* **2009**, *42*, 7474−7484.
(38) Lahmar, F.; Tzoumanekas, C.; Theodorou, D. N.; Rousseau, B. Onset of entanglements revisited. Dynamical analysis. *Macromolecules* **2009**, *42*, 7485−7494.
(39) Nikunen, P.; Vattulainen, I.; Karttunen, M. Reptational dynamics in dissipative particle dynamics simulations of polymer melts. *Phys. Rev. E: Stat., Nonlinear, Soft Matter Phys.* **2007**, *75*, 036713.
(40) Masubuchi, Y. Simulating the flow of entangled polymers. *Annu. Rev. Chem. Biomol. Eng.* **2014**, *5*, 11−33.
(41) Hua, C. C.; Schieber, J. D. Segment connectivity, chain-length breathing, segmental stretch, and constraint release in reptation models. I. Theory and single-step strain predictions. *J. Chem. Phys.* **1998**, *109*, 10018−10027.
(42) Hua, C. C.; Schieber, J. D.; Venerus, D. C. Segment connectivity, chain-length breathing, segmental stretch, and constraint release in reptation models. II. Double-step strain predictions. *J. Chem. Phys.* **1998**, *109*, 10028−10032.
(43) Hua, C. C.; Schieber, J. D.; Venerus, D. C. Segment connectivity, chain-length breathing, segmental stretch, and constraint release in reptation models. III. Shear flows. *J. Rheol.* **1999**, *43*, 701−717.
(44) Schieber, J. D.; Neergaard, J.; Gupta, S. A full-chain, temporary network model with sliplinks, chain-length fluctuations, chain connectivity and chain stretching. *J. Rheol.* **2003**, *47*, 213−233.
(45) Likhtman, A. E. Single-chain slip-link model of entangled polymers: Simultaneous description of neutron spin-echo, rheology, and diffusion. *Macromolecules* **2005**, *38*, 6128−6139.
(46) Masubuchi, Y.; Takimoto, J.-I.; Koyama, K.; Ianniruberto, G.; Marrucci, G.; Greco, F. Brownian simulations of a network of reptating primitive chains. *J. Chem. Phys.* **2001**, *115*, 4387−4394.
(47) Uneyama, T.; Masubuchi, Y. Multi-chain slip-spring model for entangled polymer dynamics. *J. Chem. Phys.* **2012**, *137*, 154902.
(48) Ramírez-Hernández, A.; Detcheverry, F. A.; Peters, B. L.; Chappa, V. C.; Schweizer, K. S.; Müller, M.; de Pablo, J. J. Dynamical simulations of coarse grain polymeric systems: Rouse and entangled dynamics. *Macromolecules* **2013**, *46*, 6287−6299.
(49) Ramírez-Hernández, A.; Müller, M.; de Pablo, J. J. Theoretically informed entangled polymer simulations: Linear and non-linear rheology of melts. *Soft Matter* **2013**, *9*, 2030.
(50) Vogiatzis, G. G.; Megariotis, G.; Theodorou, D. N. Equation of state based slip spring model for entangled polymer dynamics. *Macromolecules* **2017**, *50*, 3004−3029.
(51) Chappa, V. C.; Morse, D. C.; Zippelius, A.; Müller, M. Translationally invariant slip-spring model for entangled polymer dynamics. *Phys. Rev. Lett.* **2012**, *109*, 148302.
(52) Langeloth, M.; Masubuchi, Y.; Böhm, M. C.; Müller-Plathe, F. Recovering the reptation dynamics of polymer melts in dissipative particle dynamics simulations via slip-springs. *J. Chem. Phys.* **2013**, *138*, 104907.
(53) Wu, Z.; Kalogirou, A.; De Nicola, A.; Milano, G.; Müller-Plathe, F. Atomistic hybrid particle-field molecular dynamics combined with slip-springs: Restoring entangled dynamics to simulations of polymer melts. *J. Comput. Chem.* **2021**, *42*, 6−18.
(54) Sgouros, A. P.; Megariotis, G.; Theodorou, D. N. Slip-spring model for the linear and nonlinear viscoelastic properties of molten polyethylene derived from atomistic simulations. *Macromolecules* **2017**, *50*, 4524−4541.

https://doi.org/10.1021/acs.macromol.1c00567
Macromolecules 2021, 54, 5155−5166

(55) Wu, Z.; Milano, G.; Müller-Plathe, F. Combination of hybrid particle-field molecular dynamics and slip-springs for the efficient simulation of coarse-grained polymer models: Static and dynamic properties of polystyrene melts. *J. Chem. Theory Comput.* **2021**, *17*, 474−487.
(56) Behbahani, A. F.; Schneider, L.; Rissanou, A.; Chazirakis, A.; Bačová, P.; Jana, P. K.; Li, W.; Doxastakis, M.; Polińska, P.; Burkhart, C.; Müller, M.; Harmandaris, V. A. Dynamics and rheology of polymer melts via hierarchical atomistic, coarse-grained, and slip-spring simulations. *Macromolecules* **2021**, *54*, 2740−2762.
(57) Oberdisse, J.; Ianniruberto, G.; Greco, F.; Marrucci, G. Primitive-chain Brownian simulations of entangled rubbers. *Europhys. Lett.* **2002**, *58*, 530.
(58) Oberdisse, J.; Ianniruberto, G.; Greco, F.; Marrucci, G. Mechanical properties of end-crosslinked entangled polymer networks using sliplink Brownian dynamics simulations. *Rheol. Acta* **2006**, *46*, 95−109.
(59) Megariotis, G.; Vogiatzis, G.; Sgouros, A.; Theodorou, D. Slip spring-based mesoscopic simulations of polymer networks: Methodology and the corresponding computational code. *Polymers* **2018**, *10*, 1156.
(60) Masubuchi, Y.; Uneyama, T. Retardation of the reaction kinetics of polymers due to entanglement in the post-gel stage in multi-chain slip-spring simulations. *Soft Matter* **2019**, *15*, 5109−5115.
(61) Gula, I. A.; Karimi-Varzaneh, H. A.; Svaneborg, C. Computational study of cross-link and entanglement contributions to the elastic properties of model PDMS networks. *Macromolecules* **2020**, *53*, 6907−6927.
(62) Español, P.; Warren, P. Statistical mechanics of dissipative particle dynamics. *Europhys. Lett.* **1995**, *30*, 191.
(63) Groot, R. D.; Warren, P. B. Dissipative particle dynamics: Bridging the gap between atomistic and mesoscopic simulation. *J. Chem. Phys.* **1997**, *107*, 4423−4435.
(64) Langeloth, M.; Masubuchi, Y.; Böhm, M. C.; Müller-Plathe, F. Reptation and constraint release dynamics in bidisperse polymer melts. *J. Chem. Phys.* **2014**, *141*, 194904.
(65) Nardai, M. M.; Zifferer, G. Simulation of dilute solutions of linear and star-branched polymers by dissipative particle dynamics. *J. Chem. Phys.* **2009**, *131*, 124903.
(66) Masubuchi, Y.; Langeloth, M.; Böhm, M. C.; Inoue, T.; Müller-Plathe, F. A multichain slip-spring dissipative particle dynamics simulation method for entangled polymer solutions. *Macromolecules* **2016**, *49*, 9186−9191.
(67) Schneider, J.; Panagiotopoulos, A. Z.; Müller-Plathe, F. Polymer chain collapse upon rapid solvent exchange: Slip-spring dissipative particle dynamics simulations with an explicit-solvent model. *J. Phys. Chem. C* **2017**, *121*, 27664−27673.
(68) Schneider, J.; Süss, L. D.; Müller-Plathe, F. The influence of entanglements on the dynamics of flash nanoprecipitation: A slip-spring dissipative-particle-dynamics investigation. *J. Chem. Eng. Data* **2020**, *65*, 1264−1272.
(69) Schneider, J.; Meinel, M. K.; Dittmar, H.; Müller-Plathe, F. Different stages of polymer-chain collapse following solvent quenching−scaling relations from dissipative particle dynamics simulations. *Macromolecules* **2020**, *53*, 8889−8900.
(70) Spenley, N. A. Scaling laws for polymers in dissipative particle dynamics. *Europhys. Lett.* **2000**, *49*, 534.
(71) Williams, M. L.; Landel, R. F.; Ferry, J. D. The temperature dependence of relaxation mechanisms in amorphous polymers and other glass-forming liquids. *J. Am. Chem. Soc.* **1955**, *77*, 3701−3707.
(72) Hartmann, S. R.; Hahn, E. L. Nuclear double resonance in the rotating frame. *Phys. Rev.* **1962**, *128*, 2042−2053.
(73) James, H. M.; Guth, E. Theory of the increase in rigidity of rubber during cure. *J. Chem. Phys.* **1947**, *15*, 669−683.
(74) Masubuchi, Y.; Uneyama, T. Multi-chain slip-spring simulations for polyisoprene melts. *Korea-Aust. Rheol. J.* **2019**, *31*, 241−248.
(75) Anogiannakis, S. D.; Tzoumanekas, C.; Theodorou, D. N. Microscopic description of entanglements in polyethylene networks and melts: Strong, weak, pairwise, and collective attributes. *Macromolecules* **2012**, *45*, 9475−9492.
(76) Tassieri, M.; Ramírez, J.; Karayiannis, N. C.; Sukumaran, S. K.; Masubuchi, Y. i-Rheo GT : Transforming from time to frequency domain without artifacts. *Macromolecules* **2018**, *51*, 5055−5068.
(77) Ramírez, J.; Sukumaran, S. K.; Vorselaars, B.; Likhtman, A. E. Efficient on the fly calculation of time correlation functions in computer simulations. *J. Chem. Phys.* **2010**, *133*, 154103.
(78) Langley, N. R. Elastically effective strand density in polymer networks. *Macromolecules* **1968**, *1*, 348−352.
(79) Boudara, V. A. H.; Read, D. J.; Ramírez, J. Reptate rheology software: Toolkit for the analysis of theories and experiments. *J. Rheol.* **2020**, *64*, 709−722.
(80) Likhtman, A. E.; McLeish, T. C. B. Quantitative theory for linear dynamics of linear entangled polymers. *Macromolecules* **2002**, *35*, 6332−6343.
(81) Ngai, K. L.; Capaccioli, S.; Plazek, D. J. *The Science and Technology of Rubber*, 4th ed.; Mark, J. E., Erman, B., Roland, C. M., Eds.; Academic Press: Boston, 2013; pp 193−284.
(82) Uneyama, T.; Masubuchi, Y. Plateau moduli of several single-chain slip-link and slip-spring models. *Macromolecules* **2021**, *54*, 1338−1353.
(83) Masubuchi, Y.; Ianniruberto, G.; Greco, F.; Marrucci, G. Entanglement molecular weight and frequency response of sliplink networks. *J. Chem. Phys.* **2003**, *119*, 6925−6930.
(84) Masubuchi, Y.; Uneyama, T. Comparison among multi-chain models for entangled polymer dynamics. *Soft Matter* **2018**, *14*, 5986−5994.
(85) Everaers, R. Topological versus rheological entanglement length in primitive-path analysis protocols, tube models, and slip-link models. *Phys. Rev. E: Stat., Nonlinear, Soft Matter Phys.* **2012**, *86*, 022801.
(86) Auhl, D.; Ramirez, J.; Likhtman, A. E.; Chambon, P.; Fernyhough, C. Linear and nonlinear shear flow behavior of monodisperse polyisoprene melts with a large range of molecular weights. *J. Rheol.* **2008**, *52*, 801−835.
(87) Ramírez-Hernández, A.; Peters, B. L.; Andreev, M.; Schieber, J. D.; de Pablo, J. J. A multichain polymer slip-spring model with fluctuating number of entanglements for linear and nonlinear rheology. *J. Chem. Phys.* **2015**, *143*, 243147.
(88) Mooney, M. A theory of large elastic deformation. *J. Appl. Phys.* **1940**, *11*, 582−592.
(89) Rivlin, R. S.; Saunders, D. W.; Andrade, E. N. D. C. Large elastic deformations of isotropic materials VII. Experiments on the deformation of rubber. *Philos. Trans. R. Soc., A* **1951**, *243*, 251−288.
(90) Schlögl, S.; Trutschel, M.-L.; Chassé, W.; Riess, G.; Saalwächter, K. Entanglement effects in elastomers: Macroscopic vs microscopic properties. *Macromolecules* **2014**, *47*, 2759−2773.
(91) Everaers, R.; Karimi-Varzaneh, H. A.; Fleck, F.; Hojdis, N.; Svaneborg, C. Kremer−Grest models for commodity polymer melts: Linking theory, experiment, and simulation at the Kuhn scale. *Macromolecules* **2020**, *53*, 1901−1916.
(92) Rubinstein, M.; Panyukov, S. Elasticity of polymer networks. *Macromolecules* **2002**, *35*, 6670−6686.
(93) Svaneborg, C.; Everaers, R.; Grest, G. S.; Curro, J. G. Connectivity and entanglement stress contributions in strained polymer networks. *Macromolecules* **2008**, *41*, 4920−4928.
(94) Sliozberg, Y. R.; Chantawansri, T. L. Computational study of imperfect networks using a coarse-grained model. *J. Chem. Phys.* **2013**, *139*, 194904.
(95) Patel, S. K.; Malone, S.; Cohen, C.; Gillmor, J. R.; Colby, R. H. Elastic modulus and equilibrium swelling of poly(dimethylsiloxane) networks. *Macromolecules* **1992**, *25*, 5241−5251.

https://doi.org/10.1021/acs.macromol.1c00567
Macromolecules 2021, 54, 5155−5166

5 Conclusion and Outlook

In the past years, multi-chain slip-spring (MC-SS) simulations have evolved into different directions. On one hand, chemistry-specific, mesoscopic particle-field models were derived from atomistic or experimental data[106–111, 113], and existing models were parameterized for implementation in hierarchical models[105]. On the other hand, the applicability of generic models to experiments[98, 99] and their transferability among each other[101, 102], even for varying slip-spring densities[103], was shown. In the spirit of the latter, we used and modified our simple and intuitive slip-spring dissipative-particle-dynamics (DPD) method[88] to probe its applicability to new fields; namely, the investigation of collapse and precipitation dynamics of polymer chains and solutions, and the viscoelastic properties of elastomeric networks. The results were presented in the previous chapters and are briefly summarized here.

The objective of the first part of this thesis was to study flash nanoprecipitation[138][139] (FNP) *via* slip-spring DPD. FNP is a production technique for nanoparticles that allows great control over, for example, the particle size and dispersity. Its precipitation pathway is not fully understood, and the nanoparticles show an unpredicted aggregation behavior which is hypothesized to be influenced by topological chain interactions during the precipitation. In a preceding publication[158] that originated in my master thesis, we studied, among other things, the influence of self-entanglements, introduced by a varying number of slip springs, on the collapse behavior of $N = 100$ bead chains. As expected from additional attractions inflicted on an isolated chain, a slight contraction was observed. Beside effects of the pre-collapsed conformation, we were, however, not able to find any influence of slip springs on the collapse pathway or the final globular structure. We could also not identify different collapse stages but found intermediate pearl-necklace-like structures, which indicated that our DPD chains followed the well-known collapse mechanism of Halperin and Goldbart[147].
Two studies were inspired by these findings: in the (chronologically) first study[160] (section 4.2), the single-chain system was extended to a solution of many long, $N = 75 - 200$ polymer chains. Instantaneous exchange of $50\ \%$ of the solvent beads by nonsolvent quenched the chains from good- to poor solvent conditions. The precipitating chains were studied by their radii of gyration and a cluster analysis for the influence of topological interactions, re-introduced by different (fixed) numbers of slip springs. The polymers precipitated into a network-like intermediate structure, where some chains were already globular and others connected them. We were, however, not able to identify an influence of slip springs, or the chain length, on the stability of this structure, which quickly rearranged into separated globules as the stretched chains were retracted. To probe our initial hypothesis that slip springs, which were usually in an inactive position between neighboring beads (see section 3.3), would not be mobile enough to switch from intra- to inter-chain positions, we investigated drastically higher slip-spring mobilities with the same outcome. Thus, we conclude the role of entanglements during flash nanoprecipitation to be insignificant. The reason is essentially that the precipitation of monomers from solution is so fast, that the chains have no

time to explore whether and how they are entangled. If they start out in solution in an entangled topology, they keep it during the collapse and precipitation.
In a second publication[159], we returned to investigate the collapse behavior of single chains, with a focus on the identification and scaling behavior of different collapse stages (section 4.1). Our $N = 50 - 1000$ bead chains showed a distinct pearl-necklace collapse pathway. We identified local structures, such as blobs and bridges, from a cluster analysis and inspected their evolution during the collapse. This allowed us to measure the scaling coefficients of the three early collapse stages predicted by Halperin and Goldbart[147], namely blob formation, bridge-stretching, and the collapse of the pearl-necklace. They were similar to the predicted ones, and differences could be attributed to the relevance of different dissipative mechanisms rather than a single, dominant one.
The second part of this thesis concerns the investigation of elastomeric networks by slip-spring DPD. Simulations of networks are popular for their ability to explicitly control and access network structures, but commonly struggle to monitor the rheology of larger systems over a longer time. The study presented in section 4.3 [137] shows that slip-spring DPD can overcome these issues while correctly sampling entanglement effects. Networks were created by cross-linking equilibrated melts of bead-spring DPD chains. Slip springs were not allowed to populate cross-linked beads, and were thus trapped on their respective chains and network strands due to the applied cross-linking recipe. We used the Mooney-Rivlin[161, 162] and Rubinstein-Panyukov[64] models to extract the cross-link and entanglement contributions to the shear moduli of networks with and without slip springs under stress-strain experiments. Networks with slip springs turned off followed the phantom network model with no signs of topological strand interaction. Comparison with hard-core reference systems[134] revealed that slip springs, on the other hand, fully restored the entanglement contribution to the networks' shear moduli. This success motivated the comparison to experimental polyisoprene (PI) rubber data. In a first step, excellent mapping was achieved between the storage- and loss moduli of a monodisperse PI melt and a respective slip-spring DPD melt, where the only adjusted parameters were the time, moduli, and experimental isoprene monomers per DPD bead (here: 7.7). Without further approximations, cross-linking of the DPD melt gave a good model for experimental PI rubbers with similar strand-length distributions. Slip-spring DPD was capable to model the dynamical moduli up to a real time of ≈ 0.1 s, that is, $10^6 - 10^8$ times longer than what would be possible with, for example, atomistic or weakly coarse-grained models.

At this point, the discussion of our results requires a reflection of the employed methods. Clearly, the question arises whether the inability to find an influence of topological interactions in collapse and precipitation dynamics stems from their absence or an insufficient method. In section 4.2, we discussed whether a grand-canonical slip-spring approach, as proposed by Uneyama and Masubuchi[84] and Chappa *et al.*[83], would be better capable of sampling precipitation dynamics. We doubted this as the number of slip springs depends on global properties in these models. Some more recent works[96, 106], on the other hand, suggest a slip-spring number depending on the local environment of the chain end chosen for slip-spring insertion. It would be interesting to see how these models cope with the rapid conformational changes and heterogeneities during FNP. We do, however, note that slip springs are persisting in a reservoir between bonded beads in our simulations, and that an improved mobility of slip springs did not alter our observations. Thus, we believe that a different relocation criterion (or replacement by insertion/deletion dynamics) would not qualitatively challenge our results that entanglements are of a minor importance in FNP.

Insertion of slip springs introduces an additional attractive potential between polymer chains. Whether or not this must be compensated for is an ongoing discussion. While an exact compensation is necessary in order to leave the chain statistics undisturbed[83, 84], many authors report only a minor influence of the artificial chain attraction if the nonbonded interactions are repulsive enough[88, 91, 92, 106, 111]. Our own DPD studies showed the same, weak influence of slip springs on the chain conformation, which increased with a growing number of slip springs[160]. A problem with the compensating potential of Chappa *et al.*[83] is that it acts between all polymer beads within a range potentially accessible by slip springs. To reduce the computational impact of its derivation, respective works[83, 105] employ finitely extensible slip springs, which introduce singularities that necessitate smaller integration steps. Whether an exact chain structure is needed for quantitative predictions or an efficient computation is required for large, qualitative applications has likely to be decided case by case.

The capability of slip-spring DPD to correctly model topological effects in elastomeric networks opens a door for further applications. For example, slip-spring DPD could be used to study the influence of large network defects, such as loops and unconnected chain ends, on rheological properties. Modern network theories, such as the real elasticity network theory[163–168], the Miller-Macosko-theory[169], and combinations of both[170] discuss these effects and could serve as references. In section 4.3, we found that our systems follow the prediction of Everaers[136], who postulated that two slip springs correspond to a rheological entanglement. It would be interesting to investigate whether this relation holds between trapped slip springs and trapped entanglements[118]. Lastly, our network studies could be extended to filled rubbers, which are of a high industrial importance.
As a method that explicitly incorporates hydrodynamic interactions, slip-spring DPD could be used for studies of entanglement effects in hydrogels or swollen networks. Experiments have shown that swelling reduces the number of topological interactions to a point where no entanglement contribution to the shear modulus is detectable[171]. However, a small, persisting number of trapped entanglements contribute as additional cross-links.

The slip-spring DPD method presented here follows a simple and efficient approach to model soft-matter systems. Despite the successful top-down mapping to experimental rheological data of polyisoprene, it is clear that the simple functional form and mesoscopic mapping of several monomers per DPD bead come with a loss of chemical detail. Chemistry-specific slip-spring models exist and are mostly based on particle-field approaches[106, 111]. However, the constant evolution of more sophisticated DPD models trends towards a higher chemical specificity as well[7]. If desired, the underlying DPD sequence of the method at hand could be changed accordingly.

To conclude, we presented extensions and applications of an existing dissipative-particle-dynamics software that incorporates entanglement effects in soft matter systems *via* slip springs. Investigated systems were precipitating chains in simulations of flash nanoprecipitation and elastomeric networks. We could not find an influence of slip springs on the dynamics of a collapsing single chain or a precipitating polymer solution. Networks, on the other hand, have shown to be a highly interesting playground for slip-spring simulations, and slip springs were found to be capable to restore the topological interactions found in hard-core reference systems as well as the dynamic moduli of experimental networks. Further applications could be directed towards models of defect elastomers, filled nanocomposites, and gels, which are all of a high scientific and industrial relevance.

References to Chapters 1–3 and 5

(The subsections of Chapter 4 each have their own bibliographies.)

[1] T. E. Gartner, A. Jayaraman, *Macromolecules* **2019**, *52*, 755–786.

[2] J. T. Padding, W. J. Briels, *J. Phys.: Condens. Matter* **2011**, *23*, 233101.

[3] F. Müller-Plathe, *ChemPhysChem* **2002**, *3*, 754–769.

[4] E. Brini, E. A. Algaer, P. Ganguly, C. Li, F. Rodríguez-Ropero, N. F. A. van der Vegt, *Soft Matter* **2013**, *9*, 2108–2119.

[5] C. Peter, K. Kremer, *Soft Matter* **2009**, *5*, 4357–4366.

[6] P. J. Hoogerbrugge, J. M. V. A. Koelman, *Europhys. Lett.* **1992**, *19*, 155.

[7] P. Español, P. B. Warren, *J. Chem. Phys.* **2017**, *146*, 150901.

[8] P. Español, P. Warren, *Europhys. Lett.* **1995**, *30*, 191.

[9] R. D. Groot, P. B. Warren, *J. Chem. Phys.* **1997**, *107*, 4423–4435.

[10] J. R. Spaeth, I. G. Kevrekidis, A. Z. Panagiotopoulos, *J. Chem. Phys.* **2011**, *134*, 164902.

[11] D. Long, P. Sotta, *Macromolecules* **2006**, *39*, 6282–6297.

[12] P. Kindt, W. J. Briels, *J. Chem. Phys.* **2007**, *127*, 134901.

[13] X. Guerrault, B. Rousseau, J. Farago, *J. Chem. Phys.* **2004**, *121*, 6538–6546.

[14] G. Deichmann, V. Marcon, N. F. A. van der Vegt, *J. Chem. Phys.* **2014**, *141*, 224109.

[15] P. Español, M. Revenga, *Phys. Rev. E* **2003**, *67*, 026705.

[16] I. Pagonabarraga, D. Frenkel, *J. Chem. Phys.* **2001**, *115*, 5015–5026.

[17] N. A. Spenley, *Europhys. Lett.* **2000**, *49*, 534.

[18] W. Jiang, J. Huang, Y. Wang, M. Laradji, *J. Chem. Phys.* **2007**, *126*, 044901.

[19] M. M. Nardai, G. Zifferer, *J. Chem. Phys.* **2009**, *131*, 124903.

[20] Z. Wu, S. A. N. Alberti, J. Schneider, F. Müller-Plathe, *J. Phys.: Condens. Matter* **2021**, *33*, 244001.

[21] H. Meyer, E. Horwath, P. Virnau, *ACS Macro Lett.* **2018**, *7*, 757–761.

[22] S. F. Edwards, *Proc. Phys. Soc.* **1967**, *92*, 9.

[23] P. G. de Gennes, *J. Chem. Phys.* **1971**, *55*, 572–579.

[24] Y. Masubuchi, *Annu. Rev. Chem. Biomol. Eng.* **2014**, *5*, 11–33.

[25] J. T. Padding, W. J. Briels, *J. Chem. Phys.* **2001**, *115*, 2846–2859.

[26] J. T. Padding, W. J. Briels, *J. Chem. Phys.* **2002**, *117*, 925–943.

[27] J. T. Padding, W. J. Briels, *J. Chem. Phys.* **2003**, *118*, 10276–10286.

[28] S. Kumar, R. G. Larson, *J. Chem. Phys.* **2001**, *114*, 6937–6941.

[29] F. Lahmar, C. Tzoumanekas, D. N. Theodorou, B. Rousseau, *Macromolecules* **2009**, *42*, 7485–7494.

[30] G. Pan, C. W. Manke, *Int. J. Mod. Phys. B* **2003**, *17*, 231–235.

[31] F. Goujon, P. Malfreyt, D. J. Tildesley, *J. Chem. Phys.* **2008**, *129*, 034902.

[32] M. Yamanoi, O. Pozo, J. M. Maia, *J. Chem. Phys.* **2011**, *135*, 044904.

[33] F. Goujon, P. Malfreyt, D. J. Tildesley, *Macromolecules* **2009**, *42*, 4310–4318.

[34] T. W. Sirk, Y. R. Slizoberg, J. K. Brennan, M. Lisal, J. W. Andzelm, *J. Chem. Phys.* **2012**, *136*, 134903.

[35] N. Iwaoka, K. Hagita, H. Takano, *J. Chem. Phys.* **2018**, *149*, 114901.

[36] V. Symeonidis, G. E. Karniadakis, B. Caswell, *Phys. Rev. Lett.* **2005**, *95*, 076001.

[37] P. Nikunen, I. Vattulainen, M. Karttunen, *Phys. Rev. E* **2007**, *75*, 036713.

[38] H. Liu, Y.-H. Xue, H.-J. Qian, Z.-Y. Lu, C.-C. Sun, *J. Chem. Phys.* **2008**, *129*, 024902.

[39] N. Hoda, R. G. Larson, *J. Rheol.* **2010**, *54*, 1061–1081.

[40] W. Kuhn, *J. Polym. Sci.* **1946**, *1*, 380–388.

[41] F. T. Wall, P. J. Flory, *J. Chem. Phys.* **1951**, *19*, 1435–1439.

[42] F. T. Wall, *J. Chem. Phys.* **1942**, *10*, 485–488.

[43] F. T. Wall, *J. Chem. Phys.* **1942**, *10*, 132–134.

[44] F. T. Wall, *J. Chem. Phys.* **1943**, *11*, 527–530.

[45] H. M. James, E. Guth, *J. Chem. Phys.* **1943**, *11*, 455–481.

[46] H. M. James, *J. Chem. Phys.* **1947**, *15*, 651–668.

[47] H. M. James, E. Guth, *J. Chem. Phys.* **1947**, *15*, 669–683.

[48] H. M. James, E. Guth, *J. Polym. Sci.* **1949**, *4*, 153–182.

[49] P. J. Flory, M. Gordon, P. J. Flory, N. G. McCrum, *Proc. R. Soc. A* **1976**, *351*, 351–380.

[50] M. Rubinstein, R. H. Colby, *Polymer physics*, Oxford University Press, New York, Oxford, **2003**.

[51] J. E. Mark, B. Erman, *Rubberlike elasticity: A molecular primer*, 2nd ed., Cambridge University Press, New York, New York, **2007**.

[52] G. Ronca, G. Allegra, *J. Chem. Phys.* **1975**, *63*, 4990–4997.

[53] P. J. Flory, *J. Chem. Phys.* **1977**, *66*, 5720–5729.

[54] B. Erman, P. J. Flory, *J. Chem. Phys.* **1978**, *68*, 5363–5369.

[55] P. J. Flory, B. Erman, *Macromolecules* **1982**, *15*, 800–806.

[56] B. Erman, P. J. Flory, *Macromolecules* **1982**, *15*, 806–811.

[57] R. C. Ball, M. Doi, S. F. Edwards, M. Warner, *Polymer* **1981**, *22*, 1010–1018.

[58] S. F. Edwards, T. Vilgis, *Polymer* **1986**, *27*, 483–492.

[59] T. A. Vilgis, B. Erman, *Macromolecules* **1993**, *26*, 6657–6659.

[60] M. Doi, F. S. Edwards, *J. Chem. Soc. Faraday Trans. 2* **1978**, *74*, 1789–1801.

[61] M. Doi, F. S. Edwards, *J. Chem. Soc. Faraday Trans. 2* **1978**, *74*, 1818–1832.

[62] S. F. Edwards, T. Vilgis, *Rep. Prog. Phys.* **1988**, *51*, 243–297.

[63] M. Rubinstein, S. Panyukov, *Macromolecules* **1997**, *30*, 8036–8044.

[64] M. Rubinstein, S. Panyukov, *Macromolecules* **2002**, *35*, 6670–6686.

[65] M. Kaliske, G. Heinrich, *Rubber Chem. Technol.* **1999**, *72*, 602–632.

[66] J. D. Davidson, N. C. Goulbourne, *J. Mech. Phys. Solids* **2013**, *61*, 1784–1797.

[67] Y. R. Sliozberg, T. L. Chantawansri, *J. Chem. Phys.* **2013**, *139*, 194904.

[68] S. P. O. Danielsen, H. K. Beech, S. Wang, B. M. El-Zaatari, X. Wang, L. Sapir, T. Ouchi, Z. Wang, P. N. Johnson, Y. Hu, D. J. Lundberg, G. Stoychev, S. L. Craig, J. A. Johnson, J. A. Kalow, B. D. Olsen, M. Rubinstein, *Chem. Rev.* **2021**, *121*, 5042–5092.

[69] M. Doi, *J. Polym. Sci. Part B* **1983**, *21*, 667–684.

[70] S. T. Milner, T. C. B. McLeish, *Phys. Rev. Lett.* **1998**, *81*, 725–728.

[71] A. E. Likhtman, T. C. B. McLeish, *Macromolecules* **2002**, *35*, 6332–6343.

[72] S. T. Palmer, *Modelling a single polymer entanglement*, Ph.D. Thesis, University of Reading, Reading, **2012**.

[73] M. Doi, F. S. Edwards, *J. Chem. Soc. Faraday Trans. 2* **1978**, *74*, 1802–1817.

[74] C. C. Hua, J. D. Schieber, *J. Chem. Phys.* **1998**, *109*, 10018–10027.

[75] S. Shanbhag, R. G. Larson, J. Takimoto, M. Doi, *Phys. Rev. Lett.* **2001**, *87*, 195502.

[76] M. Doi, J.-i. Takimoto, *Phil. Trans. R. Soc. Lond. A* **2003**, *361*, 641–652.

[77] Y. Masubuchi, J.-I. Takimoto, K. Koyama, G. Ianniruberto, G. Marrucci, F. Greco, *J. Chem. Phys.* **2001**, *115*, 4387–4394.

[78] J. Oberdisse, G. Ianniruberto, F. Greco, G. Marrucci, *EPL* **2002**, *58*, 530.

[79] J. D. Schieber, M. Andreev, *Annu. Rev. Chem. Biomol. Eng.* **2014**, *5*, 367–381.

[80] T. Uneyama, Y. Masubuchi, *Macromolecules* **2021**, *54*, 1338–1353.

[81] D. Becerra, A. Córdoba, M. Katzarova, M. Andreev, D. C. Venerus, J. D. Schieber, *J. Rheol.* **2020**, *64*, 1035–1043.

[82] A. E. Likhtman, *Macromolecules* **2005**, *38*, 6128–6139.

[83] V. C. Chappa, D. C. Morse, A. Zippelius, M. Müller, *Phys. Rev. Lett.* **2012**, *109*, 148302.

[84] T. Uneyama, Y. Masubuchi, *J. Chem. Phys.* **2012**, *137*, 154902.

[85] J. D. Schieber, *J. Chem. Phys.* **2003**, *118*, 5162–5166.

[86] M. Müller, K. C. Daoulas, *J. Chem. Phys.* **2008**, *129*, 164906.

[87] Y. Masubuchi, *J. Chem. Phys.* **2015**, *143*, 224905.

[88] M. Langeloth, Y. Masubuchi, M. C. Böhm, F. Müller-Plathe, *J. Chem. Phys.* **2013**, *138*, 104907.

[89] M. Langeloth, Y. Masubuchi, M. C. Böhm, F. Müller-Plathe, *J. Chem. Phys.* **2014**, *141*, 194904.

[90] A. Nikoubashman, R. L. Davis, B. T. Michal, P. M. Chaikin, R. A. Register, A. Z. Panagiotopoulos, *ACS Nano* **2014**, *8*, 8015–8026.

[91] Y. Masubuchi, M. Langeloth, M. C. Böhm, T. Inoue, F. Müller-Plathe, *Macromolecules* **2016**, *49*, 9186–9191.

[92] A. Ramírez-Hernández, M. Müller, J. J. de Pablo, *Soft Matter* **2013**, *9*, 2030.

[93] A. Ramírez-Hernández, F. A. Detcheverry, B. L. Peters, V. C. Chappa, K. S. Schweizer, M. Müller, J. J. de Pablo, *Macromolecules* **2013**, *46*, 6287–6299.

[94] D. Q. Pike, F. A. Detcheverry, M. Müller, J. J. de Pablo, *J. Chem. Phys.* **2009**, *131*, 084903.

[95] A. Ramírez-Hernández, B. L. Peters, M. Andreev, J. D. Schieber, J. J. de Pablo, *J. Chem. Phys.* **2015**, *143*, 243147.

[96] A. Ramírez-Hernández, B. L. Peters, L. Schneider, M. Andreev, J. D. Schieber, M. Müller, J. J. de Pablo, *J. Chem. Phys.* **2017**, *146*, 014903.

[97] A. Ramírez-Hernández, B. L. Peters, L. Schneider, M. Andreev, J. D. Schieber, M. Müller, M. Kröger, J. J. de Pablo, *Macromolecules* **2018**, *51*, 2110–2124.

[98] Y. Masubuchi, *Macromolecules* **2018**, *51*, 10184–10193.

[99] Y. Masubuchi, T. Uneyama, *Korea-Aust. Rheol. J.* **2019**, *31*, 241–248.

[100] Y. Masubuchi, T. Uneyama, *Soft Matter* **2019**, *15*, 5109–5115.

[101] Y. Masubuchi, T. Uneyama, *Soft Matter* **2018**, *14*, 5986–5994.

[102] Y. Masubuchi, T. Uneyama, *ECS Trans.* **2018**, *88*, 161.

[103] Y. Masubuchi, Y. Doi, T. Uneyama, *arXiv* **2020**, No. arXiv:2011.03222v1.

[104] T. Uneyama, *J. Chem. Phys.* **2019**, *150*, 024901.

[105] A. F. Behbahani, L. Schneider, A. Rissanou, A. Chazirakis, P. Bačová, P. K. Jana, W. Li, M. Doxastakis, P. Polińska, C. Burkhart, M. Müller, V. A. Harmandaris, *Macromolecules* **2021**, *54*, 2740–2762.

[106] G. G. Vogiatzis, G. Megariotis, D. N. Theodorou, *Macromolecules* **2017**, *50*, 3004–3029.

[107] A. P. Sgouros, G. Megariotis, D. N. Theodorou, *Macromolecules* **2017**, *50*, 4524–4541.

[108] G. Megariotis, G. G. Vogiatzis, A. P. Sgouros, D. N. Theodorou, *Polymers* **2018**, *10*, 1156.

[109] A. P. Sgouros, A. T. Lakkas, G. Megariotis, D. N. Theodorou, *Macromolecules* **2018**, *51*, 9798–9815.

[110] A. P. Sgouros, G. G. Vogiatzis, G. Megariotis, C. Tzoumanekas, D. N. Theodorou, *Macromolecules* **2019**, *52*, 7503–7523.

[111] Z. Wu, A. Kalogirou, A. D. Nicola, G. Milano, F. Müller-Plathe, *J. Comput. Chem.* **2021**, *42*, 6–18.

[112] G. Milano, T. Kawakatsu, *J. Chem. Phys.* **2009**, *130*, 214106.

[113] Z. Wu, G. Milano, F. Müller-Plathe, *J. Chem. Theory Comput.* **2021**, *17*, 474–487.

[114] J. Zhang, H. Meyer, P. Virnau, K. C. Daoulas, *Macromolecules* **2020**, *53*, 10475–10486.

[115] S. A. N. Alberti, J. Schneider, F. Müller-Plathe, *Macromolecules (submitted)* **2021**.

[116] M. Langeloth, *Artificial entanglements in polymer chains*, Ph.D. Thesis, Technische Universität Darmstadt, Darmstadt, **2015**.

[117] R. Wang, M. K. Sing, R. K. Avery, B. S. Souza, M. Kim, B. D. Olsen, *Acc. Chem. Res.* **2016**, *49*, 2786–2795.

[118] N. R. Langley, *Macromolecules* **1968**, *1*, 348–352.

[119] K. Kremer, G. S. Grest, *J. Chem. Phys.* **1990**, *92*, 5057–5086.

[120] G. S. Grest, K. Kremer, *Macromolecules* **1990**, *23*, 4994–5000.

[121] G. S. Grest, K. Kremer, *J. Phys. France* **1990**, *51*, 2829–2842.

[122] E. R. Duering, K. Kremer, G. S. Grest, *Phys. Rev. Lett.* **1991**, *67*, 3531–3534.

[123] E. R. Duering, K. Kremer, G. S. Grest, *Macromolecules* **1993**, *26*, 3241–3244.

[124] E. R. Duering, K. Kremer, G. S. Grest, *J. Chem. Phys.* **1994**, *101*, 8169–8192.

[125] R. Everaers, K. Kremer, *Macromolecules* **1995**, *28*, 7291–7294.

[126] R. Everaers, K. Kremer, *Phys. Rev. E* **1996**, *53*, R37–R40.

[127] R. Everaers, K. Kremer, *J. Mol. Model.* **1996**, *2*, 293–299.

[128] R. Everaers, *New J. Phys.* **1999**, *1*, 12.1–12.54.

[129] G. S. Grest, M. Pütz, R. Everaers, K. Kremer, *J. Non-Cryst. Solids* **2000**, *274*, 139–146.

[130] A. A. Gavrilov, A. V. Chertovich, P. G. Khalatur, A. R. Khokhlov, *Soft Matter* **2013**, *9*, 4067.

[131] A. A. Gavrilov, A. V. Chertovich, P. G. Khalatur, A. R. Khokhlov, *Macromolecules* **2014**, *47*, 5400–5408.

[132] A. A. Gavrilov, A. V. Chertovich, *Polym. Sci. Ser. A* **2014**, *56*, 90–97.

[133] I. C. Tsimouri, F. Schwarz, W. Caseri, P. J. Hine, A. A. Gusev, *Macromolecules* **2020**, *53*, 5371–5380.

[134] I. A. Gula, H. A. Karimi-Varzaneh, C. Svaneborg, *Macromolecules* **2020**, *53*, 6907–6927.

[135] C. Svaneborg, R. Everaers, G. S. Grest, J. G. Curro, *Macromolecules* **2008**, *41*, 4920–4928.

[136] R. Everaers, *Phys. Rev. E* **2012**, *86*, 022801.

[137] J. Schneider, F. Fleck, H. A. Karimi-Varzaneh, F. Müller-Plathe, *Macromolecules* **2021**, *54*, 5155–5166.

[138] B. K. Johnson, R. K. Prud'homme, *AIChE J.* **2003**, *49*, 2264–2282.

[139] B. K. Johnson, R. K. Prud'homme, *Aust. J. Chem.* **2003**, *56*, 1021–1024.

[140] C. Sosa, R. Liu, C. Tang, F. Qu, S. Niu, M. Z. Bazant, R. K. Prud'homme, R. D. Priestley, *Macromolecules* **2016**, *49*, 3580–3585.

[141] C. Sosa, V. E. Lee, L. S. Grundy, M. J. Burroughs, R. Liu, R. K. Prud'homme, R. D. Priestley, *Langmuir* **2017**, *33*, 5835–5842.

[142] V. E. Lee, C. Sosa, R. Liu, R. K. Prud'homme, R. D. Priestley, *Langmuir* **2017**, *33*, 3444–3449.

[143] A. Nikoubashman, V. E. Lee, C. Sosa, R. K. Prud'homme, R. D. Priestley, A. Z. Panagiotopoulos, *ACS Nano* **2016**, *10*, 1425–1433.

[144] T. I. Morozova, V. E. Lee, A. Z. Panagiotopoulos, R. K. Prud'homme, R. D. Priestley, A. Nikoubashman, *Langmuir* **2019**, *35*, 709–717.

[145] T. I. Morozova, A. Nikoubashman, *J. Phys. Chem. B* **2018**, *122*, 2130–2137.

[146] C. Williams, F. Brochard, H. L. Frisch, *Annu. Rev. Phys. Chem.* **1981**, *32*, 433–451.

[147] A. Halperin, P. M. Goldbart, *Phys. Rev. E* **2000**, *61*, 565–573.

[148] P. G. de Gennes, *J. Physique Lett.* **1985**, *46*, 639–642.

[149] A. Y. Grosberg, S. K. Nechaev, E. I. Shakhnovich, *J. Phys. France* **1988**, *49*, 2095–2100.

[150] A. Y. Grosberg, D. V. Kuznetsov, *Macromolecules* **1993**, *26*, 4249–4251.

[151] R. D. Schram, G. T. Barkema, H. Schiessel, *J. Chem. Phys.* **2013**, *138*, 224901.

[152] J. M. Polson, M. J. Zuckermann, *J. Chem. Phys.* **2000**, *113*, 1283–1293.

[153] J. M. Polson, M. J. Zuckermann, *J. Chem. Phys.* **2002**, *116*, 7244–7254.

[154] R. Chang, A. Yethiraj, *J. Chem. Phys.* **2001**, *114*, 7688–7699.

[155] G. Reddy, A. Yethiraj, *Macromolecules* **2006**, *39*, 8536–8542.

[156] T. T. Pham, M. Bajaj, J. R. Prakash, *Soft Matter* **2008**, *4*, 1196–1207.

[157] C. Pierleoni, J.-P. Ryckaert, *J. Chem. Phys.* **1992**, *96*, 8539–8551.

[158] J. Schneider, A. Z. Panagiotopoulos, F. Müller-Plathe, *J. Phys. Chem. C* **2017**, *121*, 27664–27673.

[159] J. Schneider, M. K. Meinel, H. Dittmar, F. Müller-Plathe, *Macromolecules* **2020**, *53*, 8889–8900.

[160] J. Schneider, L. D. Süss, F. Müller-Plathe, *J. Chem. Eng. Data* **2020**, *65*, 1264–1272.

[161] M. Mooney, *J. Appl. Phys.* **1940**, *11*, 582–592.

[162] R. S. Rivlin, D. W. Saunders, E. N. D. C. Andrade, *Philos. Trans. R. Soc. A* **1951**, *243*, 251–288.

[163] M. Zhong, R. Wang, K. Kawamoto, B. D. Olsen, J. A. Johnson, *Science* **2016**, *353*, 1264–1268.

[164] Y. Gu, J. Zhao, J. A. Johnson, *Trends Chem.* **2019**, *1*, 318–334.

[165] S. Panyukov, *Macromolecules* **2019**, *52*, 4145–4153.

[166] M. Lang, *Macromolecules* **2019**, *52*, 6266–6273.

[167] T.-S. Lin, R. Wang, J. A. Johnson, B. D. Olsen, *Macromolecules* **2019**, *52*, 1685–1694.

[168] S. Panyukov, *Polymers* **2020**, *12*, 767.

[169] D. R. Miller, C. W. Macosko, *Macromolecules* **1976**, *9*, 206–211.

[170] A. A. Gusev, F. Schwarz, *Macromolecules* **2019**, *52*, 9445–9455.

[171] S. Schlögl, M.-L. Trutschel, W. Chassé, G. Riess, K. Saalwächter, *Macromolecules* **2014**, *47*, 2759–2773.

Supporting Information: Different Stages of Polymer-Chain Collapse Following Solvent Quenching – Scaling Relations from Dissipative-Particle-Dynamics Simulations

Jurek Schneider,* Melissa K. Meinel, Han Dittmar, and Florian Müller-Plathe*

Eduard-Zintl-Institut für Anorganische und Physikalische Chemie and Profile Area Thermofluids and Interfaces, Technische Universität Darmstadt, Alarich-Weiss-Str. 8, D-64287 Darmstadt, Germany

E-mail: j.schneider@theo.chemie.tu-darmstadt.de;
f.mueller-plathe@theo.chemie.tu-darmstadt.de

Non-Gaussian Parameter

In addition to the chain properties investigated in the main article, the chain collapse can be studied employing the non-Gaussian parameter[S1] $\alpha_2(t)$, which is defined using the displacement of any bead at time t

$$\alpha_2(t) = \frac{3\langle (r(t) - r(0))^4 \rangle}{5\langle (r(t) - r(0))^2 \rangle^2} - 1. \tag{1}$$

The angular brackets denote the average over all polymer beads in the system. $\alpha_2(t)$ is averaged over all 100 independent runs. If all beads follow Brownian motion, α_2 is zero. A value of $\alpha_2 = -0.4$ denotes a uniform displacement of all beads, and a positive non-Gaussian

parameter indicates a heterogeneous motion. The non-Gaussian parameter derived from the displacement of single beads is shown in Figure S1. The course of $\alpha_2(t)$ appears to be

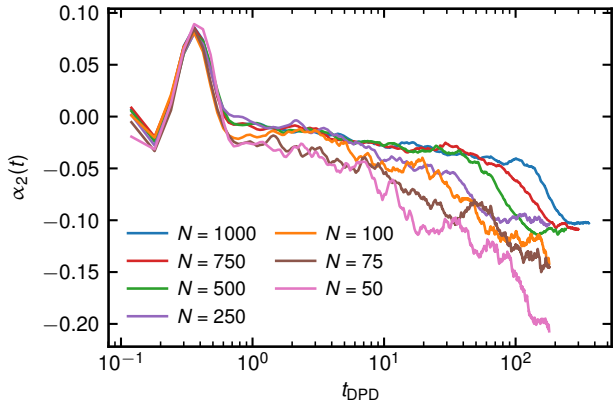

Figure S1: Non-Gaussian parameter α_2 (Equation 1) of collapsing chains of different length N as a function of time. All lines show the average over 100 independent runs after a quench from $a_{\mathrm{PS}} = 25$ to $a_{\mathrm{PS}} = 75$ at $t = 0$.

qualitatively similar for all chain lengths: Immediately after the quench, all beads move in a close-to-Gaussian fashion, with $\alpha_2 \approx 0$. This is followed by a transition to a distinct regime with $\alpha_2 > 0$ before returning to an approximately Gaussian motion. Eventually, the non-Gaussian parameter decays to a negative value. The latter is due to the collective translational motion of all polymer beads as the globular chain diffuses through the nonsolvent. Here, α_2 increases for longer chains as larger globules show a smaller displacement. The regime of heterogeneous motion ($0.18 - 0.66\ t_{\mathrm{DPD}}$) coincides with the pearling stage. At this point, some beads are members of a blob graining in their close vicinity, while others are fully exposed to nonsolvent and have to displace further to join a blob or bridge. The local dynamics of this process appear to be fully independent of the chain length, which is in line with the observations made in the main article. We note that the non-Gaussian parameter can also be derived for larger structures, e.g. the centers of mass of subchains of different lengths. However, the center-of-mass motion of these structures looses significance over the overall chain motion, and a meaningful discussion likely requires larger data sets.

Alternative Presentation of Figure 11

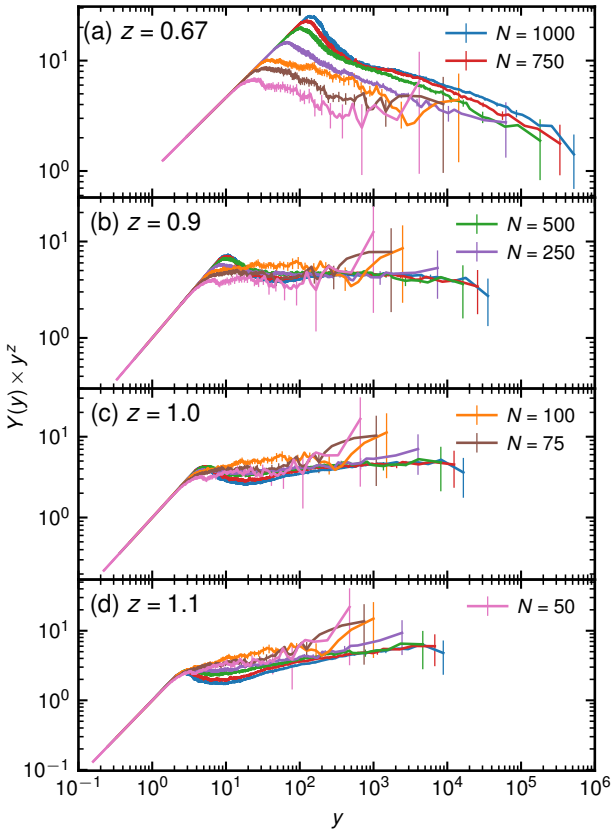

Figure S2: Results of the finite-size scaling analysis for different values of the scaling coefficient z in an alternative presentation to Figure 11. The scaling function $Y(y)$ and scaling variable y are derived from the number-averaged blob size. Error bars are shown for every fifth data point.

Figure S2 gives an alternative presentation of Figure 11 (main article), which shows the results of the finite-size scaling analysis. Scaling of the y-axis by y^z indicates a $\propto y^{-z}$ behavior as a horizontal line, which confirms that the correct scaling exponent z is chosen. This is best fulfilled for $z = 1.0$, which also shows the best collapse of curves within the error bars.

References

(S1) Aichele, M.; Gebremichael, Y.; Starr, F. W.; Baschnagel, J.; Glotzer, S. C. Polymer-specific effects of bulk relaxation and stringlike correlated motion in the dynamics of a supercooled polymer melt. *J. Chem. Phys.* **2003**, *119*, 5290–5304, DOI: 10.1063/1.1597473.

Erklärungen laut Promotionsordnung

§8 Abs. 1 lit. c PromO
Ich versichere hiermit, dass die elektronische Version meiner Dissertation mit der schriftlichen Version übereinstimmt und für die Durchführung des Promotionsverfahrens vorliegt.

§8 Abs. 1 lit. d PromO
Ich versichere hiermit, dass zu einem vorherigen Zeitpunkt noch keine Promotion versucht wurde und zu keinem früheren Zeitpunkt an einer in- oder ausländischen Hochschule eingereicht wurde. In diesem Fall sind nähere Angaben über Zeitpunkt, Hochschule, Dissertationsthema und Ergebnis dieses Versuchs mitzuteilen.

§9 Abs. 1 PromO
Ich versichere hiermit, dass die vorliegende Dissertation selbstständig und nur unter Verwendung der angegebenen Quellen verfasst wurde.

§9 Abs. 2 PromO
Diese Arbeit hat bisher noch nicht zu Prüfungszwecken gedient.

Darmstadt, 20. Juli 2021

Jurek Schneider

Erklärung zum Eigenanteil an den Veröffentlichungen

Im Folgenden ist aufgelistet, mit welchem Anteil ich an den Veröffentlichungen beteiligt war.

Mein Anteil an der folgenden Veröffentlichung beträgt $95\ \%$:
J. Schneider, L. D. Süss, F. Müller-Plathe, *The Influence of Entanglements on the Dynamics of Flash Nanoprecipitation: A Slip-Spring Dissipative-Particle-Dynamics Investigation*, J. Chem. Eng. Data **65**, 1264-1272 (2020).

Mein Anteil an der folgenden Veröffentlichung beträgt $80\ \%$:
J. Schneider, M. K. Meinel, H. Dittmar, F. Müller-Plathe, *Different Stages of Polymer-Chain Collapse Following Solvent Quenching – Scaling Relations from Dissipative Particle Dynamics Simulations*, Macromolecules **53**, 8889-8900 (2020).

Mein Anteil an der folgenden Veröffentlichung beträgt $90\ \%$:
J. Schneider, F. Fleck, H. A. Karimi-Varzaneh, F. Müller-Plathe, *Simulation of Elastomers by Slip-Spring Dissipative Particle Dynamics*, Macromolecules **54**, 5155-5166 (2021).

Darmstadt, 20. Juli 2021

Jurek Schneider

Erklärung zur Begutachtung der Veröffentlichungen

Referent: Prof. Dr. Florian Müller-Plathe 20. Juli 2021
Koreferent: Prof. Dr. Nico van der Vegt

Weder Referent (Prof. Dr. Florian Müller-Plathe) noch Koreferent (Prof. Dr. Nico van der Vegt) der vorliegenden kumulativen Doktorarbeit waren an der Begutachtung nachstehender Veröffentlichungen beteiligt:

J. Schneider, L. D. Süss, F. Müller-Plathe, *The Influence of Entanglements on the Dynamics of Flash Nanoprecipitation: A Slip-Spring Dissipative-Particle-Dynamics Investigation*, J. Chem. Eng. Data **65**, 1264-1272 (2020).

J. Schneider, M. K. Meinel, H. Dittmar, F. Müller-Plathe, *Different Stages of Polymer-Chain Collapse Following Solvent Quenching – Scaling Relations from Dissipative Particle Dynamics Simulations*, Macromolecules **53**, 8889-8900 (2020).

J. Schneider, F. Fleck, H. A. Karimi-Varzaneh, F. Müller-Plathe, *Simulation of Elastomers by Slip-Spring Dissipative Particle Dynamics*, Macromolecules **54**, 5155-5166 (2021).

Referent
(Prof. Dr. Florian Müller-Plathe)

Koreferent
(Prof. Dr. Nico van der Vegt)